NASA CR 121117

DEVELOPMENT OF WELDED METAL BELLOWS HAVING MINIMUM EFFECTIVE DIAMETER CHANGE

by

J. K. Henschel, J. B. Stevens
SEALOL, INC.

an EG&G Company

and

A. C. Harvey, J. S. Howland, S. S. Rhee
FOSTER-MILLER ASSOCIATES, INC.

Prepared for

NATIONAL AERONAUTICS AND SPACE ADMINISTRATION

NASA Lewis Research Center

Contract NAS 3-12004

1. Report No. CR 121117	2. Government Accession No.	3. Recipient's Catalog No.
4. Title and Subtitle Development of Welded Metal Bellows Having Minimum Effective Diameter Change		5. Report Date November 1972 6. Performing Organization Code
7. Author(s) J. K. Henschel & J. B. Stevens, Sealol, Inc. and A. C. Harvey, J. S. Howland & S. S. Rhee, Foster-Miller Associates, Inc.		8. Performing Organization Report No. 10. Work Unit No.
9. Performing Organization Name and Address Sealol, Inc. P.O. Box 2158 Providence, RI 02905		11. Contract or Grant No. NAS3-12004 13. Type of Report and Period Covered Contractor Report
12. Sponsoring Agency Name and Address National Aeronautics and Space Administration Washington, DC 20546		14. Sponsoring Agency Code
15. Supplementary Notes Project Manager, D. D. Scheer, Chemical Propulsion Division NASA-Lewis Research Center, Cleveland, OH 44135		

16. Abstract

A program of analysis, design and fabrication was conducted to develop welded metal bellows having a minimum change in effective diameter for cryogenic turbomachinery face seal applications. Linear analysis of the principle types of bellows provided identification of concepts capable of meeting basic operation requirements. For the 6-inch (.152 m) mean diameter, 1.5-inch (3.8×10^{-2} m) free length bellows studied, nonlinear analysis showed that opposed and nested toroidal bellows plates stiffened by means of alternating stiffener rings were capable of maintaining constant effective diameter within 0.3% and 0.1% respectively under the operating conditions of interest. Changes in effective diameter were due principally to bellows axial deflection with pressure differential having a lesser influence. Fabrication problems associated with joining the thin bellows plates to the relatively heavy stiffener rings were encountered and precluded assembly and testing of a bellows core. Fabrication problems are summarized and recommended fabrication methods for future effort are presented.

17. Key Words (Suggested by Author(s))	18. Distribution Statement
Bellows Bellows Seals Effective Diameter	Unclassified-Unlimited

19. Security Classif. (of this report)	20. Security Classif. (of this page)	21. No. of Pages	22. Price*
Unclassified	Unclassified	163	$3.00

* For sale by the National Technical Information Service, Springfield, Virginia 22151

FOREWORD

This report was prepared by Sealol, Inc., Providence, R.I. under NASA Contract NAS 3-12004. A major subcontractor covering the analytical effort on the contract was Foster-Miller Associates, Waltham, Massachusetts. This is the final technical report prepared under the contract.

The authors would like to acknowledge the effort of Robert W. Rogers who was Sealol Project Manager for the greater part of the program, prior to his retirement.

TABLE OF CONTENTS

TABLE OF CONTENTS (CONT.)

LIST OF ILLUSTRATIONS

LIST OF ILLUSTRATIONS (CONT.)

LIST OF ILLUSTRATIONS (CONT.)

LIST OF ILLUSTRATIONS (CONT.)

LIST OF ILLUSTRATIONS (CONT.)

LIST OF TABLES

SUMMARY

This report presents the results of an analytical and experimental design study aimed at the development of improved welded metal bellows for application in cryogenic seals. Performance characteristics for the full range of bellows configurations were investigated in the linear and non-linear range of operation. The major characteristic of interest was the change in bellows effective diameter over the operating range. Other characteristics of major interest were the bellows spring rate and the maximum operating stresses.

The analytical work culminated in the selection of opposed and nested toroidal bellows plates stiffened by means of alternating stiffener rings as the most promising bellows configurations. Opposed toroids appear to have the capability of maintaining constant effective diameter within 0.3 percent for the conditions of interest. Radial corrugations in the plates may further improve this. Nested toroids, because more convolutions are possible, appear capable of meeting the 0.1 percent goal. Thus, the theoretical work results in the high degree of confidence that significant advancement may be made in the state of the art.

However, fabrication problems arose concerned with the joining of the flexible bellows plates and stiffener rings required for the promising configurations. These problems prevented the experimental verification of the analytical results within the scope of effort available to the program.

Thus, while the program has not resulted in final experimental conclusions regarding performance of the promising designs, it has accomplished a significant systematic evaluation of a wide range of bellows configurations from the standpoint of their ability to provide constant effective diameter. Moreover, it has provided considerable experience with the problems involved in joining of mixed bellows stacks consisting of flexible plates and stiffener elements where there are significant variations in plate thickness among the elements, particularly where there are large diameter to span ratios involved. This type of structure is felt to be inevitable in achieving substantial improvement in the state of the art and, thus, the experience gained in this program will be helpful in developing successful fabrication techniques. Finally, the test methods and apparatus developed and built for the accurate measurement of effective diameter under cryogenic conditions, and the tooling available for producing experimental bellows plates are important tools in the eventual development of constant effective diameter bellows.

It is recommended that these accomplishments be used as the basis for a continued program to improve the state of the art in bellows seals. Specifically, the next tasks should be aimed at developing improved element configurations and joining techniques to overcome the fabrication problems.

INTRODUCTION

This report presents the results of an analytical and experimental design study aimed at the development of improved welded metal bellows for application in cryogenic seals. Performance characteristics for the full range of bellows configurations were investigated in the linear and non-linear range of operation. The major characteristic of interest was the change in bellows effective diameter over the operating range. Other characteristics of major interest were the bellows spring rate and the maximum operating stresses.

The analytical work culminated in the selection of bellows configurations having a high probability of substantial advancement of the state of the art with regard to maintaining constant effective diameter over a wide operating range. However, fabrication problems associated with the joining of flexible elements and stiffener rings having disparate section thicknesses prevented experimental verification of the analytical results within the scope of the program.

The program did attain significant technical accomplishments in terms of the systematic evaluation of a wide range of bellows configurations, fabrication experience with the type of structure required to achieve a constant effective diameter bellows, and the development of test methods and apparatus for the accurate measurement of effective diameter under cryogenic conditions.

This work, which it is hoped will form the basis for future development of improved bellows seals, is covered in this report.

Background

Face contact seals are used to separate the propellant from the turbine drive gas in rocket engine turbopumps. The useful operating life of these face seals is highly dependent upon the face loading. This load must be maintained above a minimum value, determined by the allowable seal leakage, throughout the operating pressure range of the seal. Thus, the degree of control that can be maintained over the face loading throughout this pressure range determines the maximum face loading and, consequently, the life of the seal.

The common method for controlling the seal face load is to balance the force due to the pressure distribution on the seal face with an equal and opposite force due to the pressure acting on a secondary metal bellows seal. In theory, since these forces are both functions of the differential pressure across the seal, the seal face load can be maintained constant throughout the pressure range of the seal, and is determined by the value of the axial spring force present in the bellows.

This ideal situation, however, cannot be achieved in practice since the effective diameter or area of a bellows can vary considerably with differential pressure and operating temperature. Effective diameter variations of 1 to 5 percent are common over the operating pressure range within the present state-of-the-art in bellows technology. This factor represents a major limitation to the development of improved balanced seals for advanced rocket propulsion systems.

Objective

The overall objective of the program is to develop configurations for welded metal bellows which will minimize changes in effective diameter while providing acceptable nominal characteristics throughout the desired operating range. The immediate objectives of the study reported here are the identification of promising design concepts to meet the overall objective, the analysis of these concepts to determine their feasibility, and the experimental verification of this analysis using special test bellows.

Method of Approach

The method of approach used in this study consisted of the following major steps:

Conceptual Design. - The identification and classification of promising bellows configurations.

Screening Analysis. - Linear analysis and preliminary non-linear analysis to screen out concepts which are not capable of meeting nominal operating requirements or which are not promising for providing constant effective diameter.

Non-linear Analysis. - To predict the non-linear operating behavior of the most promising configurations and to select the final design configurations for subsequent experimental evaluation.

This approach provided economy in the analysis of the concepts since the most detailed non-linear analysis was performed only for those concepts having promise of success. The preliminary analysis, however, resulted in a tabulation of the salient features of the whole range of concepts and, thus, provides convenient future reference material. Furthermore, the systematic approach followed helps ensure that no important concept categories were overlooked.

DESCRIPTION OF THE SYSTEM

A typical balanced-pressure, face-contact seal with a welded metal bellows secondary seal is illustrated in Figure 1. The nomenclature and terminology for the following technical discussion are presented in Table I.

Considering the axial free-body diagrams of Figure 2, axial force equilibrium gives the following result for the contact force, F_s, at the face seal,

$$F_s = F_b - \frac{\pi}{4} (D_o^2 - D_s^2) \Delta P \tag{1}$$

where

$$\Delta P = P_o - P_i \tag{2}$$

It should be noted that it is assumed that the nature of the hydraulic pressure distribution across the face seal is known to a sufficient degree, either theoretically or by experimental measurement, to establish the effective sealing diameter, D_s. For example, if a radial pressure distribution P (r) exists across the face seal, the effective sealing diameter, D_s, can be shown to be given by,

$$D_s = \left[\frac{1}{\Delta P} (P_o D_o^2 - P_i D_i^2 - 8 \int_{D_i/2}^{D_o/2} P(r)\, r\, dr) \right]^{1/2} \tag{3}$$

The reaction force, F_b, between the bellows and the seal ring consists of a component due to the axial compression of the bellows from its free length, and a component due to the net axial pressure force acting on the bellows.

This can be expressed as,

$$F_b = k\Delta \ell + \frac{\pi}{4} (D_o^2 - D_e^2) \Delta P \tag{4}$$

where D_e is the effective diameter of the bellows. Combining Equations (1) and (4) gives the result,

$$F_s = k\Delta \ell + \frac{\pi}{4} (D_s^2 - D_e^2) \Delta P \tag{5}$$

for the contact force on the face seal.

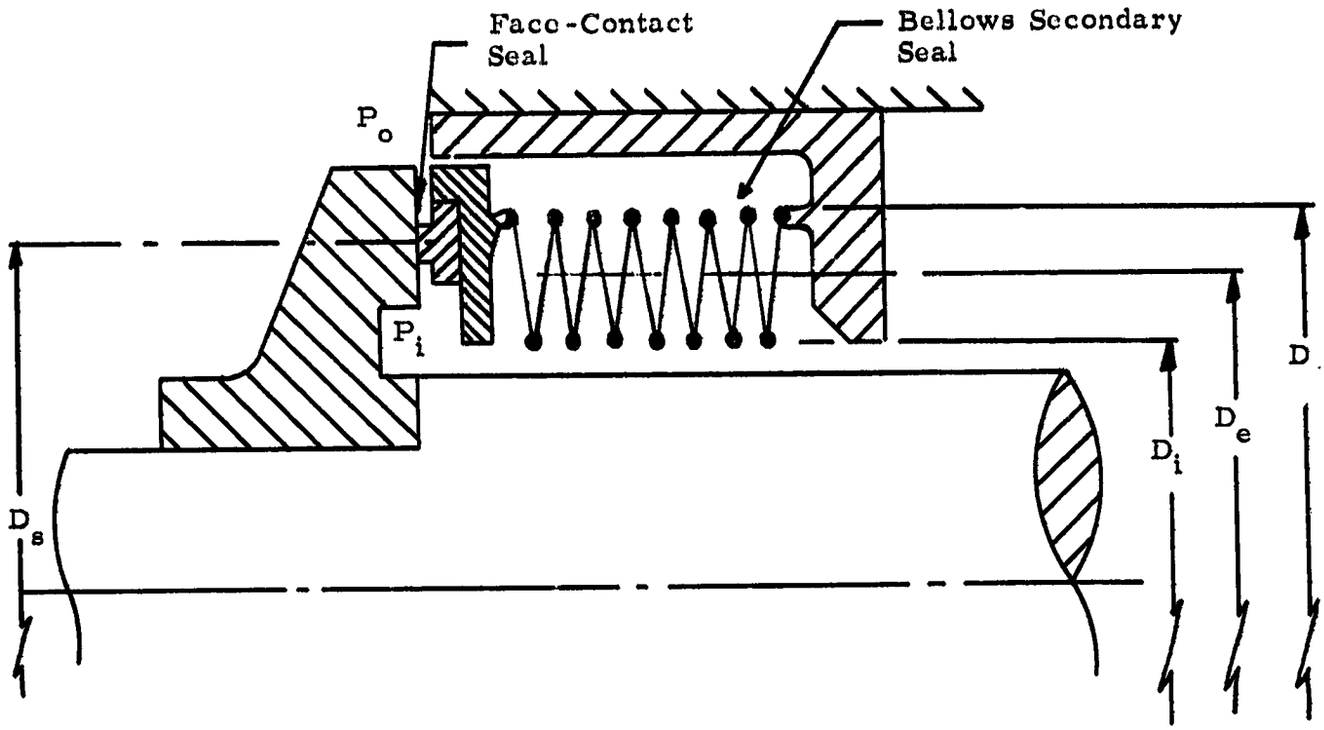

Figure 1. Schematic Diagram of a Face-Contact - Bellows Shaft Seal

TABLE I

Table of Nomenclature and Terminology

D_e	=	Effective diameter of the bellows
D_i	=	Inside diameter of the bellows
D_o	=	Outside diameter of the bellows
D_s	=	Effective sealing diameter of the face seal
F_s	=	Contact force at the face seal
F_b	=	Reaction force between the bellows and the seal ring
k	=	Bellows spring rate
ℓ	=	Bellows free length
$\Delta\ell$	=	Axial compression in bellows
P_i	=	Inside pressure
P_o	=	Outside pressure
S	=	$\frac{D_o - D_i}{2}$ - span of the bellows
t	=	Thickness of the bellows plates
core	=	Flexible element of a bellows assembly without the end fittings
convolution	=	Two bellows plates joined at the inside diameter
pitch	=	Axial distance between adjacent weld beads

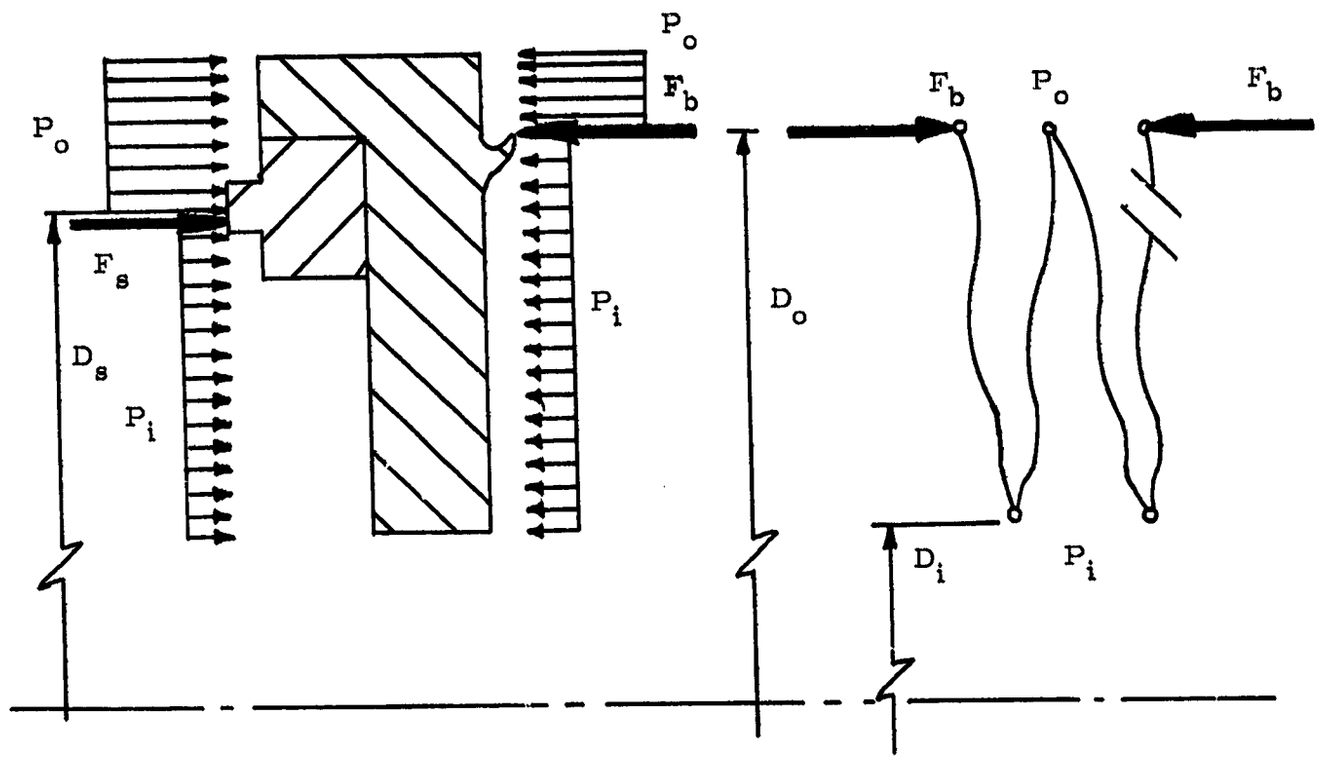

Figure 2. Idealized Axial Free-Body Diagram for the Face-Seal Ring and the Bellows

In designing a balanced pressure seal, it is attempted to set D_s equal to D_c. Thus, for the ideal case, the contact force will be independent of the differential pressure. The spring force $k\Delta\ell$ is designed to provide the minimum force necessary for adequate sealing with the minimum operational value of $\Delta\ell$, as determined by the possible shaft motion and seal wear.

In practice, however, even though D_s and D_e are balanced with no pressure differential across the bellows, the effective diameter will change with pressure differential, ΔP, unbalancing the seal. It should be noted that, in general, the spring rate, k, and the bellows free length, ℓ, will also change as a function of ΔP. However, if these quantities are considered constant in Equation (5), then any nonlinearity between seal force, F_s, and ΔP can be attributed to a variation in D_e with ΔP. This is the convention adopted in this study.

From a design point-of-view, changes in D_e have the effect of increasing the maximum force which occurs on the seal face, decreasing its life. For example, if D_e increases with ΔP, then the second term of Equation (5) will become negative as ΔP is increased. This requires a larger initial load, $k\Delta\ell$, as ΔP increases.

DESIGN GOALS

The major bellows design criteria for this program are summarized in Table II. These are discussed as follows.

The specified ranges for outside diameter, span, and free length are commensurate with the space envelope available for the bellows in the typical application.

The maximum spring rate specified is consistent with values attainable in this envelope within the bellows state-of-the-art. It may be seen from Equation (5) that the seal face load is directly proportional to the spring rate times the bellows compression, $\Delta \ell$. The compression will vary during operation due to seal wear and axial shaft motion. Thus, the seal load variation during operation can be minimized by proving minimum spring rate. For a given preload, however, the initial bellows compression is inversely proportional to spring rate. Thus, the minimum spring rate, while maintaining a reasonable value of initial compression, is a desirable design goal.

The specified axial compression ensures that the seal will not become unloaded with expected values of seal wear and shaft motion. Pressure capability of 500 psi is sufficient for the turbopump application under consideration. The ability of the bellows to withstand this pressure differential in both directions would provide maximum flexibility in the application of the bellows to various situations. However, a bellows design which is capable of providing the desired linearity but with pressure capability in only one direction would also be useful.

The 300 cycle life is adequate for the limited life applications of interest.

The seal material specified is Inconel 718 for its excellent properties at cryogenic temperatures.

The ultimate cryogenic fluids will be LH_2 and LO_2. For test purposes, however liquid and gaseous nitrogen will be used.

The specified allowable variation in bellows effective diameter of 0.1 percent ensures that the variation in seal face load due to pressure variations will be consistent with the nominal seal load. For example, typical values of the spring load, $k\Delta \ell$, in Equation (5) are of the order of 100 lbs. (444.8 newtons).

If D_e is assumed to change by an amount ΔD_e and D_s is initially equal to D_e, then Equation (5) may be rewritten in the form,

$$F_s = k\Delta \ell + \frac{\pi}{4} D_e^2 \Delta P \left[\left(\frac{\Delta D_e}{D_e} \right)^2 + 2 \frac{\Delta D_e}{D_e} \right] \qquad (6)$$

TABLE II

Design Criteria for the Bellows

Outside Diameter	5 to 7 inches
Span	not greater than 0.060 inches
Free Length	not greater than 1.5 inches
Spring Rate ($\Delta p = 0$), Room Temperature	less than 800 lb/in
Axial Compression	0.15 inches minimum
Pressure Range	0 to 500 psi, both directions
Cyclic Life	greater than 300 pressure cycles
Material	Inconel 718
Medium	LH_2 or LO_2, testing in nitrogen
Effective Diameter	Constant within 0.1 percent

for the specified conditions of Table II, this results in a possible pressure force variation of 40 lbs. (178 newtons). Within the existing state-of-the-art, however, a pressure load variation of 400 lbs. (1780 newtons) is possible resulting in much more serious seal face wear.

It should also be noted parenthetically that the bellows is expected to operate over a wide temperature range which alone will result in changes up to 0.4 percent in effective diameter and free length. Thus, to preserve pressure balancing consistent with the above specifications, the ultimate overall seal design must provide extremely uniform thermal expansion so that D_s and D_e change by an equal amount.

BELLOWS PLATE CONFIGURATIONS

At the outset of this study, a concept generation task was performed to identify and classify the major bellows convolution shapes of interest. Table III shows the range of shapes considered, classified according to family and type.

Within these generic groupings, of course, there are an infinite variety of specific configurations and it is not intended to illustrate this range. For example, many specific nested ripple configurations have been practically applied in the past. Also, useful shapes could be found which classify between the types shown. For example, the common single-sweep shape probably lies between the nested toroid and the nested ripple.

It is felt, however, based upon the results of the subsequent analytical work that the spectrum of performance characteristics for the range of practical shapes is bracketed by these generic types.

Special mention should be made of the orthotropic* flat plate and toroidal convolutions. These shapes resulted from preliminary indications that improved performance might result from increasing the radial stiffness of the plates without commensurate increases in the circumferential stiffness. For the flat plates, this can provide increased pressure resistance without corresponding increases in the spring rate. For the toroidal configuration, the resulting unbalance between radial and circumferential stiffnesses offers the possibility of maintaining the toroidal shape more perfectly under axial deflection and, thus, a more constant effective area.

Although the bellows plates were analyzed quantitatively in the range of interest as described in subsequent sections, several generalized comparisons may be noted here.

---

* Orthotropic - A specific type of anisotropy where properties (in this case, section stiffness) differ along locally orthogonal axes.

TABLE III

BELLOWS PLATE CONFIGURATIONS

Family	Type	Convolution Shape
Corrugated Plate	Nested Ripple	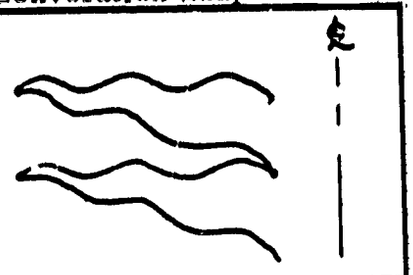
	Opposed Plate	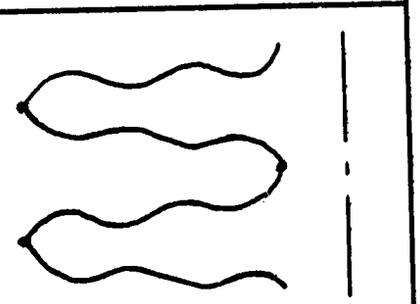
Flat Plate	Zero Inclination	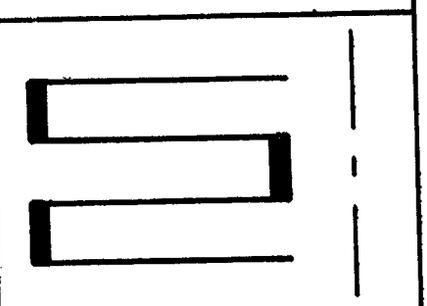
	Inclined Plate	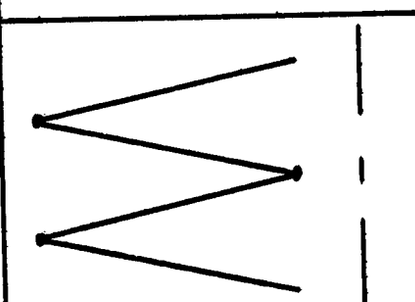
	Orthotropic (Radial Corrugations)	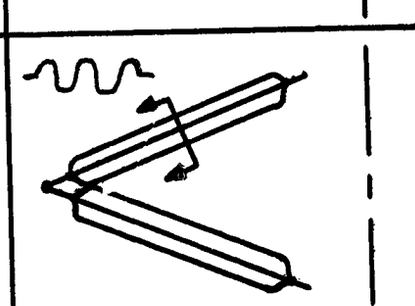

TABLE III (Cont.)

Toroidal	Full, Opposed	
	Partial, Opposed	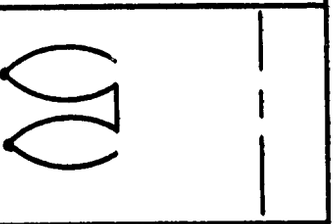
	Nested	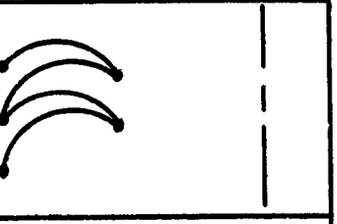
	Orthotropic (Radial Corrugations)	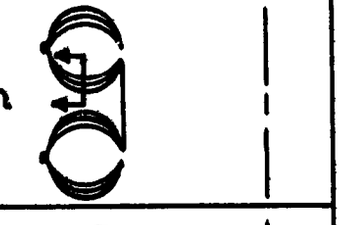
S-Shaped	Full Toroidal Segments	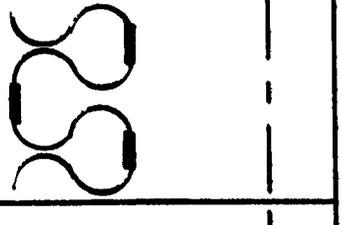
	Shallow Segments	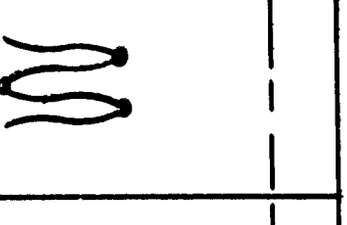
	Inclined	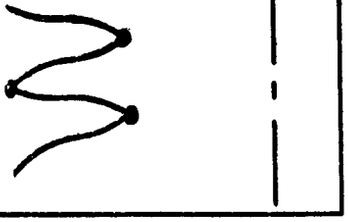

A major distinction may be drawn between full or nearly full toroidal plates and the remaining shapes. In the former the stresses due to pressure are largely membrane stresses and are nearly constant in the plate. In the latter, radial bending stresses are typically the major component and the magnitude usually varies considerably across the span depending upon the particular shape. The toroid, because of its largely membrane action, has a comparatively high resistance to pressure load for typical plate thicknesses.

The shallow shapes, however, are typically more compliant and more convolutions may be fitted into a given core length. Thus, they typically exhibit a lower spring rate and a greater capability for long stroke. Of these, those plates having a substantial portion of the span with zero inclination, such as the zero inclination flat plate and certain specific nested ripple configurations, have the lowest axial spring rate.

In general, it can be stated that any plate in an opposed or symmetric convolution will exhibit greater linearity (minimum change in effective diameter) than its counterpart in a nested convolution. Also, the full toroidal plate is theoretically the most linear configuration under pressure load alone.

The effect of the radial corrugations in the orthotropic plates is mainly the reduction in circumferential stiffness. This reduces the axial spring rate of the plates from the uncorrugated case. Radial bending stiffness is increased somewhat and the corrugations introduce circumferential bending stresses not present in the uncorrugated case. It is possible that, in some situations, the net effect would be an increased linearity over the required axial stroke without a reduction in pressure resistance.

The plate and convolution configurations described in this section serve as a basis for the detailed analytical work described in the following sections of this report.

ANALYSIS OF BASIC PERFORMANCE

The design criteria listed in Table II consist of three major types:

(a) Dimensional, Material, and Environmental Criteria

(b) Nominal Performance Criteria

(c) Linearity Criterion

The dimensional criteria specify the range of bellows diameter, span, and length of interest in this application. All of the analysis and experimentation performed in this study was concentrated in this size range. For the large diameter to span ratios of interest, there is no strong variation in performance with diameter. Thus, the size of the bellows was fixed at 6 inches (.152 m) mean diameter which allows the specified span variation within the specified envelope. In order to maintain a low spring rate and provide ease in fabrication, it is desirable to keep the span above 0.25 inches. (.0064 m) Thus, the extreme cases of 0.25 inches (.0064 m) and 0.5 inches (.127 m) were analyzed for their basic performance. The free length specification places a limitation on the maximum number of a given convolution that can be used, and also, along with the axial compression requirement, sets a minimum of 10 percent axial compression. The plate thickness represents the size parameter with the greatest possible range and the performance for each type of plate has been studied across this range.

The specified bellows material is Inconel 718 for its excellent low-temperature properties. The main effect of the material on the analytical results is that it imposes a design stress limit and thus limits the range of useful application for a given design. Since the linearity criterion is the predominant one, the design stress limit has conservatively been set as the minimum Yield Strength in the temperature range of interest. The specified 300 cycle cyclic life provides, in general, a less stringent stress limitation for Inconel 718. For reference in the remaining discussion of this report, the Yield Strength and Ultimate Strength for Inconel 718 are given in Figure 3 as functions of temperature. (1,2)*

The only environmental condition of interest presently is the surrounding medium which has the effect of imposing the temperature level at which the bellows must operate. Of the specified media, LH_2 has the lowest boiling temperature at atmospheric pressure, -423°F (20.36°F). Thus, the bellows should be capable of operating from ambient temperature down to -423°F. (20.36°F).

---

* Numbers in parentheses refer to the list of references.

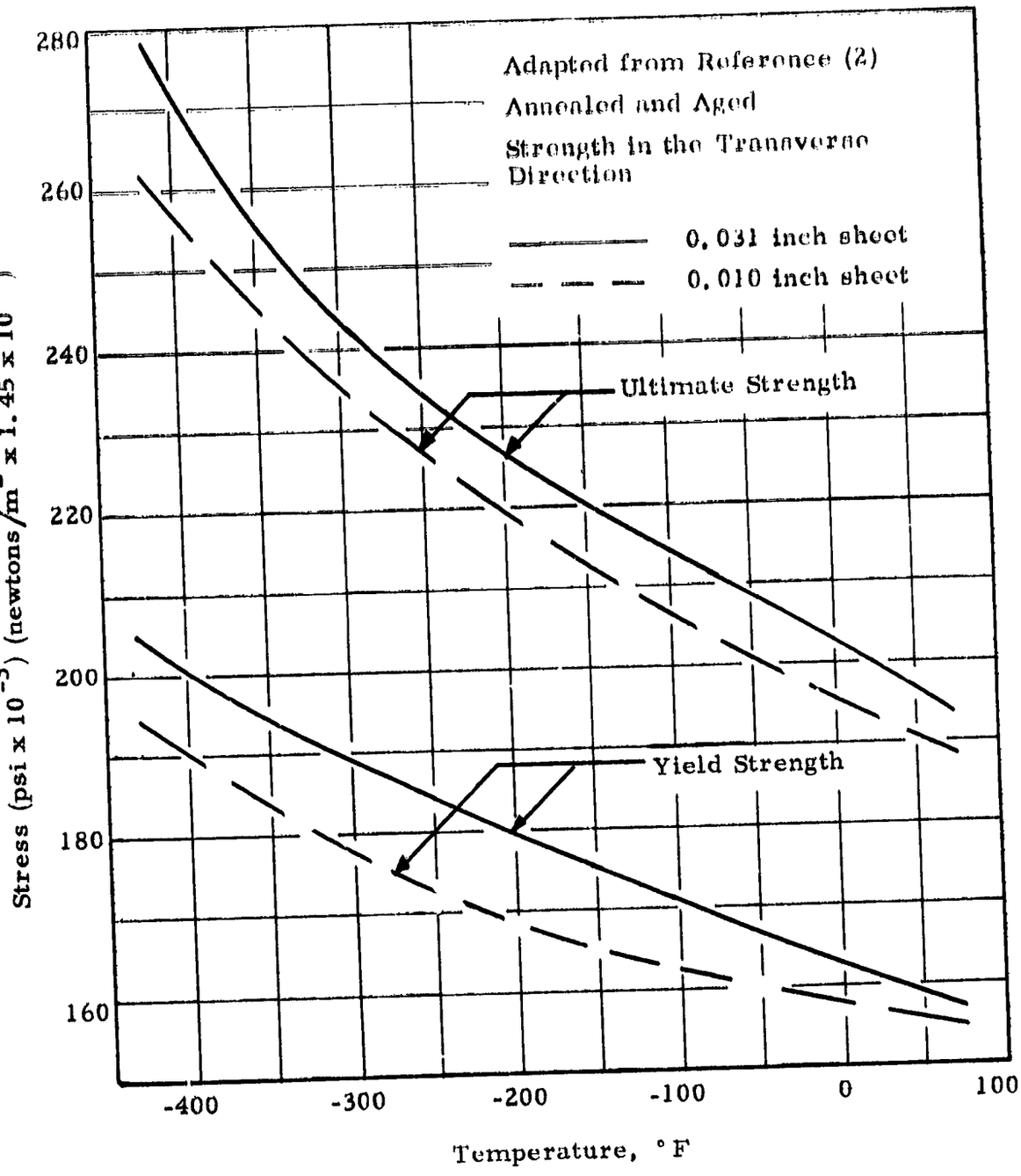

Figure 3. Ultimate Strength and Yield Strength of Inconel 718 in the Cryogenic Temperature Range

The nominal performance criteria described the capability of the bellows to perform their basic function. That is, to provide a nominal sealing force and to withstand the combined stresses due to axial deflection and pressure differential over a life of 300 cycles. If a bellows design is inherently incapable of satisfying these criteria, its linearity is of no practical interest. In general, analysis of the nonlinear behavior of a bellows is more detailed and costly than linear analysis. Thus, the method of approach followed was to screen the various types of bellows for their ability to meet the nominal performance criteria within the specified size range. This screening was accomplished by analysis of the linear range of operation, as described in the remainder of this section for the various plate shapes considered.

Nonlinear analysis to predict the change in effective bellows diameter under load was then performed only for those promising bellows shapes, predicted to meet the nominal performance criteria.

Corrugated Plates

The general convolution shape for corrugated plates was illustrated in Table III. The opposed plate convolution is of main interest in reducing the non-linearity that arises due to differences that arise in the reaction moments at the edges of asymmetric nested convolutions under load. For evaluating the capability of a given plate shape to meet the nominal performance goals of Table II, however, the nested configuration is the most favorable case. This arises from the fact that more convolutions can be included within the allowable core length, thus, minimizing the spring rate and the stresses due to the specified axial compression. For this reason, the nested configuration was analyzed in this study.

Because the nested ripple plate is in common use as a bellows seal element, considerable performance information has been accumulated. For example, it is known that the predominant stress components in these elements are the radial bending stress and the tangential direct or membrane stress. The distribution of these stresses is quite dependent upon the diameter to span ratio. For small values of this ratio (i.e. up to about 10), the magnitudes of these components are comparable and the distribution follows the plate ripples, often having large amplitude of variation across the span. In this range, considerable variations in performance can occur as the detailed shape of the plate is varied.

For large values of the diameter to span ratio, which is the range of interest in this study, however, the bending stress becomes predominant as shown in Figure 4. This approaches a straightline

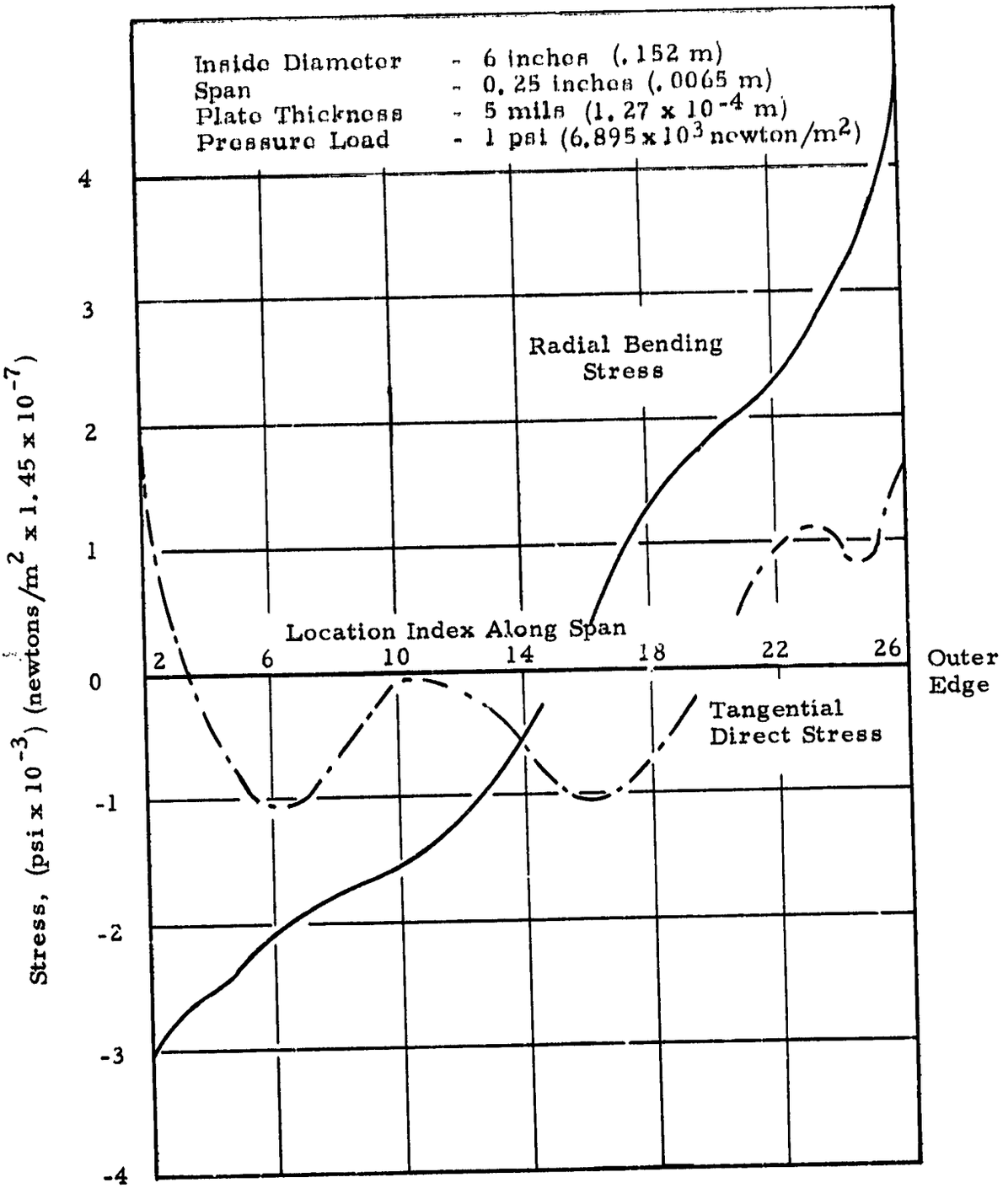

Figure 4. Predominant Stresses in a Typical Corrugated Bellows Plate in the Span to Size Range of Interest

variation across the span which is characteristic of flat plate behavior. In this range, the major factors that affect performance are the overall plate inclination and the degree of coning or inclination near the edges rather than the details of the ripples near the center of the span.

For this reason, the analysis discussed in this section is based upon a standard plate shape developed by Sealol Inc. for seal applications. It is felt that this represents a typical well-designed bellows plate of the nested ripple configuration.

The solution of Figure 4 and those upon which the remaining data of this section is based were obtained using the computer program described in Appendix A. This computer program solves the generalized shell equations as applied to bellows elements in the linear range. It, thus, provides an approximation to the nominal performance of a bellows. Significant errors would be expected for the actual magnitudes of the stresses under loads which produce large deflections and, of course, this program is not capable of predicting nonlinearity of the bellows. However, the predicted spring rates have been found empirically to hold over considerably large deflections.

The nominal performance of the tested ripple plates in the size range of interest is shown in Figures 5 and 6. In Figure 5, a mean diameter of 6 inches (.152 m) and a span of 0.25 inches (.0064 m) is assumed. The curves plot the peak maximum stress intensity as a function of plate thickness. This stress intensity combines the effects of a 500 psi (3.445×10^6 newtons/m^2) pressure load and an axial stroke of 0.15 inches (.00381 m). Figure 6 plots the same thing for a span of 0.5 inches (.0127 m).

Two curves are shown for the nested ripple plate in Figure 5. One represents a bellows core consisting of 30 convolutions regardless of plate thickness. This would provide sufficient stroke within the allowable length of the core only for plate thicknesses up to approximately 20 mils (5.08×10^{-4} m). The other curve allows the number of convolutions to vary according to the maximum that can be fit into the core length for each plate thickness between 10 and 20 mils (2.54×10^{-4} and 5.08×10^{-4} m). Below 10 mils (2.54×10^{-4} m) the number was held at 60 which is felt to be a practical, although arbitrary limit.

In both figures, the performance of the corresponding flat disk bellows is shown for comparison. This will be discussed in the next section.

Figure 7 shows the bellows spring rates for each of the cases given in Figures 5 and 6 as a function of plate thickness. The discontinuity in the 60 convolution case of Figure 7 results from the

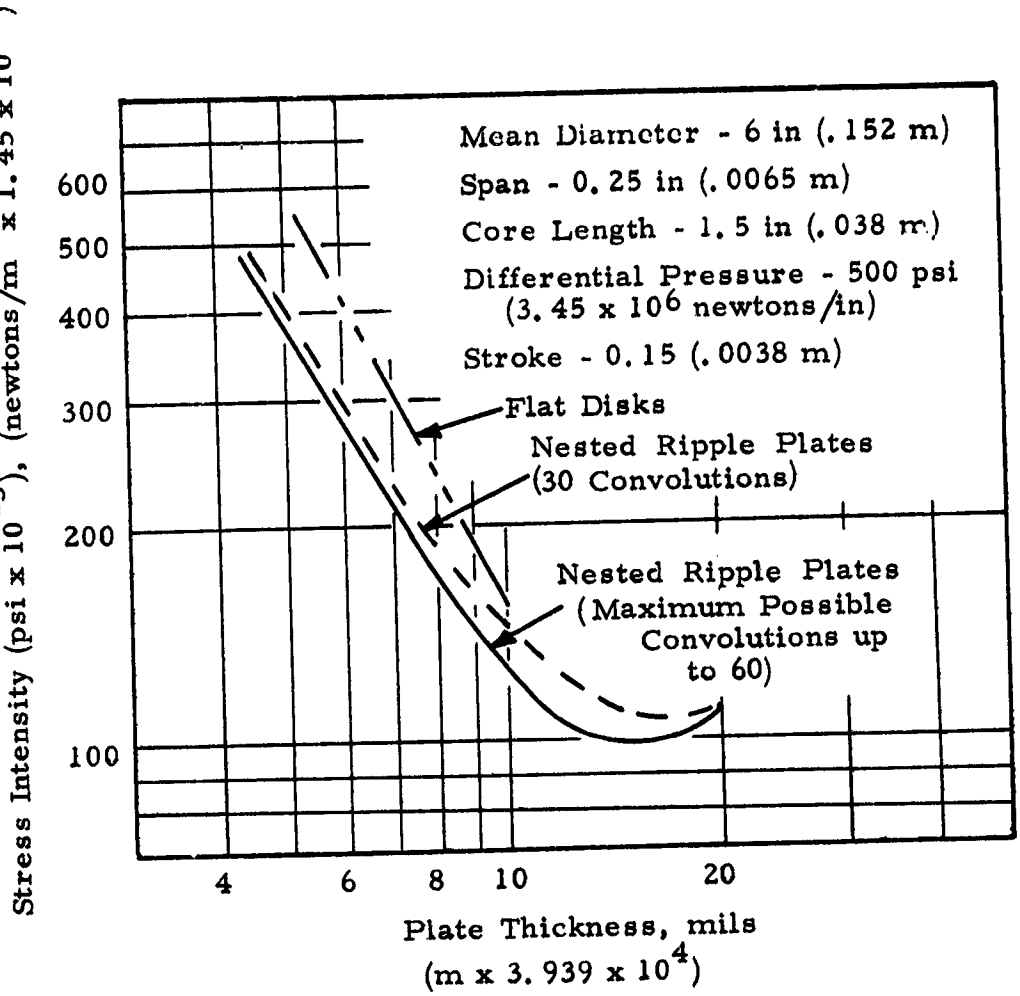

Figure 5. Combined Stress of Nested Ripple Plate Bellows Due to Pressure and Axial Deflection Compared with Flat Disks - 0.25 Inch Span

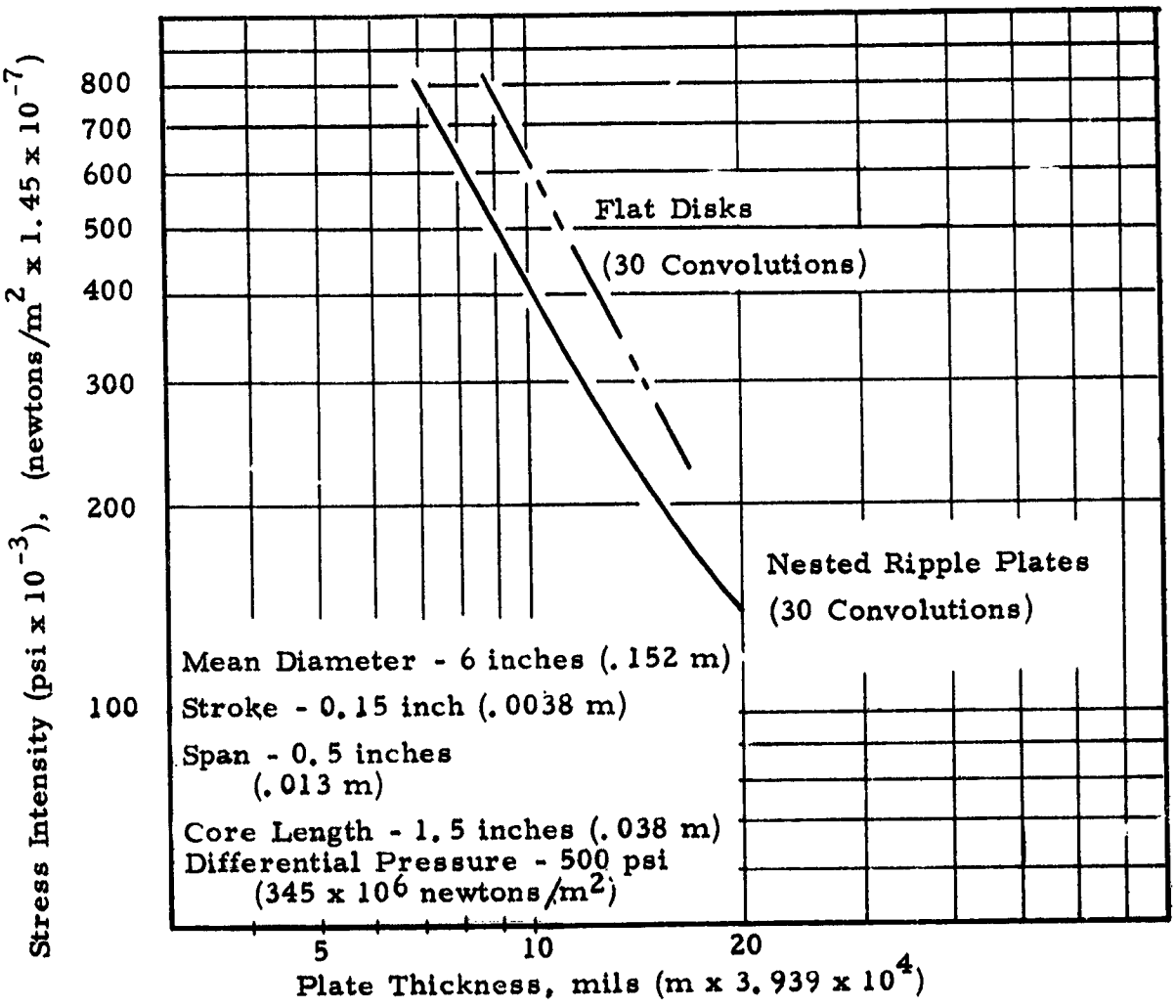

Figure 6. Combined Stress of Corrugated Plate Bellows Due to Pressure and Axial Deflection Compared with Flat Disks - 0.5 Inch Span

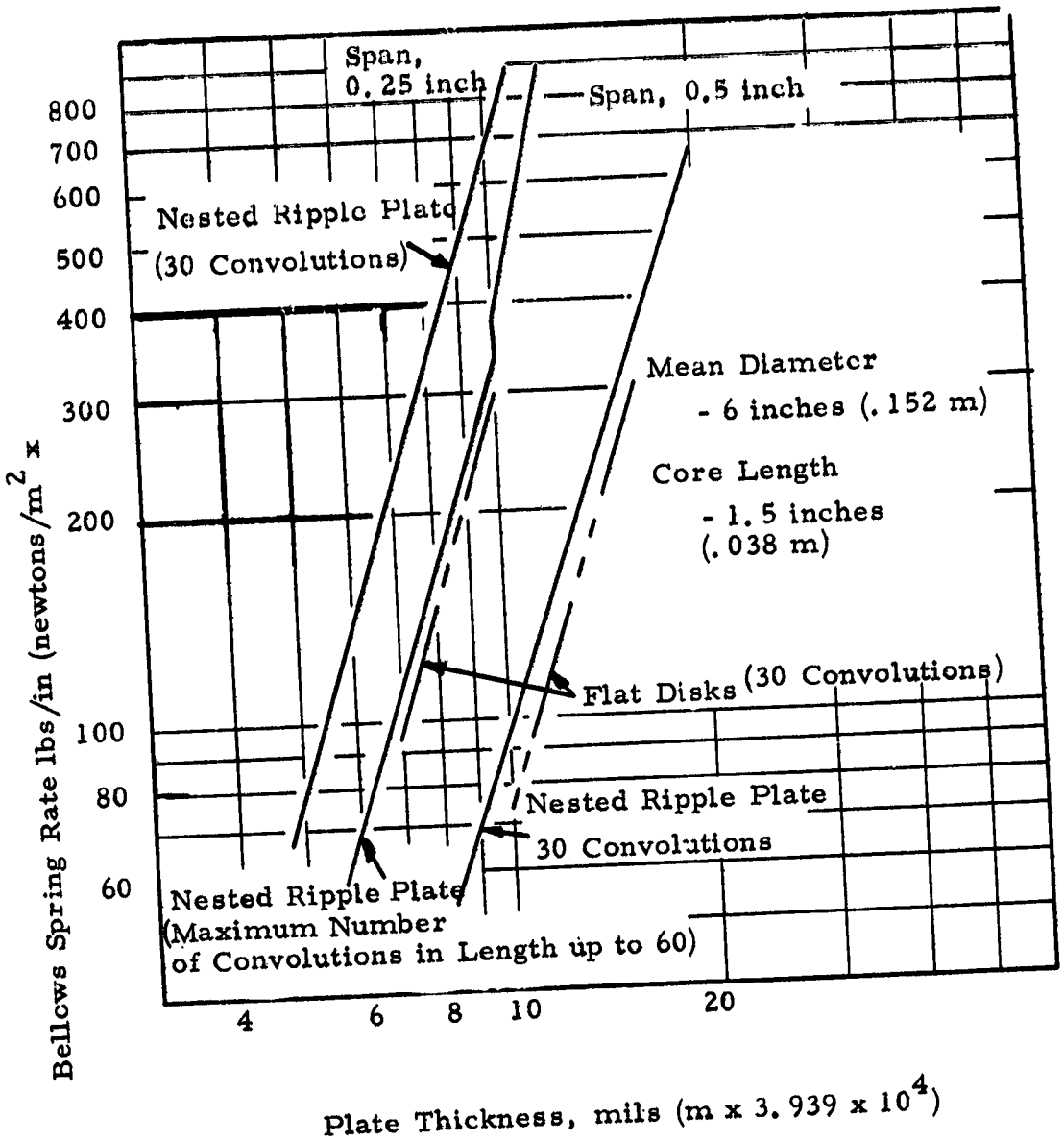

Figure 7. Comparison of Bellows Spring Rates for Corrugated Bellows and Flat Disks

fact that, with a plate thickness beyond 10 mils (2.54×10^{-5} m) 60 convolutions can no longer be fitted within the allowable core length. Thus, beyond this point, the maximum number which can be fitted in is used. This number, of course, changes as thickness is increased.

The limitations in the capability of nested ripple plates for meeting the nominal performance goals can be seen by considering the data shown in Figures 5, 6 and 7. Remembering that the maximum allowable stress intensity is approximately 150,000 psi (1.35×10^4 newtons/m^2) as shown in Figure 3, it can be seen from Figure 5 that the plate thickness for a 0.25 inch (.0064 m) span would have to be approximately 9 mils (2.285×10^{-4} m) or larger. Figure 6 shows that the 0.5 inch (.127 m) span is virtually precluded from this application since the stress does not get down to the allowable range until the plate thickness reaches 20 mils (5.08×10^{-4} m). No further reduction in stress can be achieved through additional convolutions since 30 convolutions is the maximum that can be fit into the available space for this thickness.

Figure 7 and Figure 5 show that, for the 0.25 inch (.0064 m) span, a spring rate of 800 lbs/in (1.4×10^5 newtons/m) or less can be obtained in the acceptable stress range only for plate thicknesses between 9 and 11.5 mils (2.285×10^{-4} m and 2.92×10^{-4} m).

Thus, it may be concluded that the nominal performance goals could be met only for the minimum practical span, 0.25 inches (.0064 m), with a plate thickness of approximately 10 mils (2.54×10^{-4} m) and greater than 30 convolutions. This is a very narrow range of acceptable parameters and consequently must be concluded to be a marginal situation. Any slight variation from the predicted values of either stress level or spring rate could eliminate the acceptable range entirely. For example a 27 percent error on the low side in the predicted stress value, which is easily possible for the methods used, could preclude the use of the 0.25 inch (.0064) span bellows.

For this reason, it is not felt that the nested ripple bellows configuration is suitable for this application.

Flat Disks

As noted in the preceding section, membrane stress effects are small for the corrugated plate shape in the diameter to span ratio range of interest. This implies that the corrugations and plate tilt have a relatively low importance in this range. For this reason, flat disks were analyzed for their basic performance.

Accurate relationships are available in the literature for the linear behavior of flat disks (3). Solutions are also available for the behavior of coned flat plates (i.e. Belleville washers) (4). These are somewhat unwieldy however, and it was found that, for the large diameter to span ratios of interest, the results are approximated within 10 percent by considering the plates to act as a wide straight beam with the same span, thickness, and edge conditions. This is sufficient accuracy for the purposes of this screening analysis. Thus, these approximate formulae, which are summarized below, were used to obtain the flat disk data plotted in Figures 5, 6 and 7 for comparison with the nested ripple plates.

A schematic diagram showing the initial precompression and pressure loading for the straight beam model of the flat disk bellows is given in Figure 8.

The force per unit circumference, F, required to produce the axial deflection, ΔL, is given by,

$$F = K \Delta L \tag{7}$$

where the spring rate per unit circumference, K, may be approximated by,

$$K = \frac{Et^3}{S^3 (1 - \nu^2)} \tag{8}$$

where

E = Young's Modulus

ν = Poisson's Ratio

t = plate thickness

S = span

The maximum bending stress produced by this initial precompression may be approximated by the relation,

$$\sigma_f = \frac{3 F S}{t^2} \tag{9}$$

If the bellows is then pressurized with pressure, P, an additional bending stress is produced according to the relation,

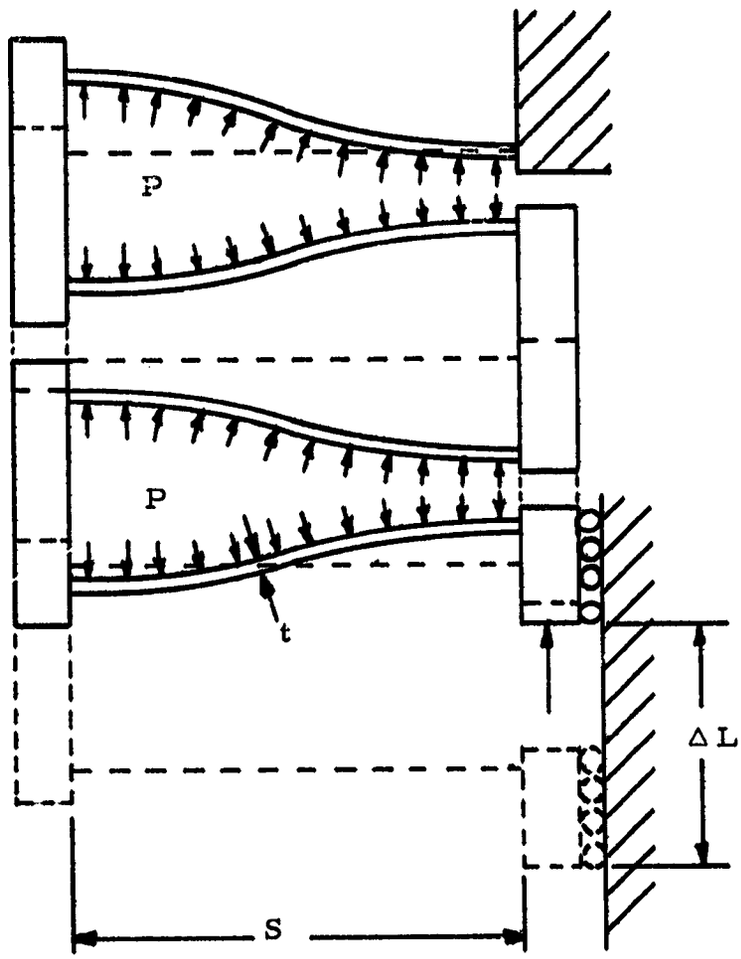

Figure 8. Schematic Diagram Showing the Deflection and Loading of the Straight Beam Model of the Flat Disk Bellows.

$$\sigma_p = \frac{P S^2}{2 t^2} \qquad (10)$$

Superposition of the two stress components given by Equations (9) and (10) at the point of maximum stress where they add was used to calculate the behavior shown in Figures 5 and 6. The spring rates shown in Figure 7 were calculated using Equation (8).

The salient conclusions that may be drawn from these results are that the flat plate bellows have a lower spring rate for the same number of convolutions than the corrugated plate bellows. Also, the bending stress due to axial compression alone is lower. However, the total stress due to both axial compression and pressure is significantly higher than that for the corrugated plates. For plate thicknesses where the stress due to pressure is acceptable, the spring rate is increased to the point where no advantage is gained in comparison with the corrugated plates. Thus, the flat plate bellows is also concluded to be unsuitable for this application.

Finally it should be noted that the performance superiority shown in Figures 5 and 6 for the corrugated bellows does not contradict the observation, made in the previous section, that corrugations near the center of the span have little effect in this size range. Rather the advantages of the corrugated plate are believed to be due to the more favorable edge conditions produced by the corrugated configuration and the resulting smaller effective span.

Orthotropic Plates

As depicted in Table III, orthotropic plates contain corrugations around their circumference, lined up along the plate radii.

As noted in the preceding section, the major drawback for flat disks was that increasing the plate thickness to obtain pressure resistance resulted in spring rates which are too high.

This can be mitigated by radially stiffening the center of the span while leaving the region near the edges of the span, where most of the bending under axial deflection occurs, unstiffened. The stiffening of the central part of the span reduces the reaction moments and the resulting stress due to pressure loading as well as the stress in the central portion of the span. At the same time, the bending stress and spring rate under axial deflection are only slightly increased since the central part of the span primarily tilts with little bending under axial deflection.

Radial corrugations are a convenient way to achieve this

stiffening using stamped plates, and they allow for the possibility of nesting the plates in a stack. The radial corrugations also provide a decreased circumferential stiffness which aids in the desired action.

As for flat plates, this configuration was analyzed using the straight beam approximation. The schematic diagram of Figure 9 shows the model used. The angularly fixed boundary condition is imposed as for the flat plate by the convolution symmetry.

It is assumed that the center of the span is corrugated to provide a section moment of inertia, I, which is n times that of the uncorrugated plate, I_o. It can be shown from the properties of the sections that,

$$n \cong \frac{6\,h^2}{t^2} \tag{11}$$

where

h = amplitude of the corrugations

t = plate thickness

Thus, a moment-of-inertia ratio of 100 can be achieved for a corrugation amplitude to thickness ratio of four.

Formulae for the spring rate, K, and the stress due to pressure, σ_p, may be computed from energy methods using the method of Castigliano. The relation for spring rate per unit circumference is,

$$K = \frac{Et^3}{S^3\,(1 - \nu^2)} \left[\frac{1}{(8x^3 - 12x^2 + 6x)\,(1 - \frac{1}{n}) + \frac{1}{n}} \right] \tag{12}$$

which is similar in form to that of Equation (8) for flat plates with the addition of the correction term. In this relation, x represents the fraction of the span which is uncorrugated at each edge of the span.

The stress due to the axial compression remains as given by Equation (9) of the preceding section where the force, F, is computed from Equation (7) using the spring rate given by Equation (12).

The maximum stress due to a pressure loading, P, is given by,

$$\sigma_p = \frac{P\,S^2}{2\,t^2} \cdot \frac{\left[(3x^2 - 2x^3)(1 - \frac{1}{n}) - \frac{1}{2n} \right]}{(\frac{1}{2n} + x - \frac{x}{n})} \tag{13}$$

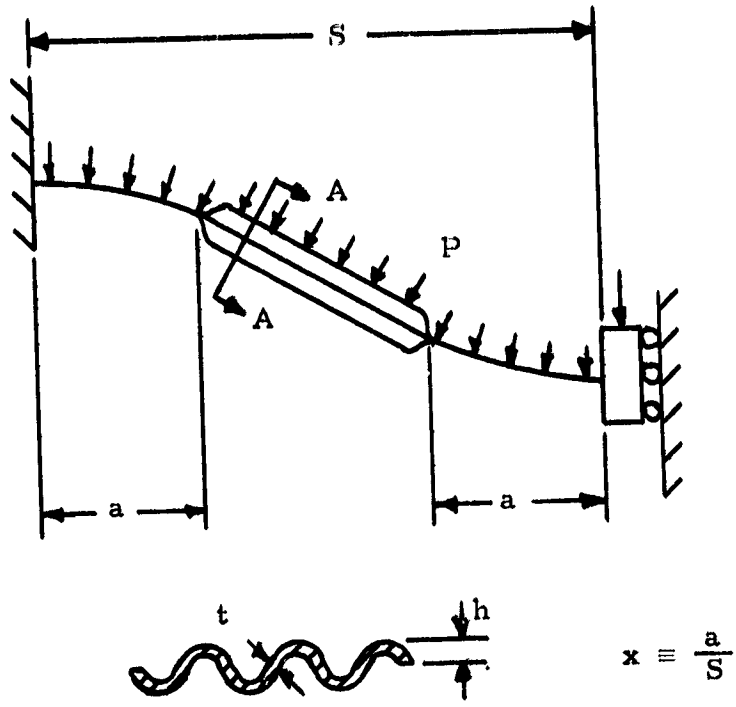

Figure 9. Schematic Diagram of the Straight Beam Model for The Orthotropic Plates.

which again is of the form of the flat plate relation, Equation (10), with a correction term. For the typically large values of n of interest for this configuration, Equation (13) reduces to,

$$\sigma_p \cong \frac{p\, s^2}{2\, t^2} \quad (3\, x - 2\, x^2) \tag{14}$$

Equations (7), (9), (12) and (14) were used to predict the performance shown in Figures 10 and 11. The number of convolutions assumed for these solutions was 30. Since there is no experience in stacking this shape, this number is open for argument. However, the minimum number used for the solutions of the previous shapes was 30 and this number represents the maximum number that can be fitted in with a plate thickness of 20 mils (5.08×10^{-4} m). It is probably a reasonable maximum, even at the lower plate thicknesses, due to the fact that stiffening rings would amost certainly need to be provided with this shape.

Comparing the stresses of Figure 10 with the corresponding flat plate solutions of Figure 5 and 6, it can be seen that the radial corrugations indeed improve performance in this respect. For example, a 50 percent reduction in stress results for the 0.25 inch (.0064 m) span with a plate thickness of 10 mils (2.54×10^{-4} m). For a 0.5 inch (.0127 m) span, the reduction is even more pronounced, almost an order of magnitude. However, the reduction in stress is achieved only at the expense of a considerably increased spring rate as may be seen from a comparison of Figures 7 and 11. The net result is that, based on the nominal characteristics of Figures 10 and 11, there is a small useable range of plate thickness for each span. This is approximately 2 mils wide for the 0.25 inch (.0064 m) span and 5 mils wide for the 0.5 inch (.0127 m) span. Above this range, the spring rate is above the 800 lbs/in (1.4×10^5 newtons/m) limit of Table II; below it, the stresses exceed the 150,000 psi (1.35×10^9 newtons/m^2) limit.

Although the nominal stresses are indeed lower than those for both the nested ripple and flat disk plates of Figure 5 in this thickness range, the design is still felt to be extremely marginal. In no case does the predicted stress level fall below approximately 80,000 psi (0.72×10^9 newtons/m^2). Local stress concentrations near edge fixtures and at the transition points between the radial corrugations and the unstiffened edge region could easily raise the stress beyond the 150,000 psi (1.35×10^9 newtons/m^2) limit.

Finally, the reduced circumferential stiffness of the plates due to the corrugations will require stiffening rings to achieve the desired degree of linearity just to resist diametral growth under pressure. Although this is a common requirement for most of the

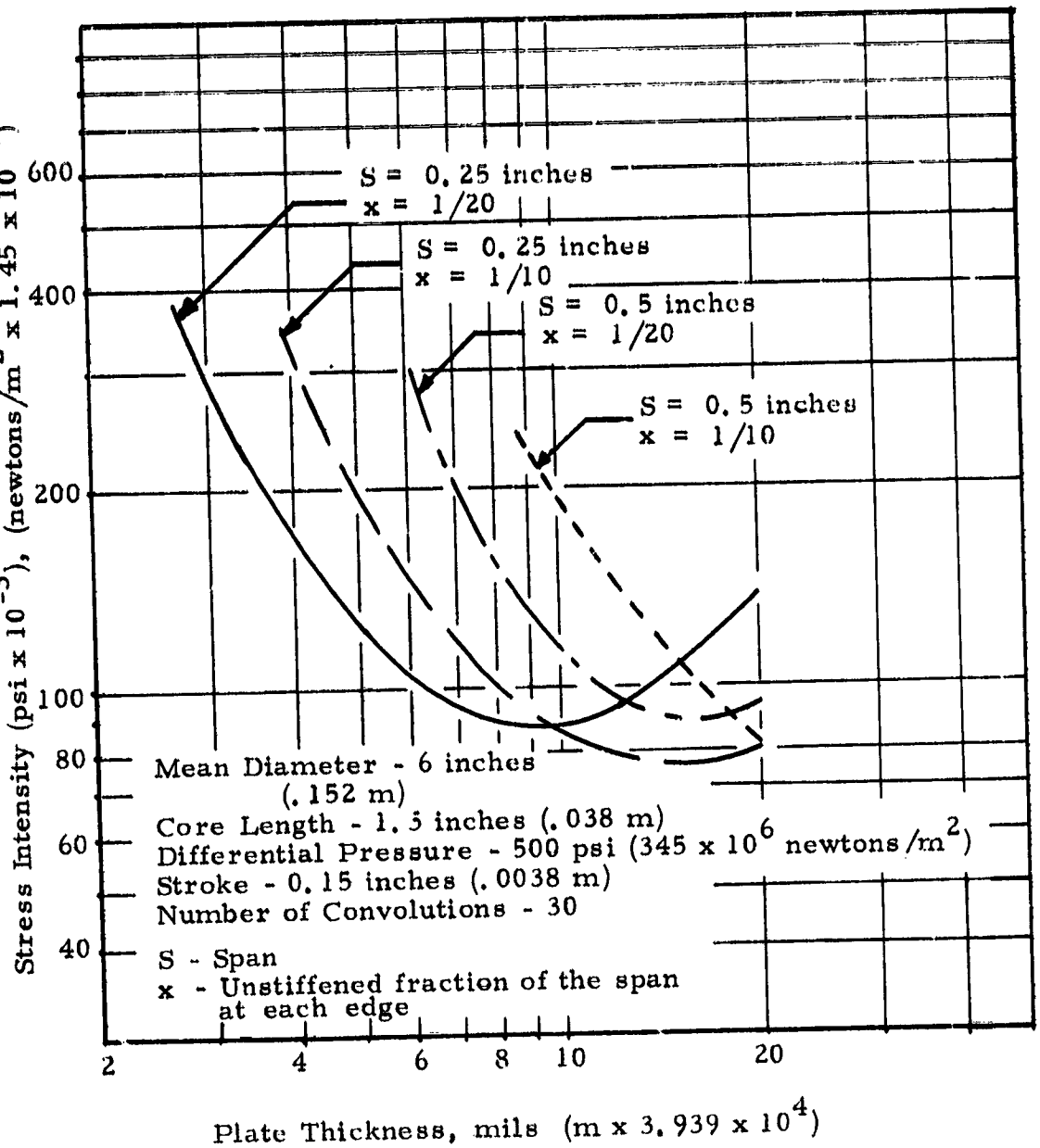

Figure 10. Combined Stress for Orthotropic Plate Bellows (Radial Corrugations) Due to Pressure and Axial Deflection.

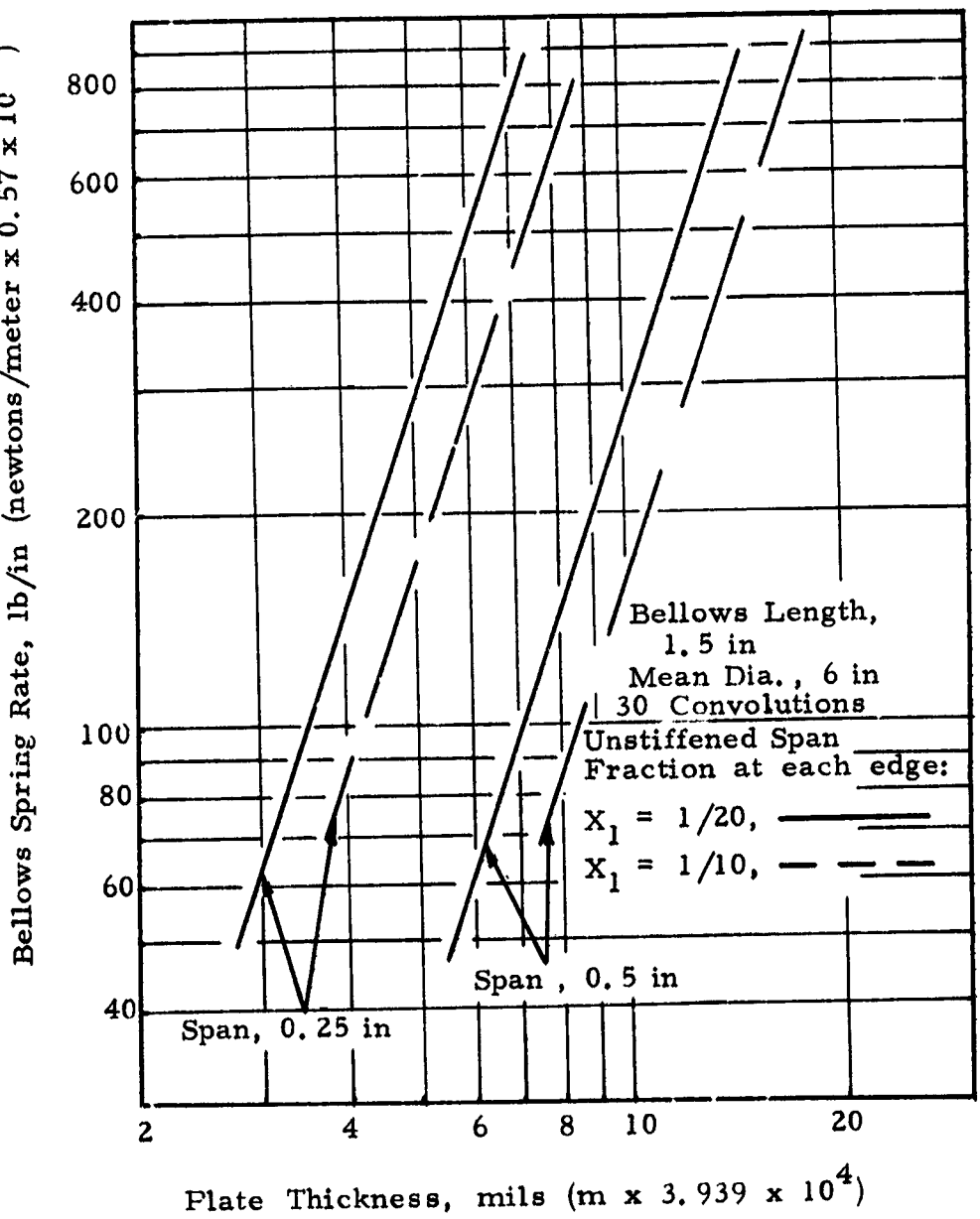

Figure 11. Bellows Spring Rate vs. Plate Thickness for Orthotropic Plate Bellows (Radial Corrugations)

shapes considered, it becomes most critical from a fabrication point of view when a large number of convolutions are required as in this case.

Thus, the net effect of the orthotropic flat plate bellows is to provide a marginal design similar to that of the normally corrugated plate only with a smaller plate thickness. For this reason, it was not carried further for evaluation in the nonlinear range.

Full Toroidal Plates

The use of toroidal convolutions is well-known for high pressure-carrying capability. The welded version would consist of two opposed semi-toriods, welded together at one edge and connected to adjacent convolutions at the other edge by stiff spacer rings.

Solutions for the behavior of toroidal convolutions are given in the literature. (3, 5). The schematic diagram of Figure 12 shows the major variables of importance.

The following formulae may be used to compute the deflection and stresses under both precompression and pressure loading in a manner entirely parallel to that discussed in the preceding sections for flat disks and orthotropic plates. The formulae are limited to regions where the following inequalites are satisfied among the bellows dimensional parameters (5).

$$\frac{S}{t} > 40 \tag{15}$$

$$\frac{S^2}{2\,t\,\bar{R}} > 1 \tag{16}$$

In this region, the spring rate per unit circumference is given by (6),

$$K = \frac{Et^2}{10.88\ R\ S\ \sqrt{1 - \nu^2}} \tag{17}$$

The maximum bending stress due to a force per unit circumference, F, is,

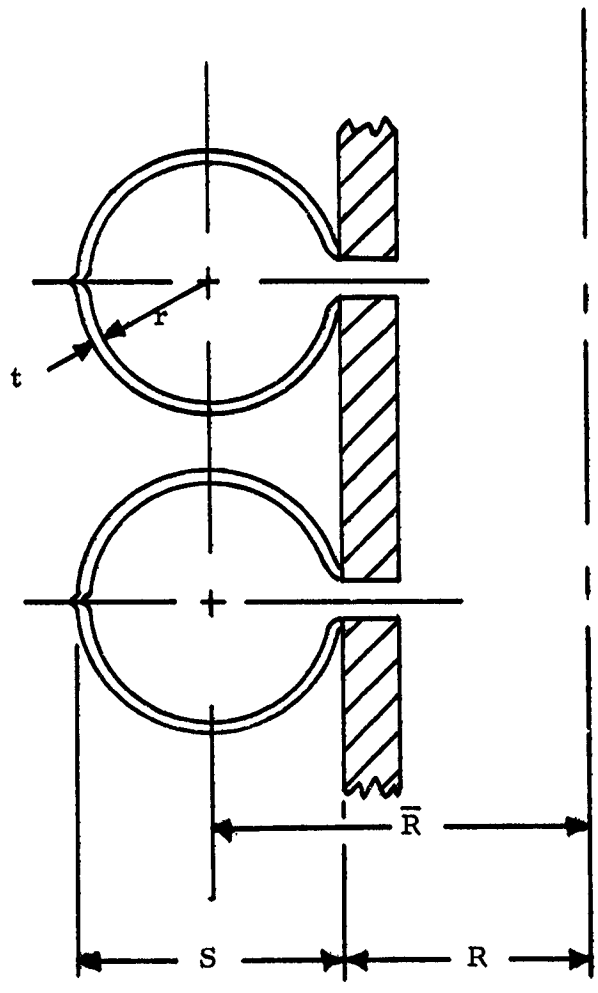

Figure 12. Schematic Diagram of the Full Opposed Toroidal Bellows.

$$\sigma_f = \frac{2.99\ F}{t\ \sqrt[6]{1 - \nu^2}} \sqrt[3]{\frac{\bar{R}\ S}{2\ t^2}} \tag{18}$$

The maximum stress due to pressure loading, P, becomes,

$$\sigma_p = \frac{P\ S}{4t}\left(1 + \frac{\bar{R}}{R}\right) \cong \frac{p\ S}{2t} \tag{19}$$

The latter stress is a membrane stress and the approximate result applies within 5 percent in the size to span region of interest in this study.

Although stability and buckling of bellows elements is always a consideration in bellows design, it is of special concern for toroidal elements which often require only relatively small plate thicknesses for pressure resistance. When externally loaded, these elements could undergo large deformations due to buckling. Since the present application has as a goal the capability of pressure loading in both direction, buckling limits were studied to determine whether they impose practical design criteria.

No previous analysis was found for the local buckling of a toroidal convolution. However, it is obvious that circumferential effects and complex curvature will make the toroid more stable than its corresponding straight tube. Available solutions for a straight tube with external pressure can be used to set an upper limit on the required plate thickness, t, as follows (3).

$$\left(\frac{t}{r}\right)^3 > \frac{4p}{E} \tag{20}$$

Substituting the design pressure loading, p, of 500 psi (3.445×10^6 newtons/m^2) and the Young's Modulus, E, of 30×10^6 psi (2.07×10^{11} newtons/m^2) into this relation gives,

$$\frac{t}{r} > 0.04 \tag{21}$$

A more conservative mode of collapse is the local buckling of the crest of the toroid. Using, as a conservative approximation, the buckling of a 90° straight arch, a lower limit for the required plate thickness (3),

$$\left(\frac{t}{r}\right)^3 > \frac{2p}{E} \cong 0.02 \tag{22}$$

for the above numerical values. Thus, the range for realistic buckling limits lies between the values of Equations (21) and (22). Above this range, the toroid is almost certainly stable and below, it is likely to be unstable.

The relationships of Equations (17) through (19) were used to predict the combined stresses for toroidal bellows having spans of 0.25 inches (.0064 m) and 0.50 inches (.0127 m) in Figures 13 and 14, respectively. The stability limits discussed above are also indicated on the graphs. The spring rates for these bellows are shown in Figure 15.

It can be seen from Figures 13 and 14 that the combined stresses for both spans are within the Yield Stress for the material (150,000 psi or 1.35×10^4 newtons/m^2) in the thickness range between 3 and 10 mils (7.62×10^{-5} m and 2.54×10^{-4} m). The stresses are most favorable for the 0.25 inch (.0064 m) span where more convolutions can be accommodated within the core length and the pressure stresses are smallest. This span, of course, also provides less restrictive stability limits. Figure 6 shows that virtually all combinations of span and number of convolutions give a spring rate within the design goals in the plate thickness range of interest.

The location of the peak combined stress is also of interest for the toroid. The stress due to pressure loading is nearly constant throughout the toroid. The bending stress due to axial loading is maximum at an angle of approximately 45° along the toroid from its mid span. Thus, the maximum combined stress does not occur at the edges of the span where stress concentrations due to the weld joints may be expected.

Modification of the toroidal plates to add radial ribs similar to those studied for the orthotropic flat plates was investigated. The purpose of this modification in the toroidal plates was the mitigation of shape changes which tend to bring about nonlinearity under axial deflection, and, as such, will be discussed in a subsequent section treating nonlinear considerations. It should be mentioned here, however, that in the orthotropic toroidal bellows, the nonuniform stresses caused by axial deflection of the bellows are expected to be relieved in addition to the provision of greater linearity.

In summary, the full opposed toroid appeared to offer basic performance which was within the desired design goals. From a practical design point of view, fewer convolutions were required and did not appear to present outstanding fabrication difficulties. Although stiffening rings would be required to achieve the desired degree of linearity, their number and cost is minimized due to the small number of convolutions. Thus, it was recommended that this configuration be further evaluated as one of the most promising for this application.

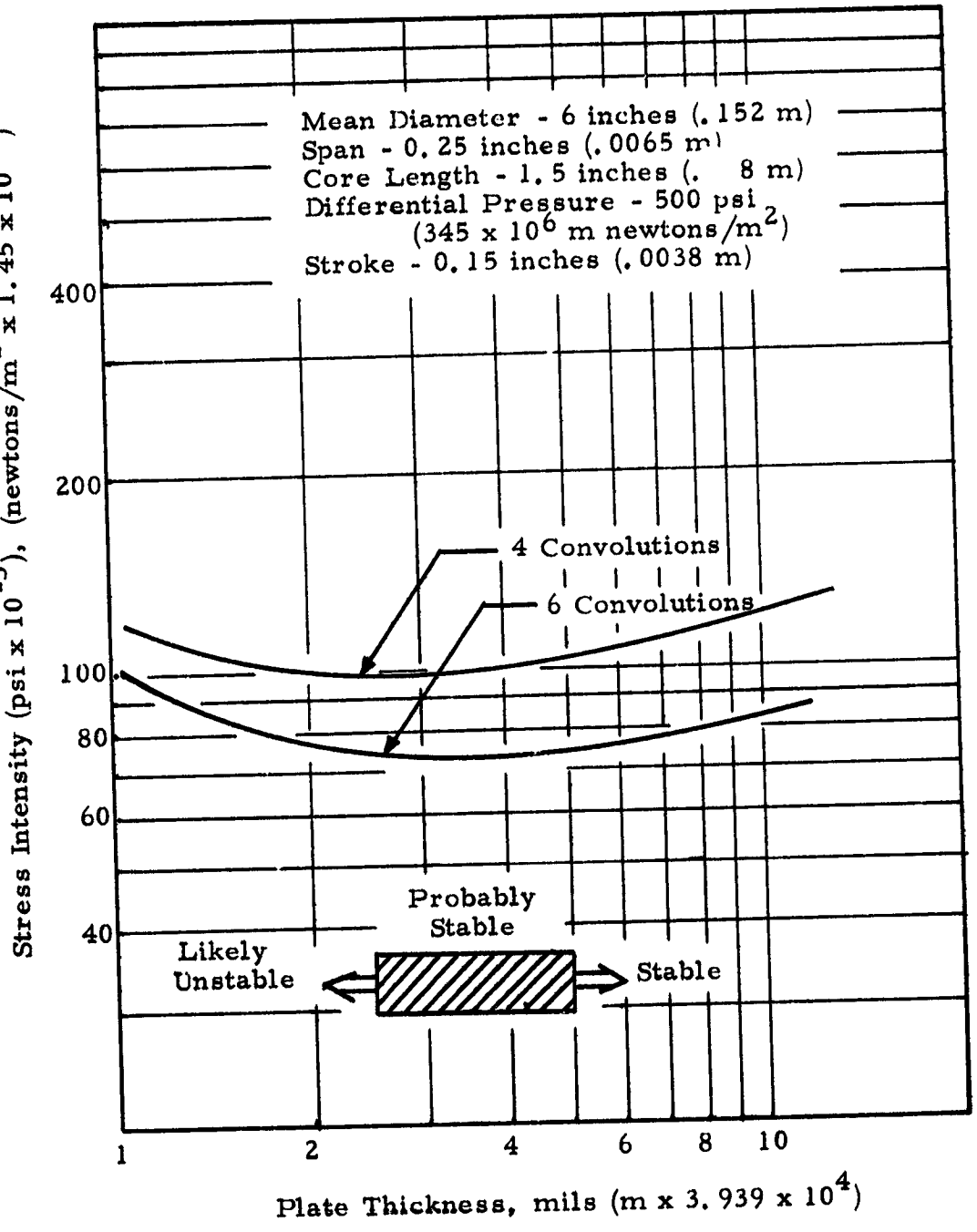

Figure 13. Combined Maximum Stresses for Toroidal Bellows with 0.25 Inch Span.

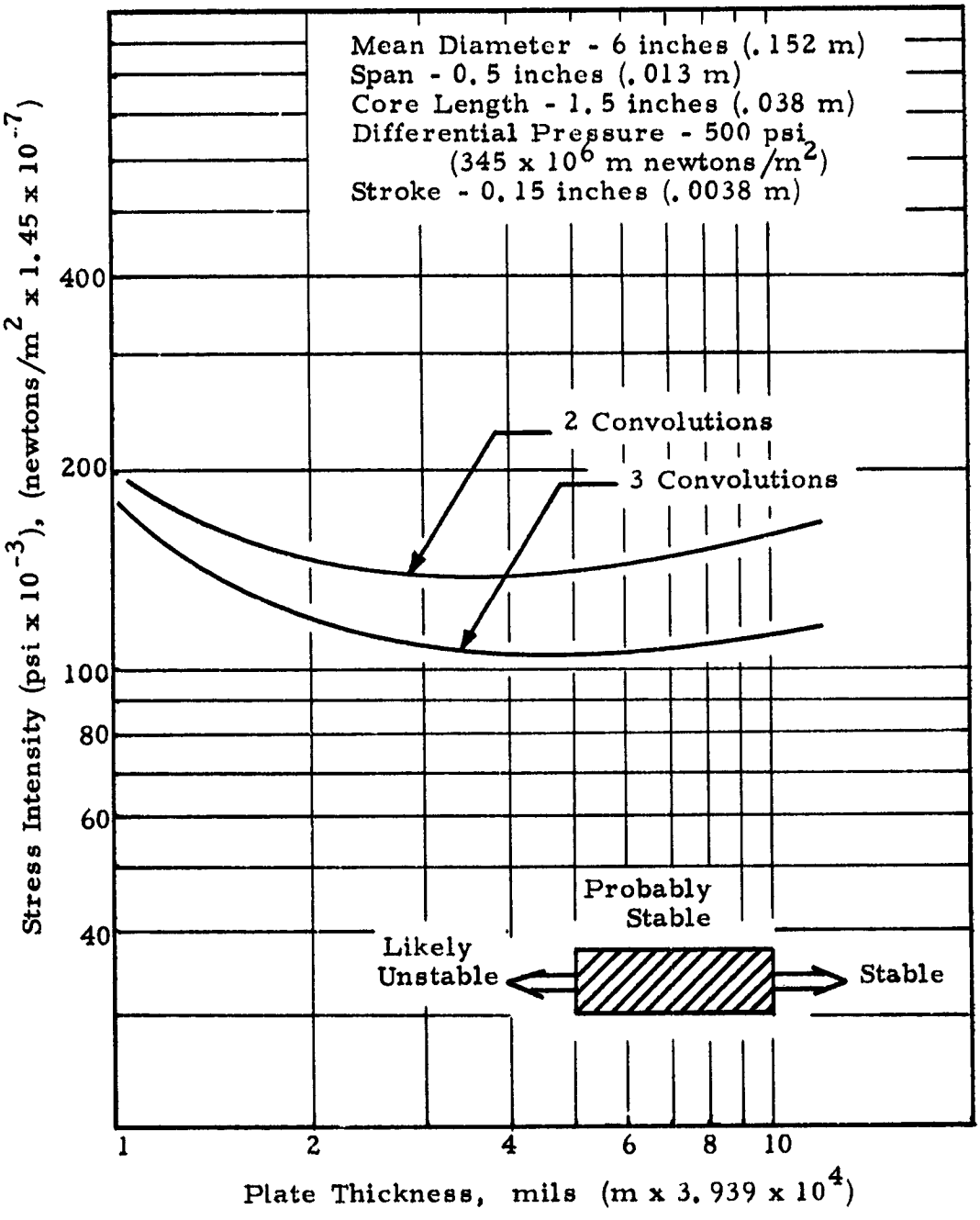

Figure 14. Combined Maximum Stresses for Toroidal Bellows with 0.5 Inch Span.

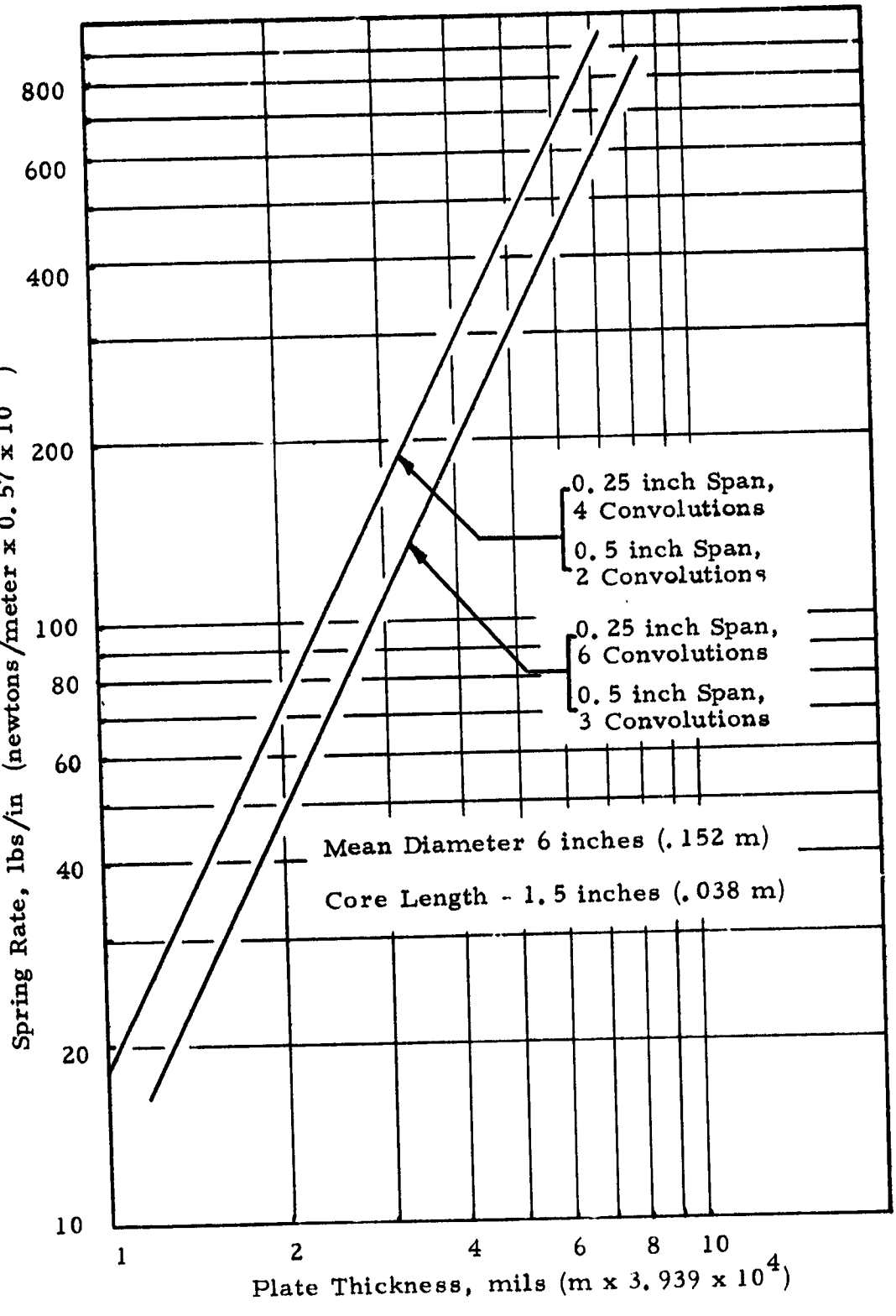

Figure 15. Spring Rates for Toroidal Bellows.

Partial Toroids

The advantages of the toroidal shell for pressure-carrying capability are apparent from the results of the previous section. These advantages are due to the membrane action which only depends upon the fact that the radius of curvature of the shell is constant across the span. Except for boundary effects near the points of attachment similar advantages would be expected for partial toroids where each plate consists of a section including less than 180°. These have the advantage that more convolutions could be fitted into a given core length if the plates were nested rather than stacked symmetrically. Thus, the basic performance of the partial toroid was investigated as described in this section.

Partial toroids can be assembled in various configurations, both with and without stiffening spacer rings as shown in Figure 16. The angular stiffness of the spacer rings is extremely important, especially for the nested configurations.

Qualitatively, the performance of the partial toroids can be understood by considering the normal toroidal membrane action coupled with the resultant reaction forces produced at the boundaries or edges of the span. The membrane stresses due to pressure loading act along a direction tangent to the plate. Thus, in Figure 16(a), the reaction forces, F_A and F_B, are almost equal in magnitude but have a small resultant force, F_R, due to their difference in direction. This reaction force tends to tilt the convolution and expand it radially away from the centerline. The effects of the reaction force which is always present for the configuration where the plates are joined directly to each other can be reduced by providing a stiff spacer ring to resist the deformation as in Figures 16(b) and (c). This will, of course, produce local bending stresses near the stiffening rings. In Figure 16(d), the convolution is oriented so that the tilting moments due to the reaction force at each end cancel each other. The convolution, however, would still tend to deflect radially outward.

By attaching the plates to either side of the stiffening ring as in Figure 16(e), the plate tangents, and thus the direction of the resultant forces can be made parallel. In this way the reaction loading on the stiffener can be reduced to a moment or couple which would have to be resisted by the stiffener if tilting is to be avoided.

If the plates are stacked in a symmetrically opposed configuration as shown in Figures 16(g) and (h), there can be no section tilting but the resultant force, F_R, tending to deflect the convolution radially is much larger. This can be resisted, of course, if sufficient radial stiffness is provided by stiffening rings as in Figure 16(h).

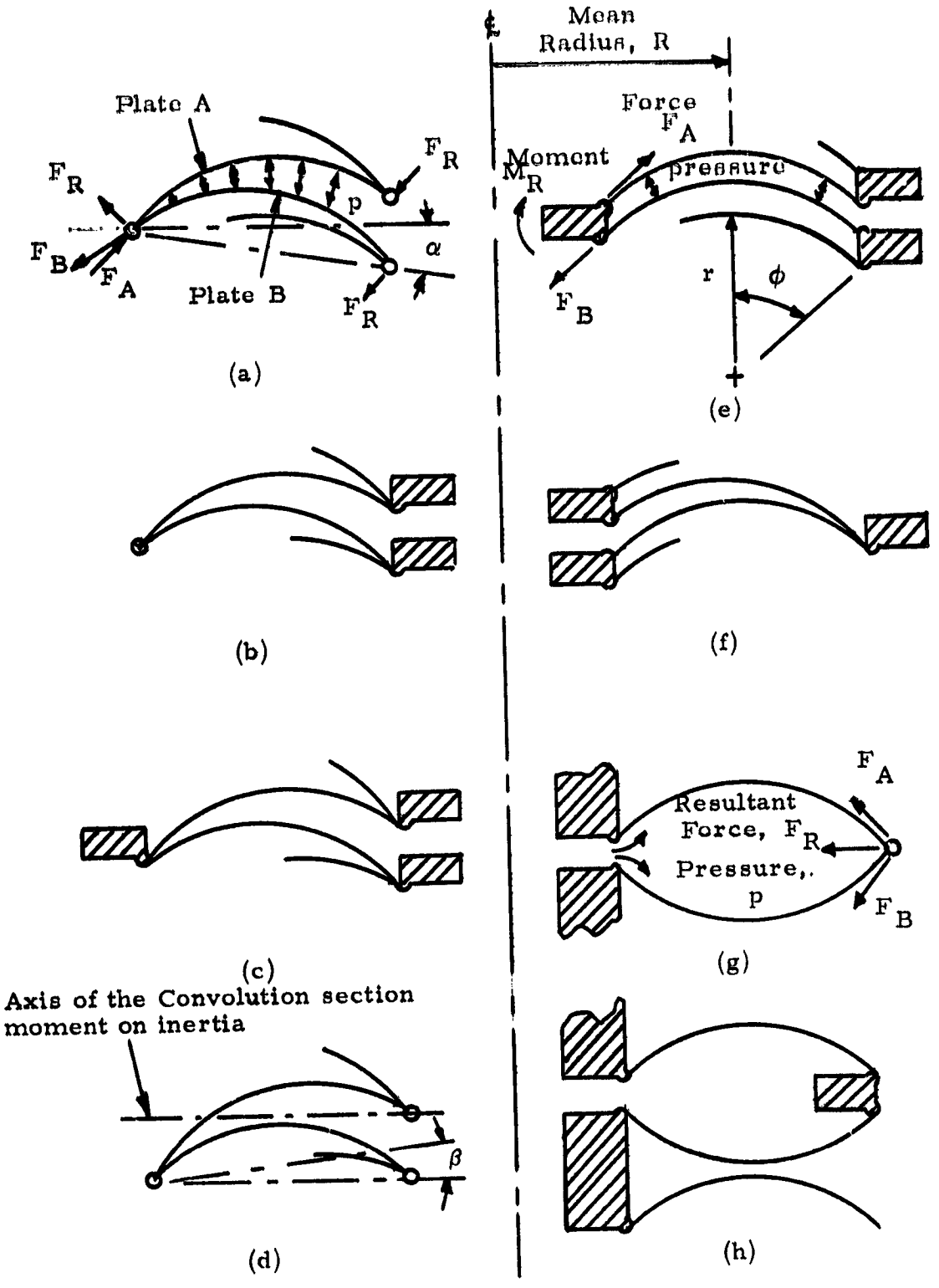

Figure 16. Partial Toroid Convolutions Having Various Configurations and Methods of Assembly.

The partial toroids were analyzed in detail, using the linear computer solution described in Appendix A, for two limiting configurations:

(a) The case where the plates are attached together by means of sufficiently stiff spacer plates so that the span edges can be considered angularly and radially fixed.

(b) The simple nested configuration of Figure 16(a) with no auxiliary stiffening.

The variation of the total combined stress and spring rate for six convolutions as a function of the arc semi-angle, ϕ , are plotted in Figure 17 for the fixed edge conditions with a plate thickness of 5 mils (1.27×10^{-4} m). The results show that the combined stresses are acceptable for this whole range of angle, ϕ , with a minimum in the range of 70°.

The variation of performance with plate thickness for a given arc segment ($\phi = 60°$) is shown in Figure 18. Here it can be seen that the stresses are at a minimum in the range of 3 to 4 mils (7.62 to 10.16×10^{-5} m) plate thickness.

Both Figures 17 and 18 show that the maximum stress intensity and the spring rate for six convolutions are acceptable within the design goals for this program provided stiffening rings are used so that the edge condition for the bellows plates approach the angularly and radially fixed case. The plates could be stacked symmetrically opposed as shown in Figure 16(h) or nested as shown in Figures 16(c), (e) or (f). In the latter case, many more than 6 convolutions could be used, further reducing the spring rate and the stress due to axial stroke.

Nested partial toroids without stiffening rings as shown in Figures 16(a) and (d) were also analyzed. The results showed that severe shape distortions occur under pressure loading and the combined stresses are intolerable.

Referring to Figures 16(a) and (d) for the definition of variables, cases were run with:

$$\phi = 60°$$

$$\alpha = 0.1 \text{ radians}$$

$$0 < \beta < 0.1 \text{ radians}$$

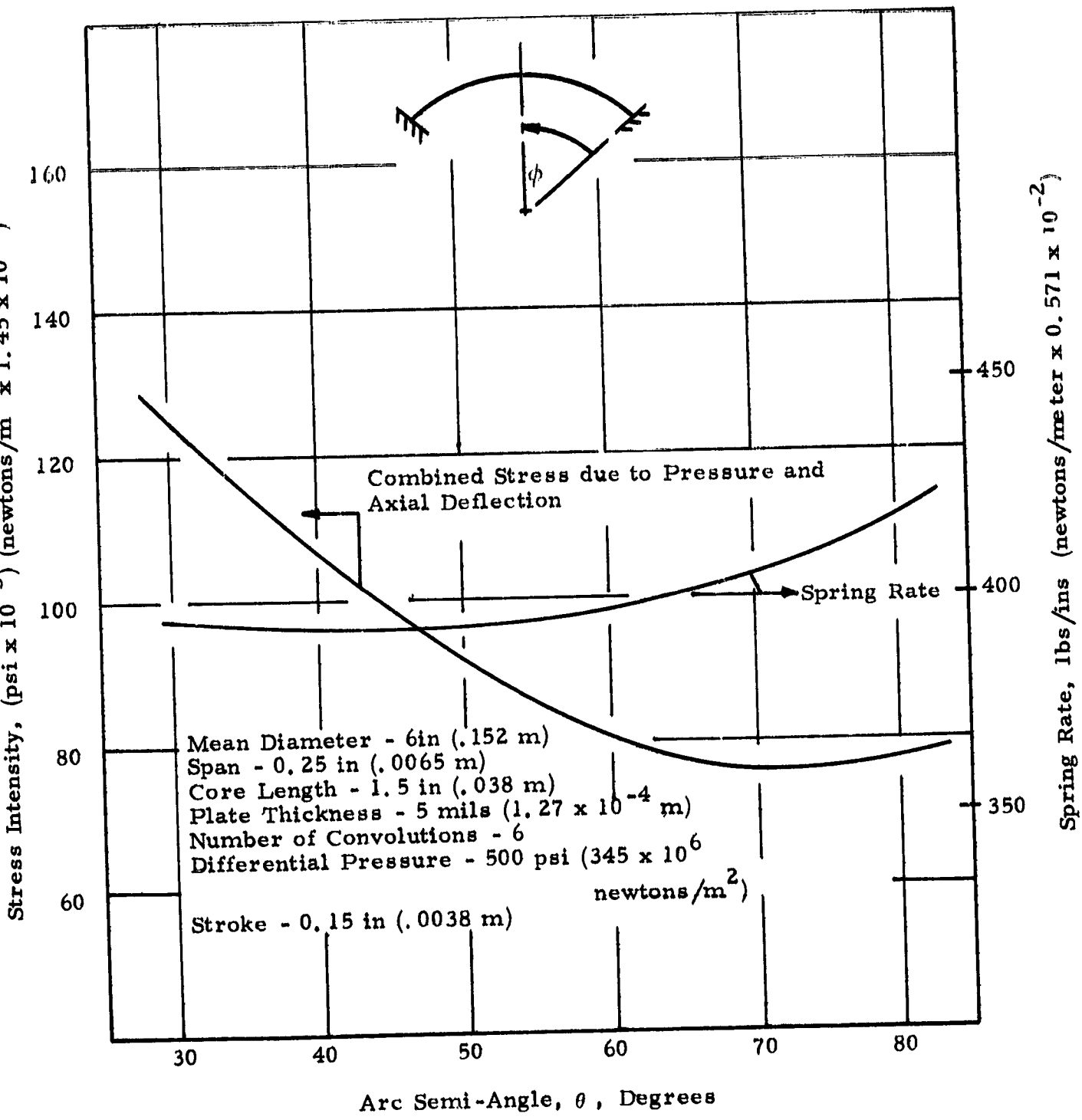

Figure 17. Variation in the Performance of Partial Toroids with Arc Length For Fixed Edge Conditions

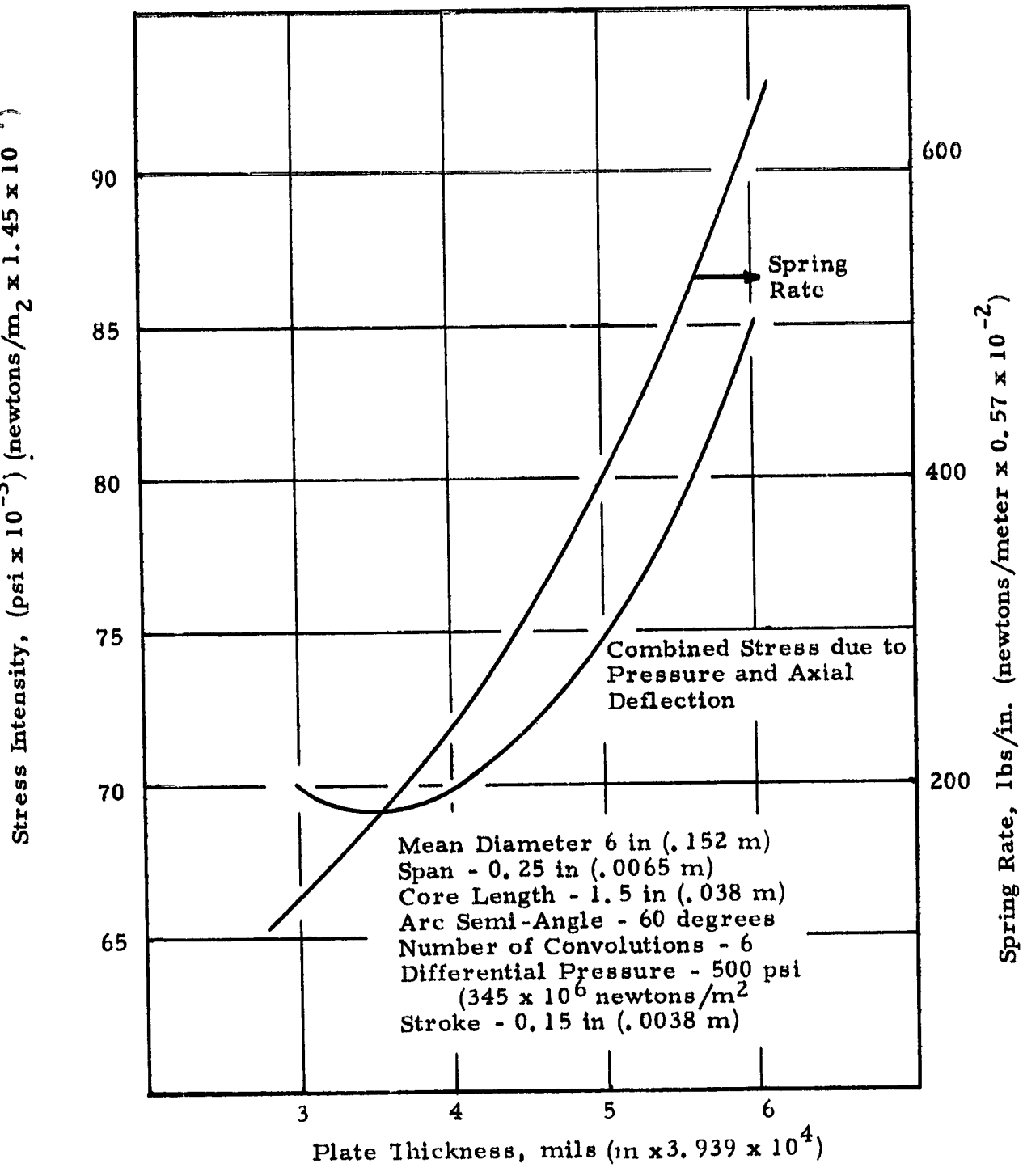

Figure 18. Variation in the Performance of Partial Toroids with Plate Thickness for Fixed Edge Conditions.

A typical convolution distortion is shown in Figure 19. Variation of the mean cone angle, β , was found to have little effect on the stresses. The major stresses, on the other hand, are approximately in direct proportion to the pitch angle.

For a span of 0.25 inch (.0064 m) and a pitch angle, , of 9.1 degrees (pitch -50 mils (1.27×10^{-3} m)), the combined stress intensity predicted is 400,000 psi, (2.76×10^{9} newtons/m^2) with a pressure differential of 500 psi (3.445×10^{6} newtons/m^2). This assumes 10 convolutions and a stroke of 0.15 inches (3.81×10^{-3} m).

In order to reduce the stresses to the level of those for the stiffened ring as shown in Figure 18, the pitch would have to be reduced by a factor of about 5. That is, approximately 50 convolutions would be required. For this case, plate clearance would be a problem and fabrication would be costly. Although span and thickness could be increased to reduce the stress or allow fewer convolutions, indications are that the basic performance would not be significantly better than the corrugated or flat plate shapes.

In summary, the partial toroid plate shape are attractive if stiffener rings are used to provide angular and radial fixity at the edges. This configuration is recommended as the most promising nested design. Without the stiffener rings, the partial toroid does not appear attractive for this application.

S-Shaped Plates

The final family of plate shapes shown in Table III to be analyzed for basic performance was the S-Shaped family. Preliminary consideration indicated the possibility that, in the nested configuration, the reaction moments of successive plates would tend to cancel due to the difference between the sign of the curvature for the two plates with respect to the pressure load. This would provide a convolution resistant to the large convolution deformation of the type shown in Figure 19. When stacked symmetrically opposed, it was not expected to offer any advantages over the previous configurations analyzed.

The dimensional parameters used to define the S-Shaped plates are defined in Figure 20. The range of these parameters considered were as follows:

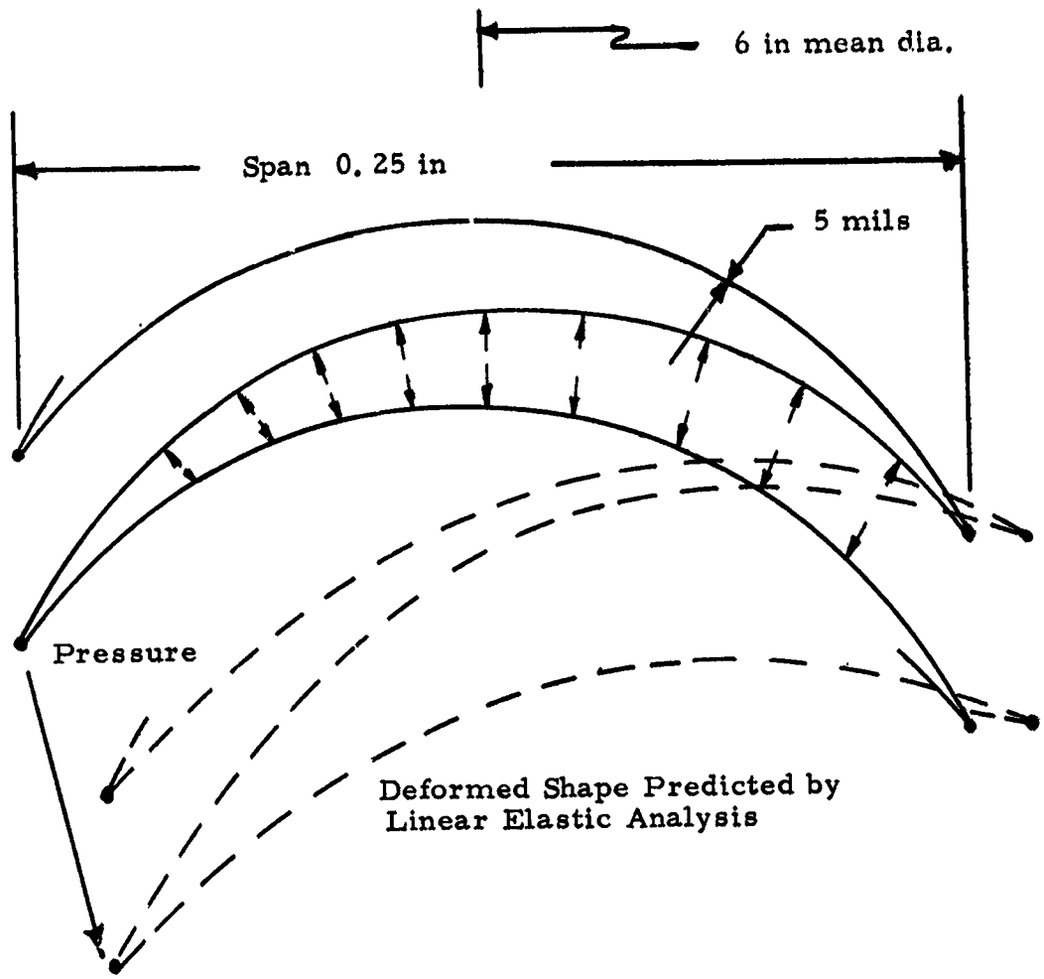

Figure 19. Distortion of a Nested Partial Toroid Convolution Under 500 psi Pressure Loading At a Fixed Axial Length.

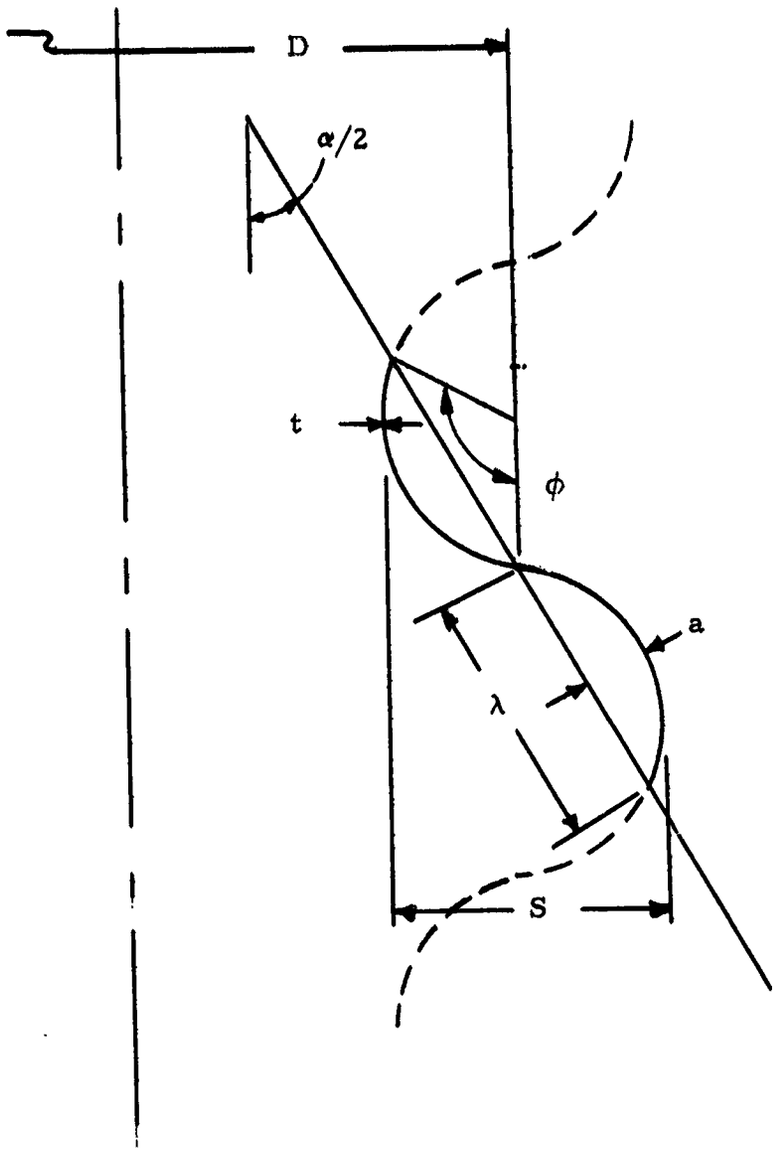

Figure 20. Definition of Dimensional Parameters for the S-Shaped Plates.

Plate Thickness, t: 5 mils and 7 mils (1.27×10^{-4} m and 1.778×10^{-4} m)

Cone Angle, α: 90°, 120°, 180°

Wave Length, λ : $\frac{S}{2}$ to $\frac{S}{2}\sqrt{2}$

Arc Angle, ϕ : 90°, 120°, 180°

Span, S: 0.25 inches (.0064 m)

Mean Diameter, D: 6 inches (.152 m)

The various shape classes formed by varying these parameters are shown schematically in Figure 21.

These shapes were analyzed for stress and deflection under both a 500 psi (3.445×10^6 newtons/m^2) pressure loading and an axial stroke of 5 mils (1.27×10^{-4} m) per convolution. This stroke is consistent with achieving the specified bellows stroke of 0.15 inches (3.81×10^{-3} m) if 30 convolutions are used. This, of course would not be possible unless the plates were nested but represents the most optimistic assumption.

The stresses and spring rates were computed with computer program, NONLIN, developed by Battelle Memorial Institute (6). This computer program which is described in Appendix B is capable of predicting the nonlinear behavior of a bellows and was also used in this study for that purpose as discussed in a later section. It is also capable of predicting the linear performance, however, and is conveniently designed for ease in treating various plate shape inputs. Thus, it was used to investigate the basic performance of the S-shaped plates.

The plates were assumed to be angularly fixed at the edges. This is again an optimistic assumption. It represents closely the case where the plates are stacked symmetrically opposed but would require stiffening rings for a nested configuration. However, it will be seen that, even under the optimistic assumptions, the pressure stresses for these plates are too high. Thus, their analysis was not carried further under more realistic assumptions.

The results of the computer analysis are plotted in Figures 22 and 23 where the results for the nested ripple and the flat disk shapes are also given for comparison. Figure 22 shows the predominant stresses as a function of plate thickness for each of the plate shapes treated under two separate loadings:

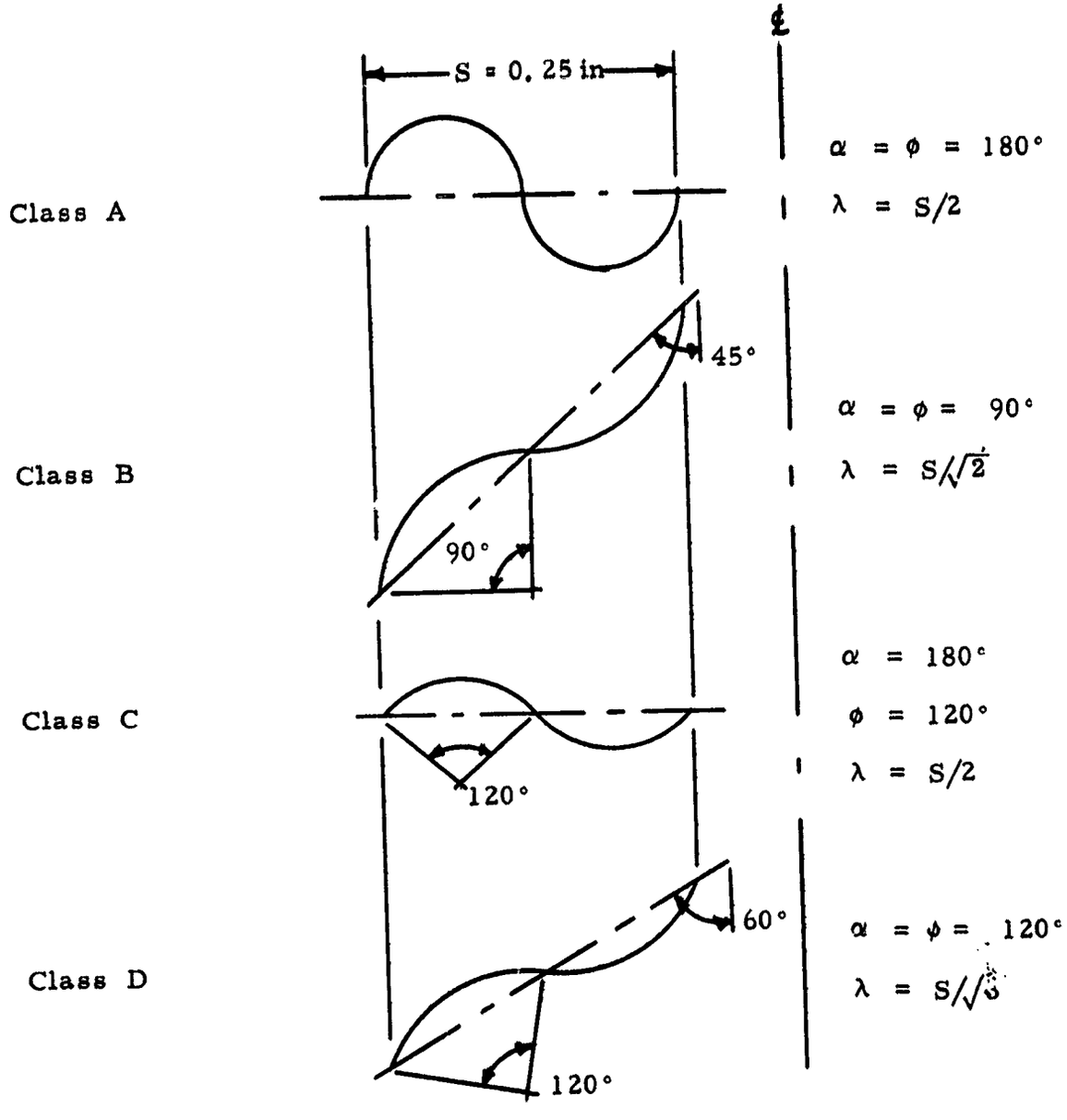

Figure 21 Classes of S-Shaped Plates Analyzed.

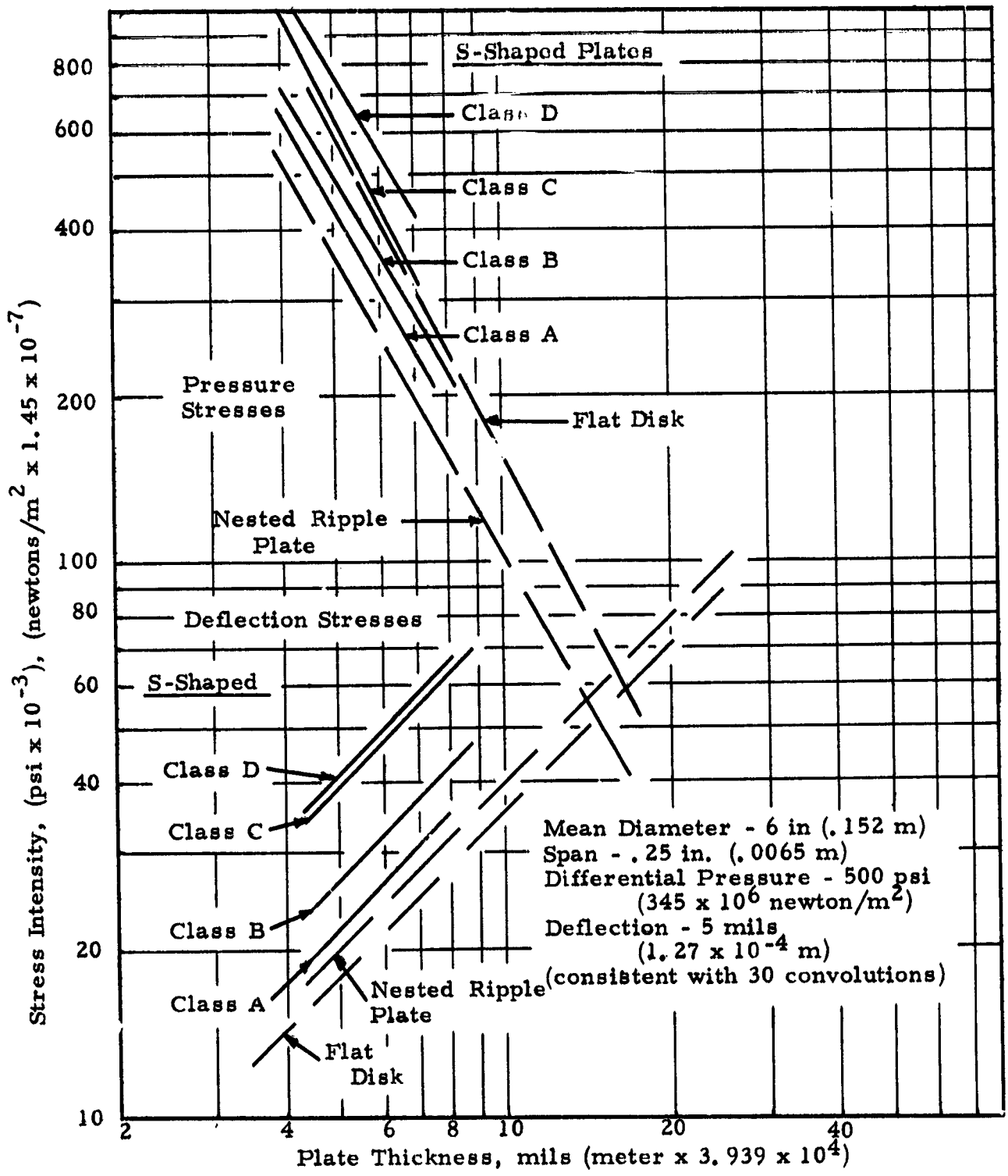

Figure 22. Stresses in S-Shaped Plates Compared with Corrugated and Flat Plate Shapes.

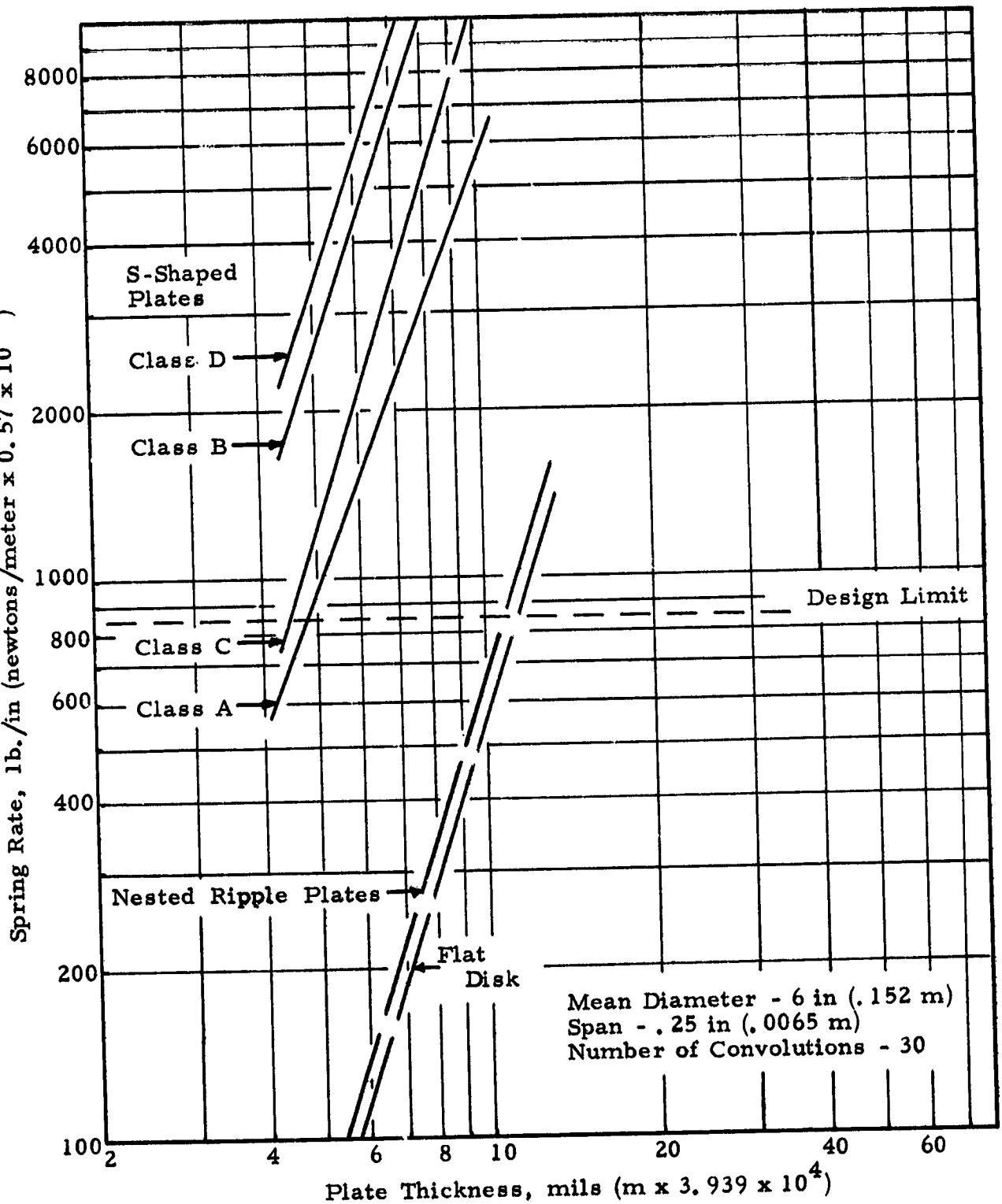

Figure 23. Spring Rates for S-Shaped Plates. Compared with Corrugated and Flat Plate Shapes.

(a) 500 psi (3.445×10^6 newtons/m^2) pressure loading with zero deflection.

(b) 5 mil (1.27×10^{-4} m) per convolution deflection with zero pressure load.

It can be seen that the general behavior is similar to the nested ripple and flat disk bellows. The stresses for the S-shaped plates under pressure are higher than those of the nested ripple plates and fall on either side of the flat disk shape depending upon detailed configuration. The stresses due to deflection are all greater than those of the nested ripple plates and flat disks.

The spring rates, given in Figure 23, also have a similar variation with thicknesses to the nested ripple plates and flat disks, but are much higher, even assuming the optimistic 30 convolutions.

It can easily be seen that, for plate thicknesses where the spring rate approaches the acceptable 800 lb/in (1.4×10^5 newtons/m) range, the stresses in the S-shaped plates are far above the design stress limit of 150,000 psi (1.35×10^9 newtons/m^2). Thus, the basic performance of the S-shaped plate does not warrant its further consideration for this application.

It might be noted parenthetically that Figures 22 and 23 provide a convenient reference, summarizing and comparing the basic linear performance of bellows plate shapes where bending stresses predominate over membrane stresses in the large size to span range. Although these families of plate shapes are not promising for the present high pressure application, they are generally useful as bellows seal elements in less demanding situations.

Summary of Basic Performance

The basic performance of bellows plates includes their pressure carrying capability and force-deflection characteristics. The analysis performed in this study shows that there are basically two categories of such performance characteristics:

(a) Bending Plates - where the plates are relatively flat across the span including multiple waves about the chord line.

(b) Membrane Plates - where the plates form a significant part of a semi-toroid.

The predominant stress in the bending plates under pressure is the radial bending stress. For a given span, this stress is relatively large and the plates must be thick to withstand it. This, in turn, leads to large spring rate and deflection stresses or, conversely, a large number of convolutions.

In the diameter to span range of interest, diameter was not found to have a strong effect on performance.

Both categories were found to be susceptible to large angular deformation or coning of the convolution section under pressure loading when the plates are nested rather than being stacked symmetrically opposed. This is most serious for the thinner membrane plates and for cases where the pitch is large and requires, in general, the use of stiff spacer rings to withstand the load.

The major conclusion drawn on the basis of the analysis of basic performance is that the membrane category offers the best combined ability to meet the pressure and spring rate requirements of Table II within the specified dimensional constraints. These can either be symmetrically opposed full toroidal plates or nested partial toroids with stiffening rings.

The corrugated plate bellows was the best of the bending plate category. It appears capable of providing marginally acceptable performance with a relatively large plate thickness and a large number of convolutions. However, its performance is inferior to both of the promising toroidal configurations and, thus, it was not evaluated further for this application.

NONLINEAR CONSIDERATIONS

The most promising bellows plate configurations for meeting the pressure and spring rate requirements of Table II within the specified dimensional constraints were found to be symmetrically opposed toroidal plates and nested toroidal plates, each with stiffening rings. In the following sections, their linearity or stability of effective diameter is studied analytically in order to select the most promising test configurations.

The design goal for the bellows is that it will maintain its effective diameter constant within 0.1 percent at a given axial compression or stroke over the entire pressure range, 0 to 500 psi (3.445×10^6 newton/m^2).

The method of approach followed was to conduct parametric studies to predict the effects of the various design parameters for each shape on the change in effective diameter. The optimum combination of parameters was then selected for further consideration in fabrication and experimental studies.

Symmetrically Opposed Toroidal Plates

The basic element of the symmetrically opposed toroidal bellows is shown schematically in Figure 24 where the principal nomenclature for this study is defined. Because of the symmetry, the plate may be assumed to be angularly rigid or fixed at the edges as shown. Also, it was determined in the preliminary study that sufficiently rigid stiffener rings can be provided so that the edges may also be considered to be radially fixed. Thus, the model used for parametric analysis as illustrated in Figure 24 is free to deflect axially under an applied loading but is fixed radially and angularly at the edges.

In addition to the parameters defined in Figure 24, the following variables will be used in the discussion.

(a) Effective Diameter

Defining an axial bellows force per unit circumference, N_p, by

$$N_p = \frac{F_b}{\pi D_s} \tag{23}$$

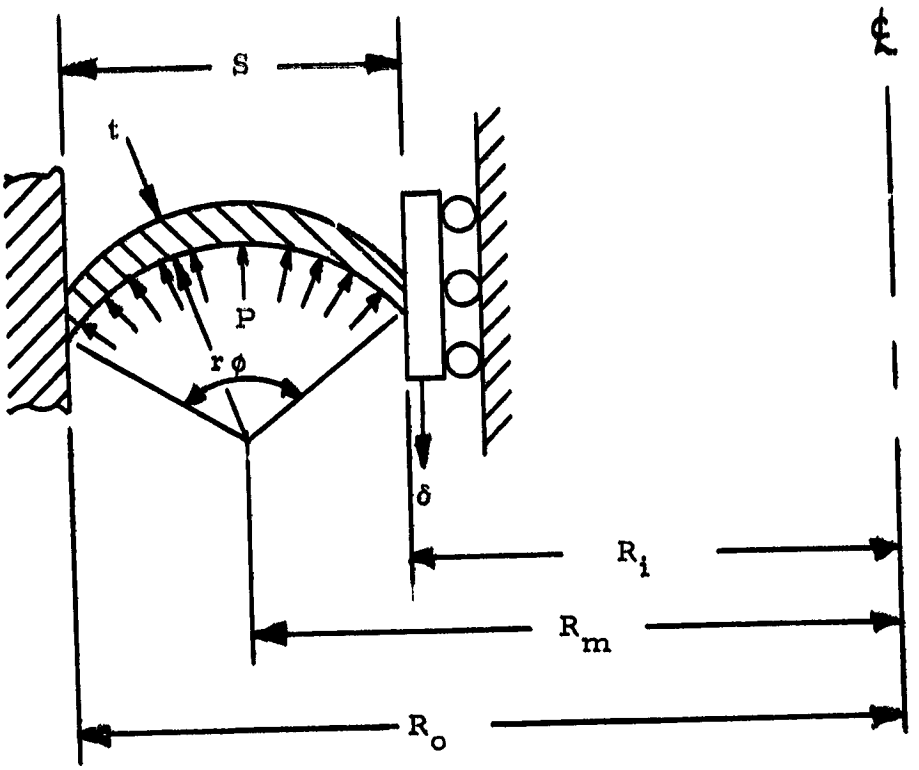

p	-	pressure
δ	-	axial deflection
S	-	span
t	-	plate thickness
r	-	radius of curvature
R_i	-	inner radius
R_m	-	mean radius
R_o	-	outer radius
ϕ	=	included angle of the toroidal segment

Figure 24. Schematic Diagram of the Symmetrically Opposed Toroidal Plate Element and the Definition of Principal Nomenclature.

where

F_b = reaction force between the bellows and the seal ring

D_s = effective sealing diameter of the face seal

and combining with Equation (4) allows the definition of an effective diameter as follows,

$$D_e^2 \equiv D_o^2 + \frac{4\ K\Delta\ell}{P} - \frac{4\ D_s N_p}{P} \tag{24}$$

where P is used to denote the differential pressure across the bellows.

(b) Nonlinearity of Effective Diameter

A small nonlinear perturbation, ΔD_e, of effective diameter about its nominal value, D_e, may be related to a perturbation in bellows force, ΔN_p, by differentiating Equation (24). Assuming that $K\Delta\ell$ and D_o are constant, this gives,

$$2\ D_e\ \Delta D_e = -\frac{4\ D_s}{P}\Delta N_p \tag{25}$$

which may be used to define a percentage change or nonlinearity in effective diameter. Defining the percentage change in effective diameter as,

$$\%\ \Delta D_e = \left|\frac{\Delta\ D_e}{D_e}\right| \times 100,$$

and combining with Equation (25) gives,

$$\%\ \Delta D_e = \frac{2\ D_s}{P\ D_e^2}\ \Delta N_p \times 100 \cong \frac{\Delta N_p}{15} \tag{26}$$

where

p = 500 psi (3.445×10^6 newtons/m^2)

$D_e \cong D_s$ = 6 inches (0.152 meter)

It should be noted that the above definition assumes that spring force, $K\Delta\ell$, is a constant under pressure load. In other words, any change that might occur in the spring load under pressure is lumped into ΔN_p and thus, by definition, into ΔD_e. This is in accordance with the convention discussed under "Description of the System." This convention is reasonable from a design point-of-view because any change in spring force with pressure appears as an effective nonlinearity between pressure force and pressure, or as a change in effective diameter. Moreover, there is no method for separating the various contributing effects to a nonlinearity detected in a solution for N_p at a given pressure level and initial deflection.

Thus, Equation (26) was used to interpret the nonlinear computer solutions in the following discussion.

The only parameter fixed for the parametric study of nonlinearity was the nominal or mean diameter, D_m, which was taken to be 6 inches (0.152 meters). The other parameters were varied in the ranges shown in Table IV.

A total of 50 computer runs using computer program NONLIN were made to study these parametric variations as well as the effects of the boundary stiffness and certain shape modifications. The detailed numerical results from these computer runs are tabulated in Appendix D. Typical stress distributions are also presented in Appendix D for plates having 60°, 120°, and 180° included angles. The effects of the variation of each of the major parameters on change in effective diameter over the desired pressure range are discussed in the following paragraphs.

Effect of Axial Deflection. - The percentage change produced in the effective diameter between small pressure loads and a pressure loading of 500 psi (3.445×10^6 newtons/m^2) as a function of the axial deflection of a single plate, δ, is shown in Figure 25 for various included angles. (Reference Run Nos. 1, 2, 3, 4, 15, 18, 19, 20, 21, 22 and 34 of Appendix D).

It can be seen that the percentage change in effective diameter is approximately linear with the axial deflection for a given included angle and that there is a marked change from a large included angle approaching a full semi-toroidal and a small toroidal section. For the large included angles, it can be seen that to achieve the desired goal of 0.1 percent or less change in effective diameter requires an axial deflection less than 5 mils per plate. Thus, for the total maximum axial compression of 0.15 inches (3.81×10^{-3} meters), at least 30 plates would be required. This is more than can be fitted into the core length available for the symmetrically opposed configuration, which is less than 1.5 inches. It appears, in fact, that only about 12 plates can be used. Thus, the $\% \Delta D_e$ can be no smaller than approximately 0.26.

TABLE IV

Range of Parameter Variation for the Nonlinear Behavior of the Symmetrically Opposed Toroidal Plates

Axial Deflection, δ	0 to 15 mils (0 to 3.81×10^{-4} m)
Thickness, t	3 to 7 mils (7.62×10^{-5} to 1.77×10^{-4} m)
Pressure, p	0 to 500 psi (0 to 3.445×10^{6} newton/m^2)
Included Angle, ϕ	60° to 180°
Span, S (Approximate)	1/8 to 1/4 inch (3.17×10^{-3} to 6.35×10^{-3} m)

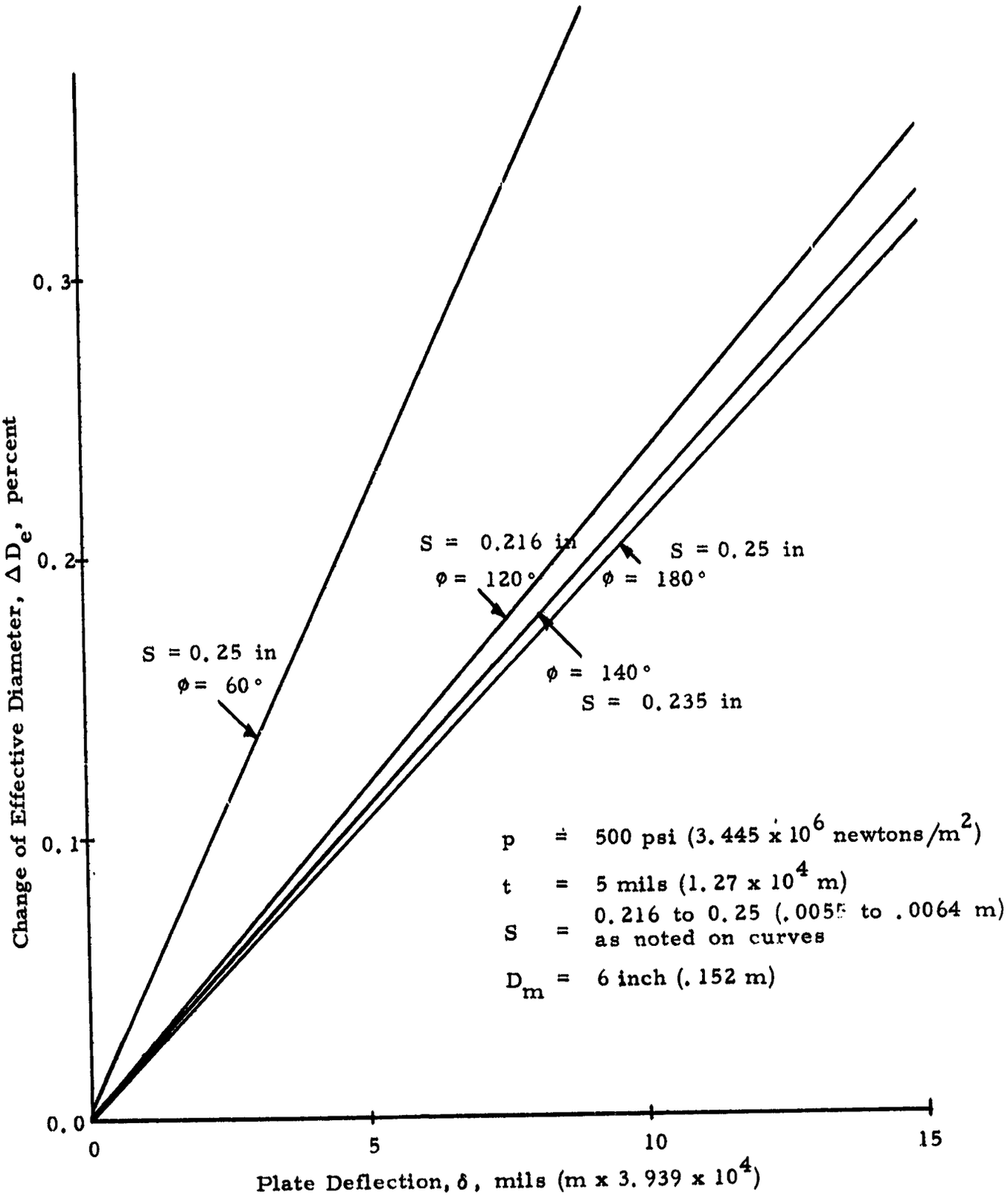

Figure 25. Effect of Deflection on Change in Effective Diameter.

Effect of Plate Thickness. - The effect of variation in plate thickness on effective diameter for various included angles is shown in Figure 26. (Reference Run Nos. 3, 5, 6, 7, 8, 21, 24, 25, 26, 27, 34 and 35 of Appendix D).

It can be seen that plate thickness has practically no effect for the large included angles. The moderate effect shown for an angle of 60° is somewhat academic for a bellows where constant effective diameter is the principle goal in view of the fact that its performance in this respect is not competitive with the larger included angles.

Effect of Pressure Loading. - The effect of pressure loading itself on change in effective diameter for a 120° plate with a nominal axial deflection of 10 mils is shown in Figure 27. (Reference Run Nos. 21, 28 and 29 of Appendix D). It can be seen that, over the pressure range of 50 to 500 psi, the nonlinear analysis predicts very little effect on the change in effective diameter due to pressure alone.

Effect of Included Angle. - The effect of included angle variation on the change in effective diameter is shown in Figure 28 for two plate deflections. (Reference Run Nos. 2, 3, 15, 19, 21 and 34 of Appendix D). This plot again shows that fact that a large included angle should be used for minimum change in effective diameter and that the variation is small between angles of 120° and 180°.

Effect of Span. - The effect of span on effective diameter can be seen by comparing Run No. 2, having a span of 1/4 inch with Run No. 12, having a 1/8 inch span, in Table D-1 of Appendix D. Here, it can be seen that the change in effective diameter is approximately the same for equal axial deflection, all other factors constant. Thus, from a design point-of-view, if more plates of a smaller span can be fitted into the available length so that the deflection per plate is reduced, the expected percent change in effective diameter would be reduced according to the behavior indicated in Figure 25. Thus, it may be concluded that minimum span is desirable which, of course, is limited ultimately by manufacturing difficulties.

Effect of Boundary Conditions. - As discussed before, the solutions used as a basis for the preceding discussion assumed edges which are both angularly and radially fixed. The angular fixity is provided automatically by symmetry for the opposed configuration. However, radial fixity depends upon the use of a sufficiently stiff ring welded between the bellows plates. The actual radial deflection of an opposed toroidal convolution plus practical stiffeners has been estimated as approximately 1 mil. To determine the degree of effective diameter change that might occur due to this actual radial deflection, a 1 mil radial deflection was imposed at the boundary of both the

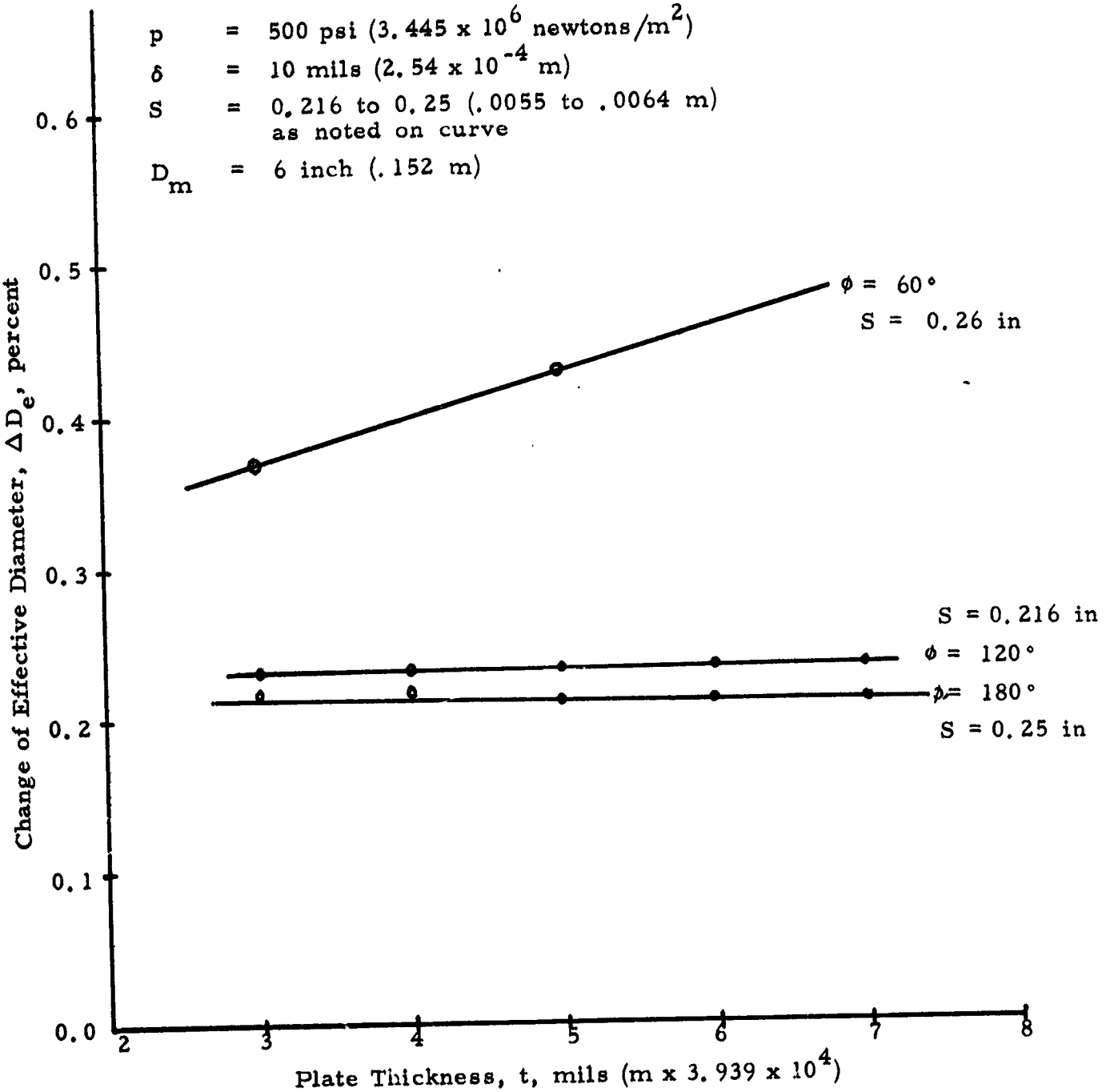

Figure 26. Effect of Plate Thickness on Change in Effective Diameter.

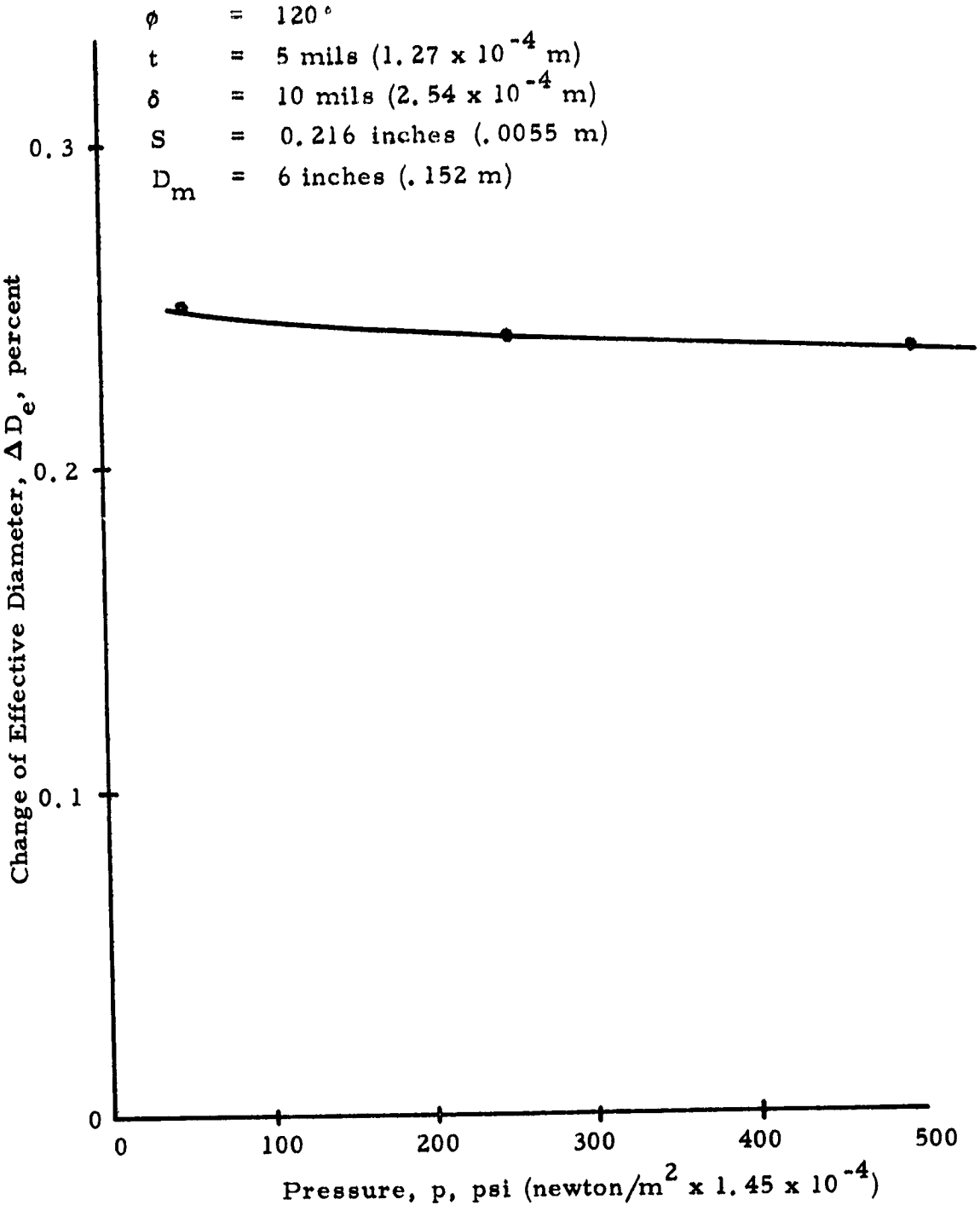

Figure 27. Effect of Pressure Loading on Change in Effective Diameter.

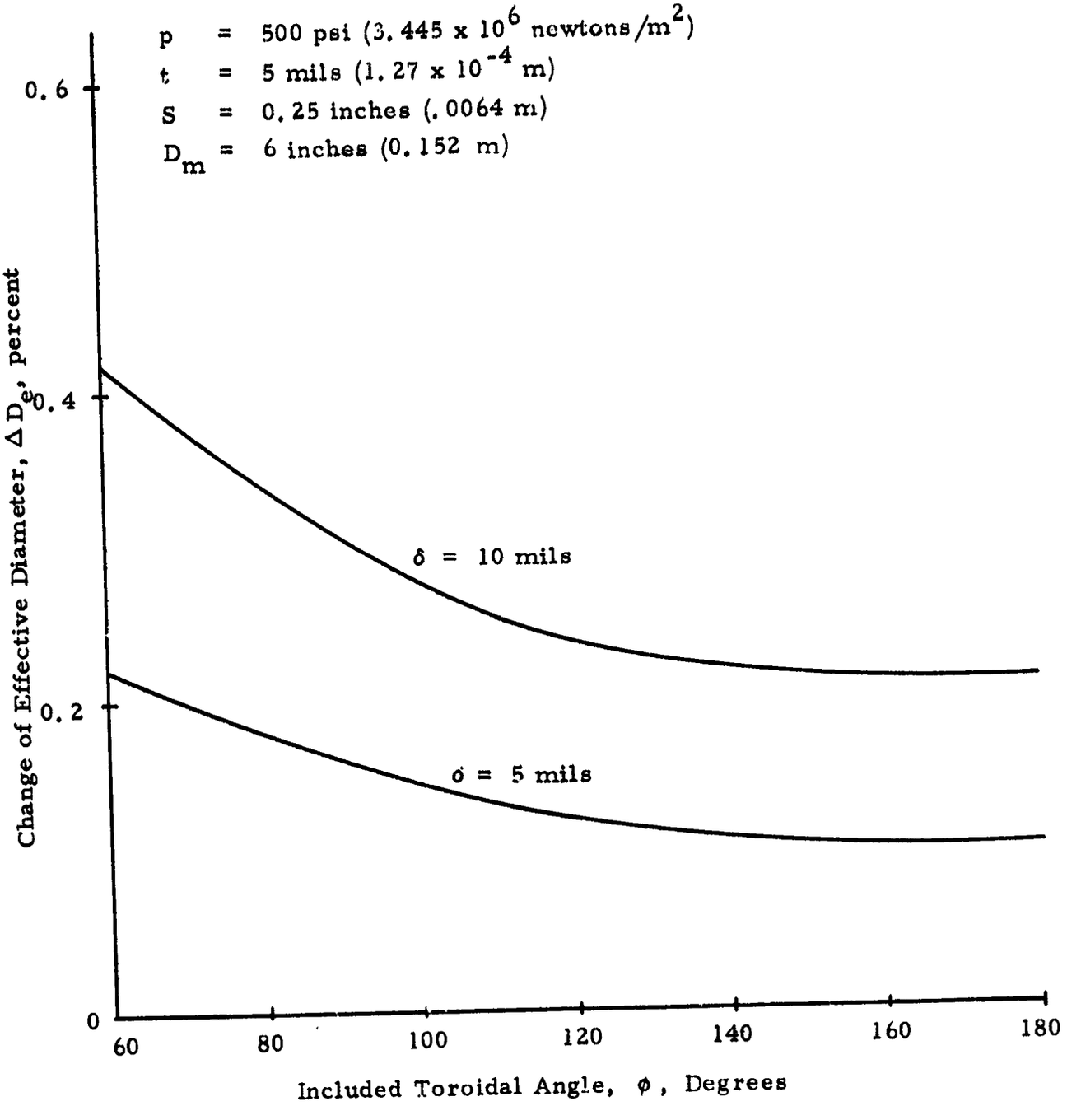

Figure 28. Effect of Included Angle on Change in Effective Diameter.

120° and 180° included angle plate (Run Nos. 13, 14, 30 and 31). The results of these runs are compared with the identical fixed cases (Runs No. 1, 3, 16 and 21) in Figure 29. It can be seen that the maximum variation of change in effective diameter occurs for the 180° plate and is only 0.01 percent out of 0.2 percent. Thus, the error introduced by assuming a fixed boundary condition is negligible.

Interpretation of Results. - The results of the parametric computer analysis summarized in the preceding paragraphs indicates that the smallest change in effective diameter that can be expected over the desired axial deflection and pressure range is approximately 0.26 percent, within the overall design constraints imposed in Table II.

It can be seen from Figures 25 and 27 that the nonlinearity or change in effective diameter is due entirely to the axial deflection of the plate and that its effects are fully present even at very low pressures. Two physical effects can combine to produce this type of nonlinearity:

(a) A nonlinear force-deflection characteristic or spring rate at large deflection which would appear in the solution for combined loading as a change in effective diameter.

(b) Distortion of the shape by the axial deflection or load so that the reaction forces produced by subsequent (or combined) pressure loading are distributed differently than with no axial deflection.

A third possible effect, distortion of the plate shape under the pressure load itself can be seen by Figure 27 to produce little change in effective diameter.

However, it can be seen from Run No. 9 of Table D-1 (Appendix D) that the total axial reaction force due to a 10 millinch axial deflection alone is only 2.6 lbs for the 180° plate. Any nonlinearity in spring force would be small compared with this total load. Run Nos. 1 and 3 for the same plate, on the other hand, show that the change in reaction force for this deflection at 500 psi pressure loading is 5.8 lbs. Thus, it is obvious that this latter nonlinearity must be almost completely due to Effect (b) above rather than (a). The same conclusion can be drawn for the 120° plate from Run Nos. 16, 21 and 23.

Effect (b) could be produced simply by the plate tilt due to the axial deflection. This was investigated by Runs No. 16 and 17 of Table D-1 where two identical cases were run with no axial deflection. They differed only in that the plate in Run No. 16 was tilted by 2.3 degrees to simulate an axial load with, of course, no shape distortion.

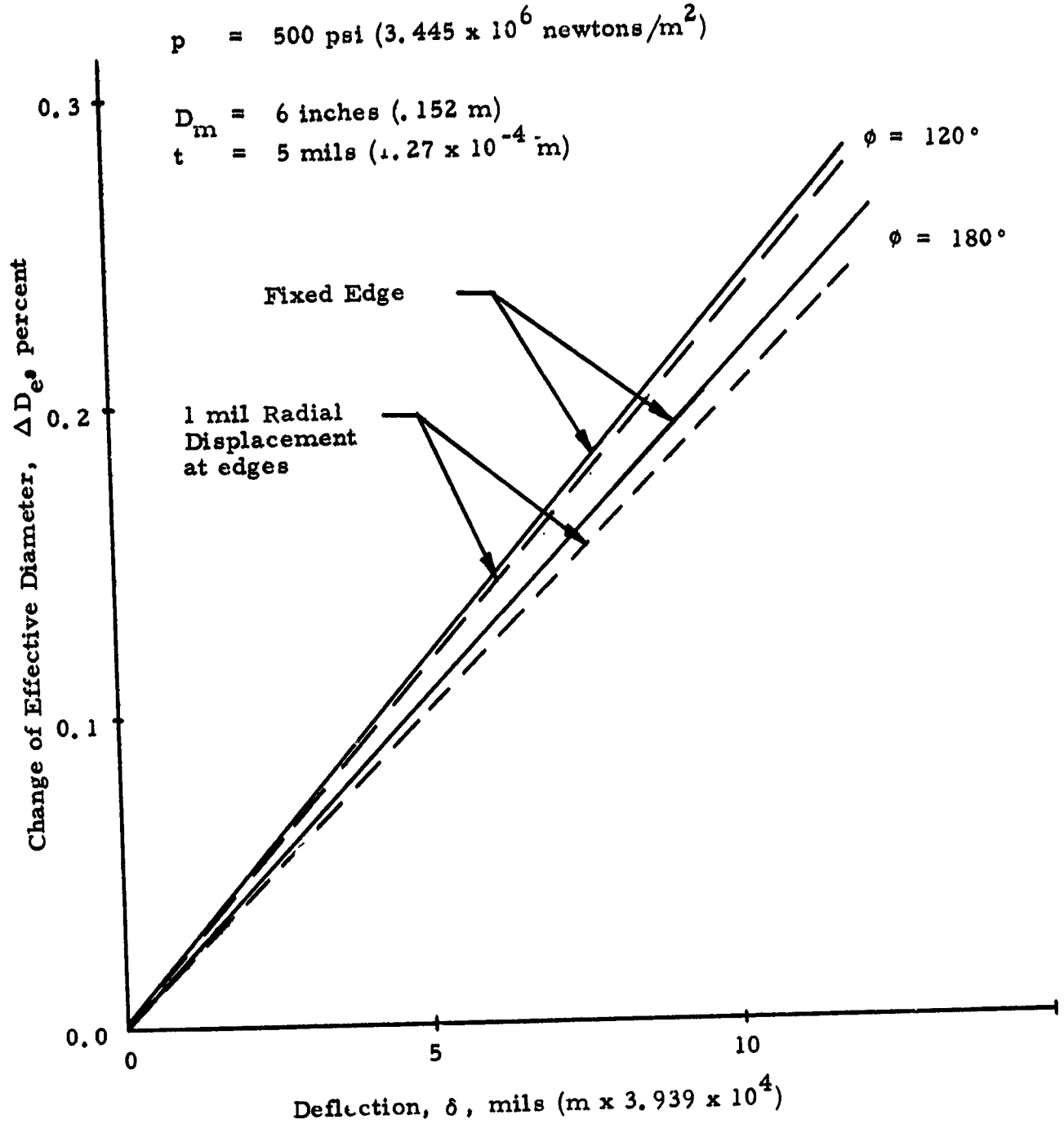

Figure 29. Comparison of Change in Effective Diameter Between Change with a Fixed Edge and a Specified Edge Displacement.

The results for the two cases were identical and virtually linear over 500 psi. Thus, the distortion of interest is actual shape distortion away from the initial toroidal shape due to the bending stresses engendered by the axial deflection.

Design Studies. - Several computer runs were devoted to an attempt to uncover design techniques for the opposed toroidal which would reduce the nonlinearity due to shape distortion under axial load. One general technique which was thought to be a possible improvement was to provide relatively compliant edges with a radially stiff span so that axial deflection is produced by plate tilt in order to minimize the plate shape distortion.

One method for approaching the above condition is to vary the compliance of the plate across the span so that the edges are relatively much more compliant for bending deflections than the center portion of the span. This was done in Run Nos. 46 to 49 of Table D-1 where the plate thickness and moduli were varied across the span in such a way that the circumferential stiffness was constant, but the meridional or radial bending stiffness was much greater at the center of the span that at the edges. For Run Nos. 46 and 47, the circumferential stiffness was equivalent to a 5 mils constant thickness plate but the bending stiffness near the center of the span was 9 times greater than that at the edges. For Run Nos. 48 and 49, the circumferential stiffness near the edge was equivalent to a 2.5 mil plate and that near the center to a 5 mil plate but the central bending stiffness was 36 times greater than that at the edges. The salient result was that the predicted change in effective area was exactly the same as that for a constant 5 mil bellows plate. The distribution of curvature change can be easily seen in Figure 30 where the angular deflection, β, is plotted across the span for these two cases and compared with a uniform thickness plate. As expected, the major effect was to concentrate the curvature change near the edges. However, it was so much greater in this region that any advantage from the stiffened central portion was offset.

A final concept for a shape change to approach the ideal distortionless toroid was the use of a non-isotropic or radially corrugated plate. Here, corrugations in the radial direction instead of thickness variation or modulus variation as described above would be used to make the circumferential stiffness negligible compared with the bending stiffness near the compliant edges. This would have the effect of approaching a "rigid-body" rotation of the ideal toroidal shape and might reduce the effective area change. This type of configuration, however, cannot be treated using available nonlinear analytical techniques. Thus, it is recommended that a critical experiment be performed to check its effect on linearity. The basis for the design of a non-isotropic opposed toroidal plate is given in Appendix F.

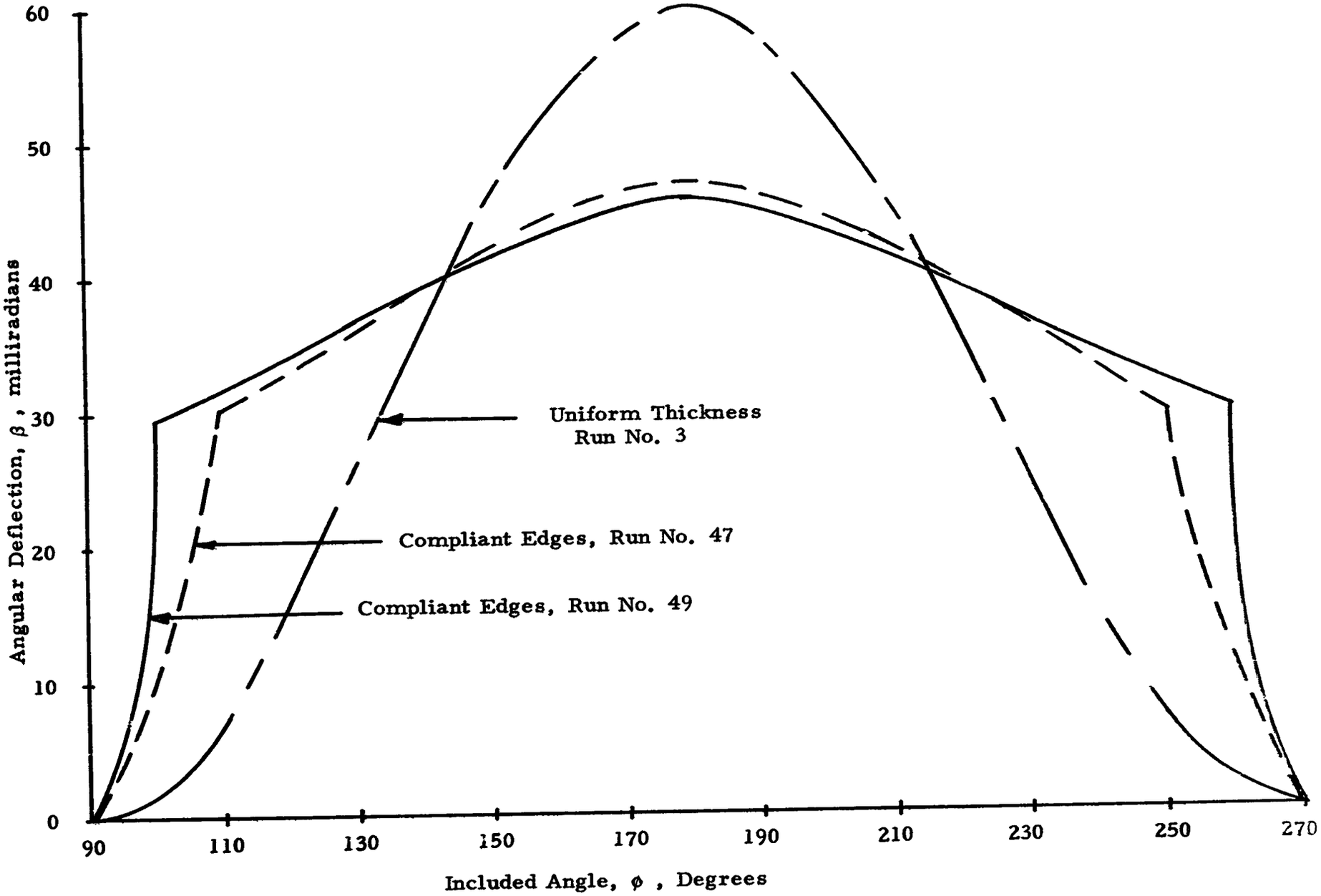

Figure 30. Comparison of the Angular Deflection Across the Span for the Uniform Thickness and Compliant Edge Cases.

Another shape parameter that might be used to reduce the change in effective diameter is the selection of an optimum initial shape so that the nonlinear effects due to distortion compensate each other. This, in essence, means varying the initial curvature of the plate away from a perfect toroid in an optimum way. It might be expected that variation of the shape so that the deflected shape would approach a perfect toroid might reduce the nonlinearity in reaction force under pressure load. This was tested by Run Nos. 42, 43 and 44. The results showed that the effective area change was identical to that of an initially undistorted plate. In fact, as might be expected, the nonlinearity is due to the shape change alone and minor changes of the starting point have no effect.

A second curvature change aimed at producing a relatively stiff central portion similar to that produced by the variable thickness cases discussed in preceding paragraphs was tested by Run No. 45. Here a peaked plate with a relatively stiff central portion was produced by reducing the radius of curvature in the central region. As before, this concept produces no advantage in terms of linearity and has, as its main effect, the increasing of the peak stress in the plate.

Nested Toroidal Plates

The principal advantage of the nested toroidal bellows is that, although the individual plate behavior is not expected to improve over the opposed plate case, many more plates can be stacked into a bellows core having a given length. Thus, each plate is required to undergo a smaller plate deflection which has been shown in the preceding section to be the major variable affecting change in effective diameter.

Another fundamental difference is that the convolution is not symmetric about a plane perpendicular to the axis as is the opposed case. Thus, the pressure load is expected to cause a rotation of the elements with a corresponding change in effective diameter even at zero axial deflection.

A series of 50 computer runs were made to investigate the effects of varying a number of parameters on the performance of the nested toroid. Two basic configurations of importance, single and multiple convolution, were studied as defined in Figure 30 where the principal nomenclature is also defined.

In order to minimize computer time, the single convolution (2 plates) case was used to determine the basic nonlinear behavior of the bellows. The multiple convolution case was then used for the more promising combinations of variables to study the effect of the end condition and select the most promising bellows plate and stiffener configuration.

It can be seen from Figure 31 that, in general, a stiffener ring is provided at each plate joint and the effect of varying the stiffness of this plate was studied. In addition, all of the parameters studied for the opposed plate were also investigated for the nested plate. The only parameter fixed was the mean diameter of the bellows plate, D_m = 6 inches (0.152 m).

The linearity of the bellows was computed as expressed in Equations (23) through (26). That is, the change in effective diameter is proportional to the change in axial reaction force, N_p, between the linear and the nonlinear solution for a given loading.

The results of the parametric study are summarized and discussed in the following paragraphs. The numerical results of the computer solutions are tabulated in Appendix E where sample stress distributions for the plates are also given.

Effect of Axial Deflection and Included Angle. - The percentage change produced in the effective diameter between small pressure loads and a pressure loading of 500 psi (3.445×10^6 newtons/m^2) as a function of the axial plate deflection, δ, is shown in Figure 32 for three included angles, (Reference Run Nos. 4, 5, 11, 12, 15 and 16 of Appendix E).

It can be seen that the change in effective diameter is again proportional to the axial deflection and has about the same overall sensitivity as the opposed toroid (related to individual plate deflection). The total change does not vary markedly with included angle in the range studied (also true of the opposed toroid in this range). The major effect of varying the included angle is to shift the curve downward so that the deflection at which there is no change in effective diameter from the linear case occurs at a finite non-zero value. This has some practical significance since, by selecting the optimum ϕ, the total range of change in absolute effective diameter over a range of deflections can be halved.

Effect of Plate Thickness. - The effect of variation in plate thickness on change in effective diameter can be seen in Figure 33 for an included angle of 140°. (Reference Run Nos. 17, 18, 21 and 22 of Appendix E). It can be seen that, for this case, the increase in thickness from 5 to 10 mils results in a smaller absolute change in effective diameter over the pressure range.

Effect of Span. - Although no specific cases were run to investigate the effect of span alone, the behavior for one case can be seen by comparing Run Nos. 5 and 7 of Table E-2 where the span decreases from 1/4 inch to 1/8 inch, all other factors except plate thickness remaining constant. There was essentially no effect on

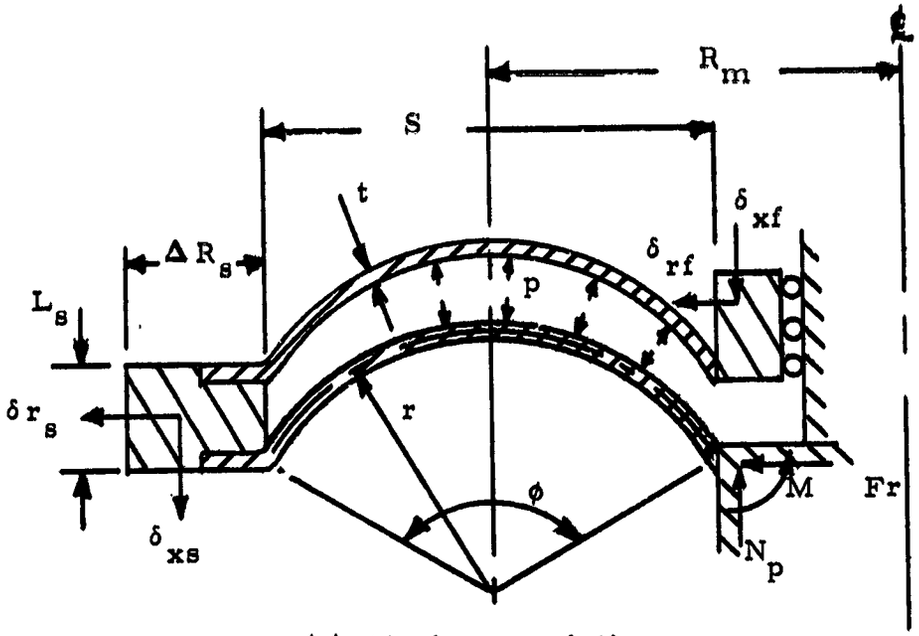

(a) Single Convolution

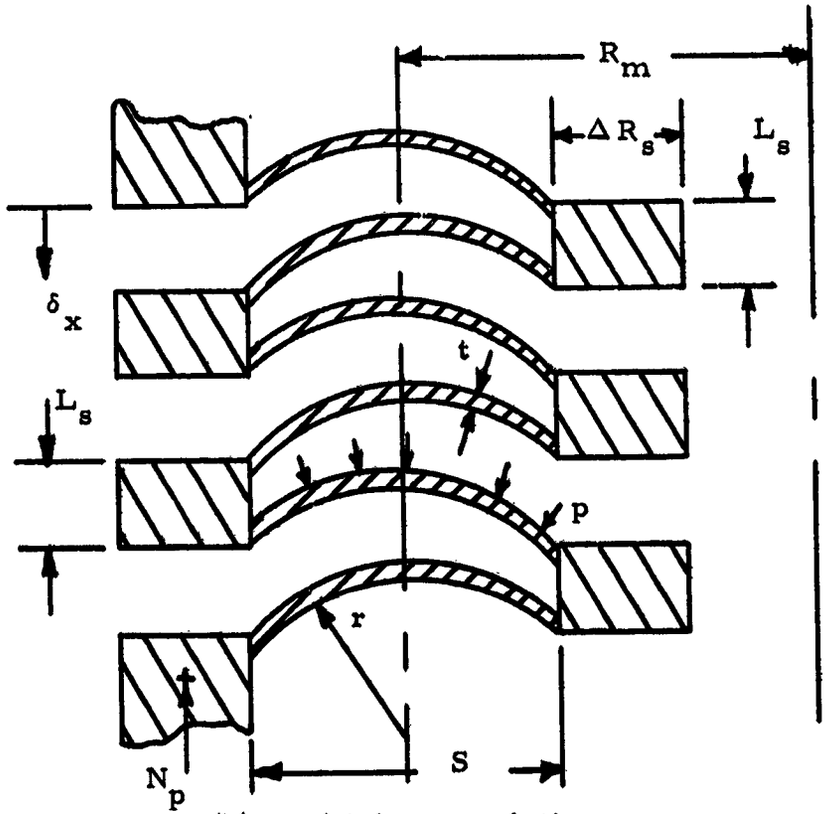

(b) Multiple Convolution

S - Span
R_m - Mean Radius
t - Plate Thickness
r - Toroid Radius
φ - Included Angle
L_s - Stiffener Ring Length
ΔR_s - Stiffener Ring Thickness
N_p - Axial Reaction Force
δ_x - Axial Deflection
δ_r - Radial Deflection
n - Number of Convolutions
p - Applied Pressure

Figure 31. Schematic Diagrams and Definition of Nomenclature for the Nested Toroidal Bellows.

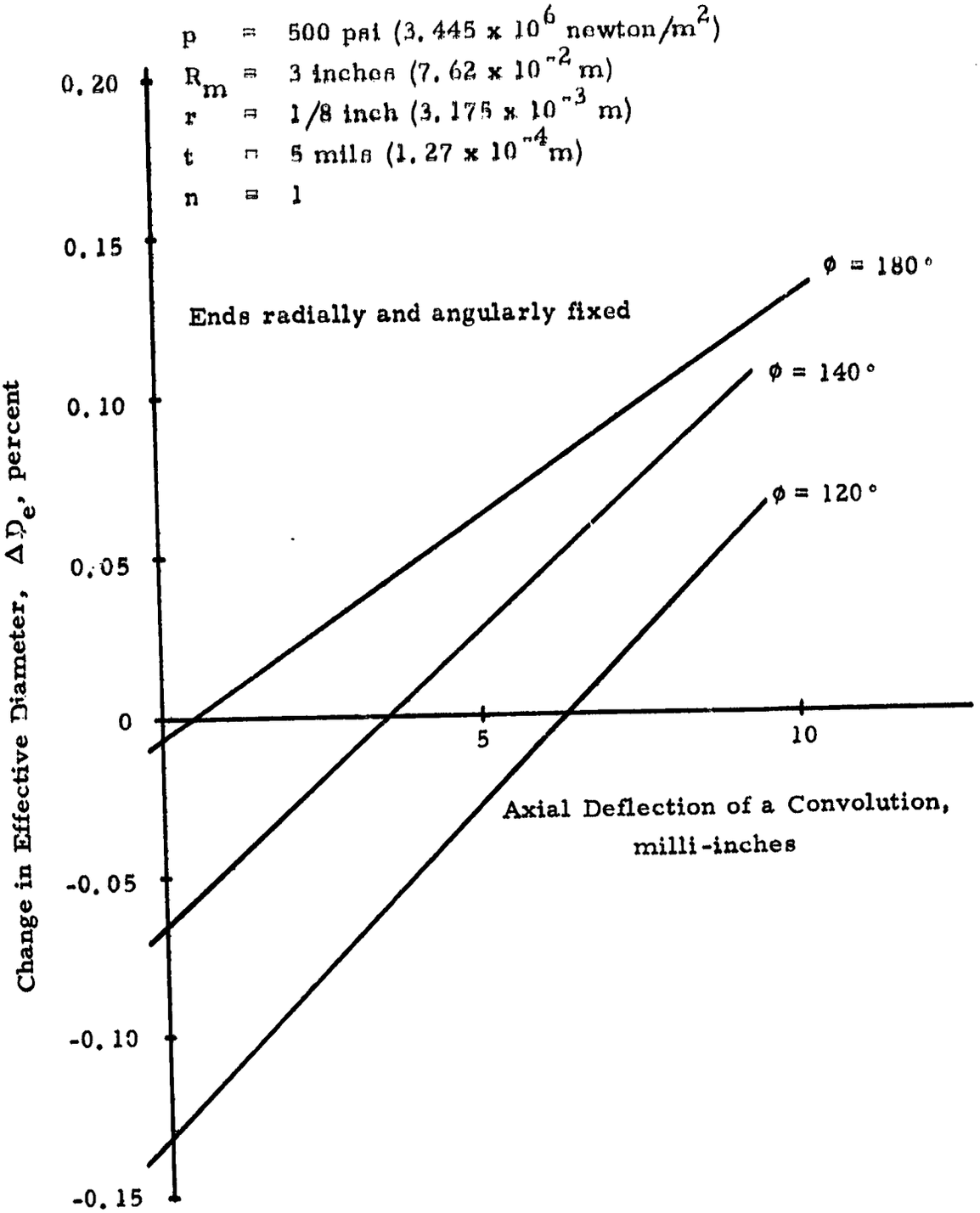

Figure 32. Effect of Axial Deflection on Change in Effective Diameter for Single Convolutions with Various Included Angles.

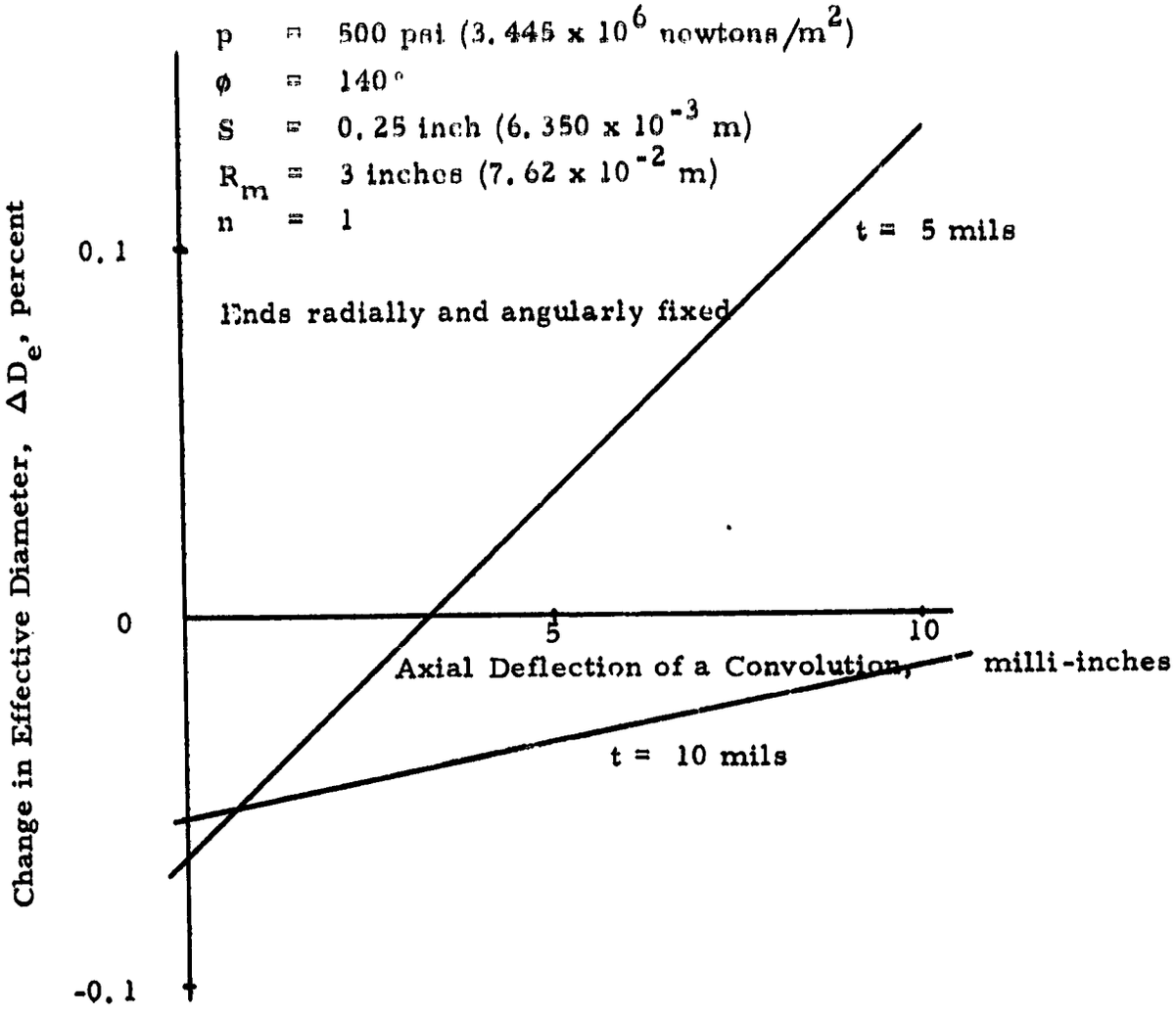

Figure 33. Effect of Plate Thickness on the Change in Effective Diameter for a Single Convolution.

change in effective diameter which is the result expected from the single plate results of the opposed toroid study. This confirms the previous conclusion that, from a design point-of-view, minimum span consistent with feasibility of fabrication is desirable since more convolutions, in general, can be fitted into a given core length.

Effect of Edge Boundary Conditions. - The edge boundary conditions on the plate are provided by the stiffness of the stiffener rings. The basic conditions used for reference in the single convolution studies assumed radially and angularly fixed edge conditions. Here, the results are not markedly different from those of the opposed toroid study in terms of the range of change in effective diameter over a given range of single plate deflection.

Several cases were devoted to checking the effect of relaxing the fixed boundary conditions. For example, the angularly fixed case for $\phi = 140$ (Reference Runs 11 and 12 of Table E-2) is compared with the angularly free case (Reference Runs 19 and 20 of Table E-2) in Figure 34, both being radially fixed. This produced very little effect on the change in effective diameter.

Also in Figure 34, the fixed case for $\phi = 180°$ (Reference Runs 4 and 5 of Table E-2) is compared with one having an imposed radial deflection of 1 mil (a reasonable value for typical stiffener rings) but remaining angularly fixed (Reference Runs 2 and 3 of Table E-2). The total range of ΔD_e remains about the same for these cases, the main effect being a shift downward. This has some practical value, as mentioned before, in that it reduces the maximum absolute change in effective diameter experienced over the range of plate deflections.

The main conclusion from these studies is that so long as reasonable radial stiffening is present, the stiffness of the edge boundary conditions does not have a major effect on the single convolution behavior.

Effect of Multiple Convolutions. - Because the nested toroid convolution is not symmetric, plate rotation must occur if the edge stiffeners are not sufficiently stiff to provide angular fixity. Thus, if the end fittings are very stiff so that the end boundary condition is essentially fixed some variation in plate behavior may be expected for succeeding convolutions away from the end fitting. The effect of multiple convolutions on the change in effective diameter was tested for a 160° toroidal plate by Run Nos. 23 through 29 of Table E-1. The results are plotted in Figure 35. Here, it may be seen that the two convolution case gives a result significantly different from the single convolution but that the difference becomes much smaller as succeeding convolutions are added. The major effect is to move the effective diameter versus convolution deflection curve down, thereby

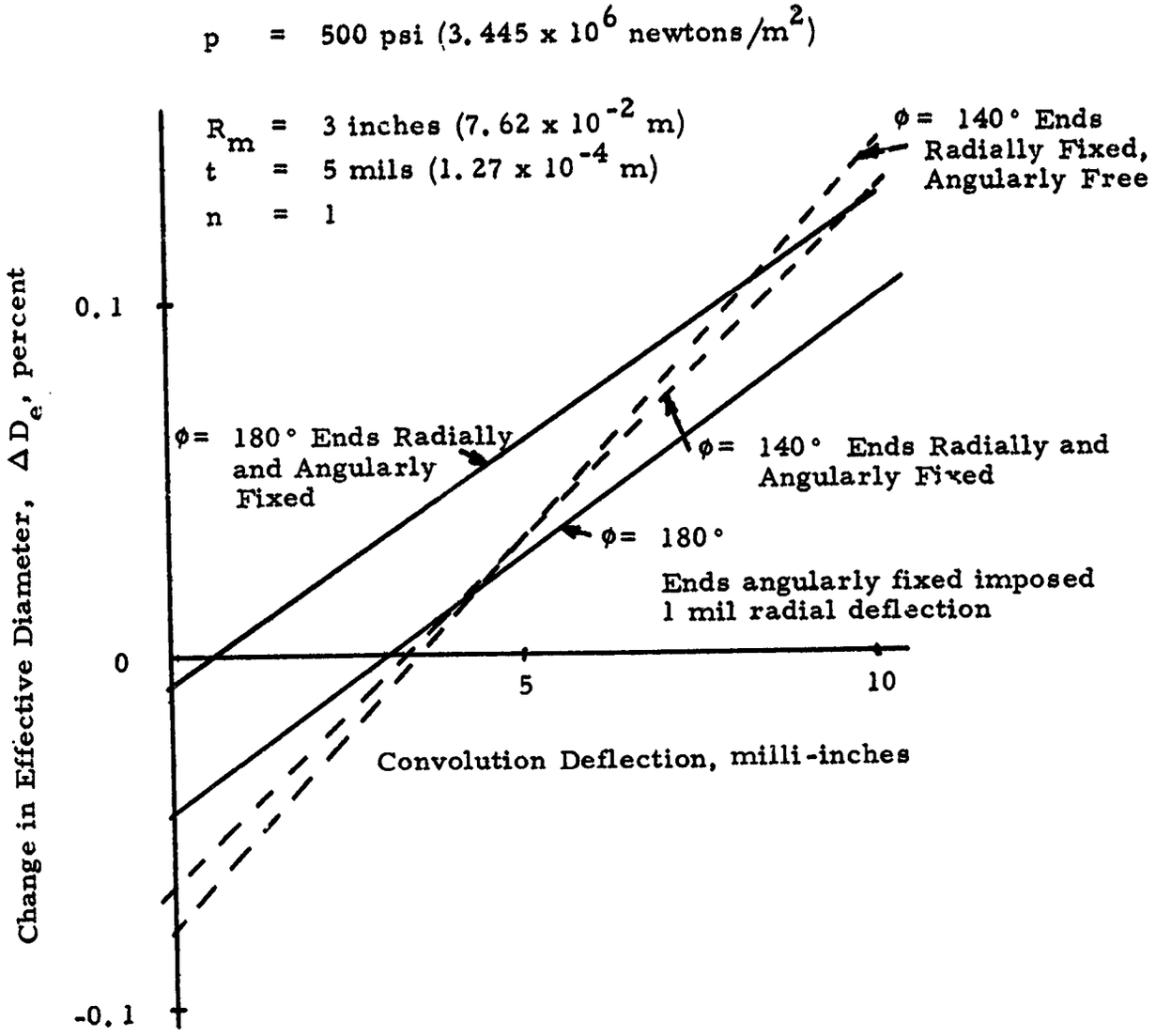

Figure 34. Effects of End Boundary Conditions on a Single Convolution.

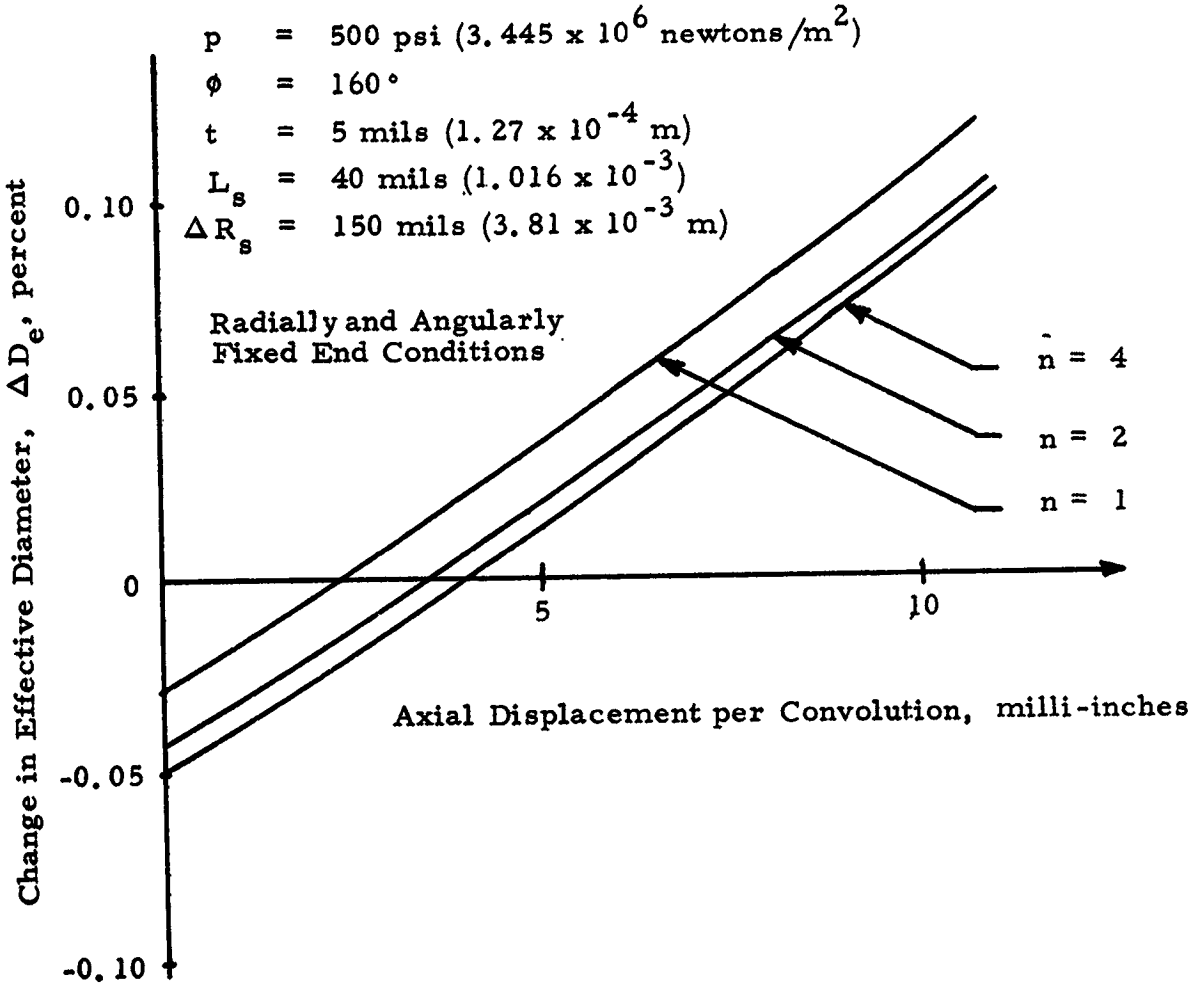

Figure 35. Effect of Multiple Convolution on Change in Effective Diameter.

taining the same sensitivity of change in effective diameter with deflection but decreasing the range of absolute change.

The specific dimensions for the plate and stiffener rings are shown in Figure E-1 of Appendix E. The decay of the effect of the end boundary conditions on the deflection of the plates can be seen graphically by comparing the plate stress distributions plotted in Figures E-2 through E-5. The stress distributions in the second and fourth plates are essentially identical and it may be expected that succeeding plates will show no differences until the end fitting on the other end of the core is approached.

Thus, it may be concluded that 4 convolutions are sufficient for a good prediction of the effective diameter change in a multiple convolution bellows of this type where edge stiffener plates are typical of those of Figure E-1 in terms of radial and angular stiffness.

Interpretation of Results. - Comparing the basic single convolution behavior shown in Figure 32 with that for the opposed toroidal plate shown in Figure 25, it can be seen that they are comparable from the standpoint of change in effective diameter over the desired pressure and deflection range. (It is important to note that the plate deflection scale of Figure 25 represents one-half the single convolution deflection for comparison with Figure 32).

The use of a partial toroid (ϕ = 120° or 140°) increases the sensitivity of change in effective diameter with deflection in each case. However, this increased sensitivity is accompanied by an adjustment in the zero change location for the nested plates. Thus, the net effect is to reduce the absolute change in effective diameter with deflection.

The major difference between the opposed and the nested cases is that the latter are inherently capable of closer spacing, thus allowing more plates within a given core length. This reduces the required deflection per plate and, thus, the change in effective diameter. Since it appears that the 15 to 30 convolutions (30 to 60 plates) required to keep the change in effective diameter below 0.1 percent for the various ϕ's can be physically fitted into the core length, this configuration, unlike the opposed toroid appears basically feasible for meeting the design goal. The analysis, of course, does not consider difficulties in fabrication which are much more critical for the nested configuration than for the opposed. These will be discussed in a later section. It also does not take into account the design trade-off associated with the variable number of plates for the various ϕ's that may be fitted into the bellows core. Several multiple-convolution solutions were devoted to this subject in order to select the most promising configuration as discussed in the following chapter.

SELECTION OF THE EXPERIMENTAL BELLOWS CONFIGURATIONS

The objective of the analytical studies of the preceding sections of this report was the identification of those bellows configurations having the best promise for meeting the linearity goal, constancy of effective diameter within $\pm$ 0.1 percent across the specified deflection and pressure range.

In fact, only the nested toroid appears theoretically capable of achieving this goal since sufficient convolutions can be used to bring the nonlinearity within this bound by reducing the individual plate deflection.

However, the opposed toroidal configuration is theoretically capable of achieving constancy of effective diameter within the 0.2 to 0.3 percent range with the number of convolutions possible. Since this is still much better than the present state-of-the-art for bellows seal applications, it was recommended as an alternative test bellows for this program. Also the opposed toroid is inherently easier to fabricate and was felt to have a considerably better probability of surviving this critical step of the development. Moreover, the radially corrugated version of the opposed toroid is felt to be promising for further reducing the effective diameter change, perhaps bringing it within the design goal.

In summary, therefore, the three most promising design configurations selected on the basis of the analytical studies for further experimental evaluation were:

(a) Opposed Toroid

(b) Radially Corrugated Opposed Toroid

(c) Nested Toroid

In addition to the nonlinear analysis discussed in the preceding section, further studies and computer runs were devoted to the selection of the optimum configuration for each of these designs. These studies are discussed in the following paragraphs.

Opposed Toroid

The nonlinear analysis of single toroidal plate showed that the axial deflection per plate and the toroid included angle have the greatest effect on change in effective diameter. For the multi-convolution case, the number of convolutions that can be fitted into the desired core length becomes important. The maximum number of convolutions can be expressed approximately from the geometry of the bellows as,

$$n < \frac{L \sin(\phi/2)}{S(1-\cos\phi/2) + L_s \sin(\phi/2)} \tag{27}$$

where

L = core length

L_s = stiffener length per convolution in excess of the toroidal plate height

S = span

ϕ = toroid included angle

This is plotted in Figure 36 for a realistic span of 0.25 inches and two stiffener lengths. In these plots, the fact that the number of convolutions must be integer is taken into account. Realizing that the individual plate deflection, δ, may be expressed by,

$$\delta = \frac{\Delta L}{2n} \tag{28}$$

the individual plate data of the preceding chapter can be modified to reflect the number of convolutions possible in the prescribed core length of 1.5 inches (0.038 m). This is plotted in Figure 37 for a 0.25 inch (.0065 m) span and a net stiffener length of 40 mils (1.02×10^{-3} m). The corresponding spring rates and combined stress are also shown in this figure.

It can be seen that, although stress and spring rate are within the prescribed limits (150,000 psi and 800 lbs/in) across this range, the stress is minimized in the 120 to 160° range of included angle. The change in effective diameter increases monotonically in this range, making 120° the optimum included angle. This is a weak optimum, however, and the choice of included angle is affected from a design point-of-view by the fact that the 160° included angle allows a reduction in the number of convolutions from 8 to 6, making the bellows significantly easier and cheaper to fabricate. The increase in change of effective diameter is felt to be small enough so that the fabrication advantage is warranted.

Thus, the 6 convolution 160° toroidal plate is recommended as the best compromise for the opposed toroidal bellows. The change in effective diameter is nearly independent of plate thickness in the realistic 4 to 6 mil range. The recommended span is 0.25 inches and the mean radius is 3 inches. For the opposed toroid, the angular stiffness of the stiffener rings is not critical because of the symmetrical load placed on them. They must only be stiff enough to resist radial deflections. This is true with stiffeners having a net increase in convolution length of 40 mils as assumed for the data of Figure 37.

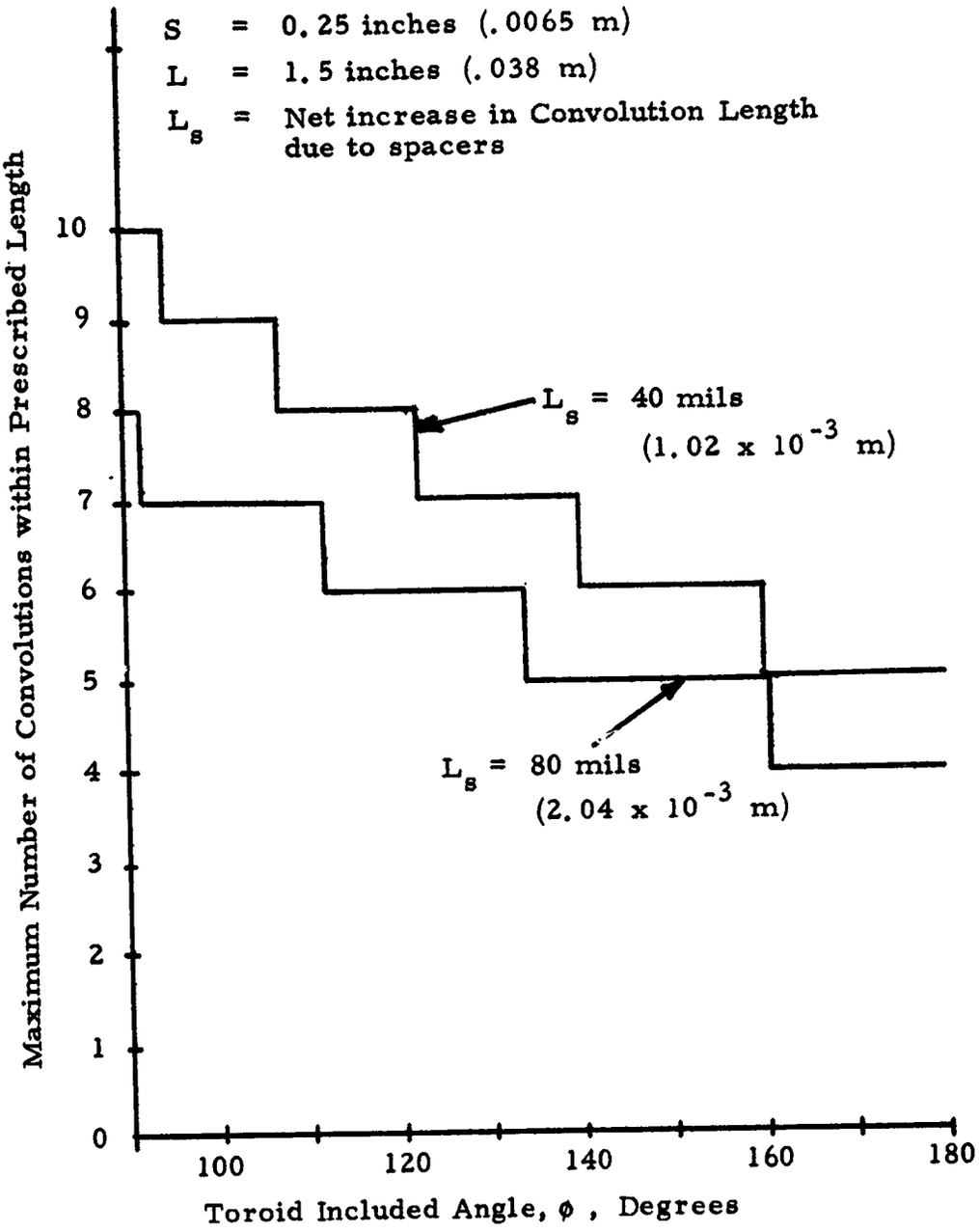

Figure 36. Maximum Number of Convolutions that can be Fitted Within the Prescribed Length for Two Typical Spacer Lengths.

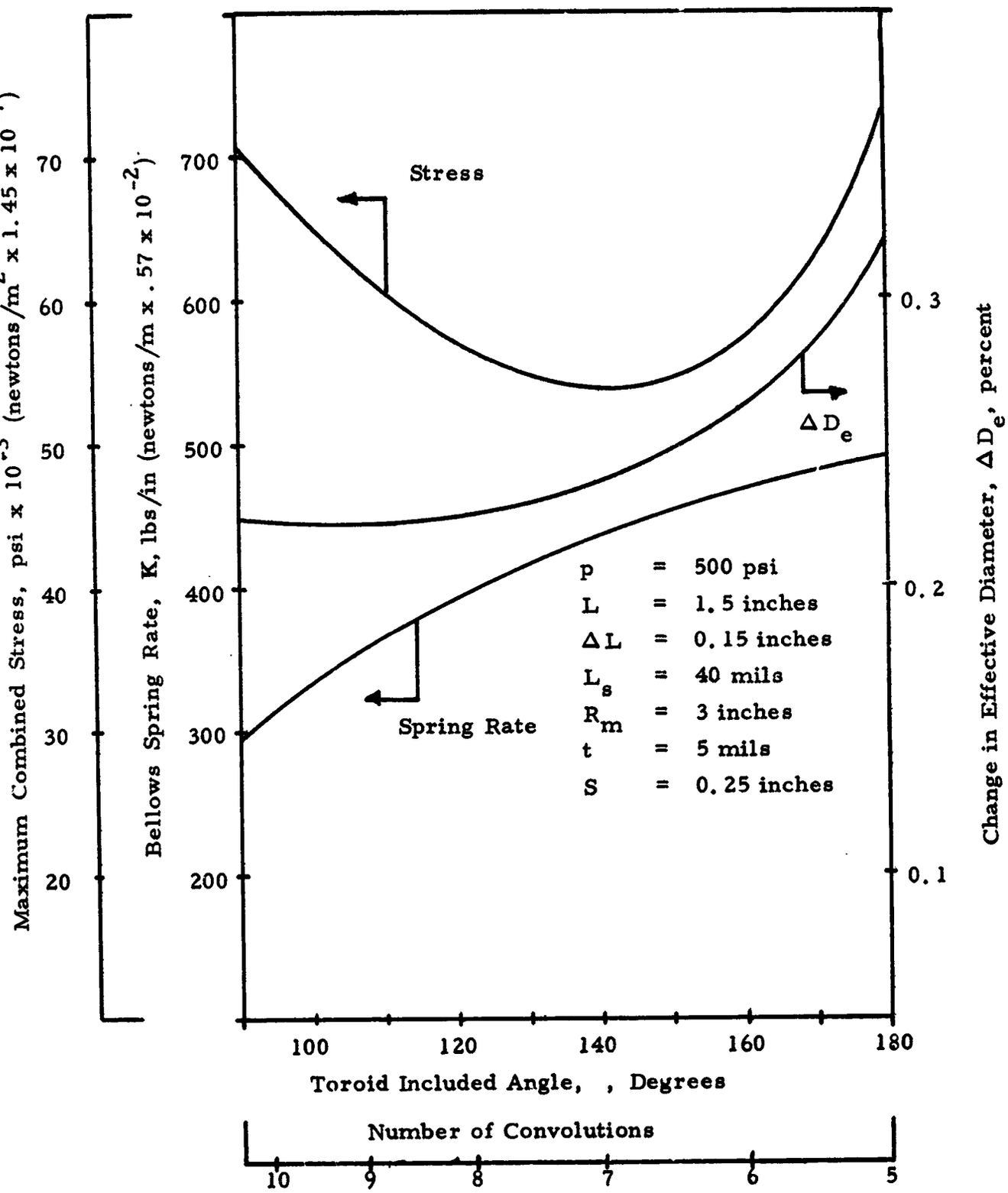

Figure 37. Performance Curves for Opposed Toroidal Bellows Having The Maximum Number of Convolutions for Each Included Angle.

For the corrugated opposed toroid, the 10 mil amplitude corrugation with a half wave-length of 50 mils described in Appendix F is recommended as providing significant stiffness ratios for experimental evaluation.

Nested Toroid

Selection of Stiffener Dimensions. - The results of the nested toroid analysis showed that, providing sufficient radial stiffening were present, the angular stiffness of the stiffening rings was not critical. Radial stiffness is provided by using the maximum cross-sectional area.

From a design point-of-view, a maximum number of plates having minimum span is desirable to minimize change in effective diameter. The minimum practical span was selected to be 0.25 inches. Since the maximum allowable span, including both toroidal plates and stiffeners, is 0.6 inches, the radial dimension or width, ΔR_s of the stiffener rings should be approximately 0.15 inch. This was used as the nominal value for the recommended design.

For the nested configuration, the stiffener ring length, L_s, can be related to the total core length, L, by

$$L_s (2n - 1) = L = 1.5 \text{ inches} \tag{29}$$

To ensure that adjacent plates still have an axial clearance, δ_c, after being compressively deflected through $\Delta\ell$, the stiffener length must meet,

$$L_s \geq \frac{t}{\cos \phi\, 2} + \frac{\Delta L}{n} + \delta_c \tag{30}$$

where

t = plate thickness

ϕ = included angle

Taking $t = \delta_c = 5$ mils, Equations (29) and (30) may be solved for various ϕ to give L_s and n. These are tabulated in Table V.

Selection of Included Angle. - Using the stiffener length tabulated in Table V and a width, ΔR_s, of 150 mils, the change in effective diameter was predicted for stacks of four convolutions. (Reference, Run Nos. 27 to 39 of Appendix E). The results of these computer solutions are plotted in Figure 38.

TABLE V

Acceptable Combinations of Stiffener Length and Number of Convolutions for Various Included Angles

Included Angle, ϕ degrees	Stiffener Length, L_s milli-inches	Number of Convolutions, n	Deflection per Convolution, milli-inches
120	25	30	5
140	30	25	6
150	35	21	7
160	40	19	8
180	55	14	10.7

t = 5 milli-inches

δ_c = 5 milli-inches

ΔL = 0.15 inches

It should be noted that a stack of four convolutions was used instead of the actual number corresponding to each included angle as shown in Table V in order to save computer time and fit within the conveniently available memory capability. Also the preliminary multi-convolution solutions showed that four convolutions was sufficient to predict the basic behavior of the bellows.

Also plotted in Figure 38 is a locus of the single convolution displacement corresponding to the total deflection of 0.15 inches and the selected maximum number of convolutions for each included angle. This convolution deflection is tabulated in Table V.

It can be readily seen by the points of intersection of the performance locus with the curves for various ϕ s that the goal of 0.1 percent absolute change in ΔD_e is only met for plates having an included angle in the range of 140 to 160°.

The combined stress and spring rate for these bellows plates are plotted in Figure 39. Here it can be seen that the stress decreases with increasing ϕ and that the spring rate, although increasing, is always well below the 800 lb/inch limitation. Thus, it appears that the optimum choice for included angle is 160°.

Selection of Plate Thickness. - In order to test the effects of a significant thickness increase on the performance of the bellows, Run Nos. 40 through 42 of Appendix E were made using 8 mil plates. The results showed slight improvement of effective diameter change and stress but a nearly five-fold increase in spring rate. Since it is felt that this spring rate increase more than offsets any advantage gained in constancy of effective diameter and that the increased thickness may lead to increased fabrication difficulties, it was decided to use the 5 mil plate thickness.

Effects of a Welding Flange. - Later fabrication studies indicated the desirability of providing a lip or flange at the edge of the toroidal plate for welding onto the stiffener rings. Two versions of this type of flange are shown schematically in Figure 40.

These were treated analytically by Run Nos. 43 through 50 of Appendix E.

The circular flange of Figure 40(b) would not converge to a solution having acceptable accuracy on the computer. Thus, a flat flange model as shown in Figure 40(c) was used and valid solutions were obtained.

The general results indicated that there is no significant effect on change in effective diameter from this type of flange. Also, the spring rate is not affected.

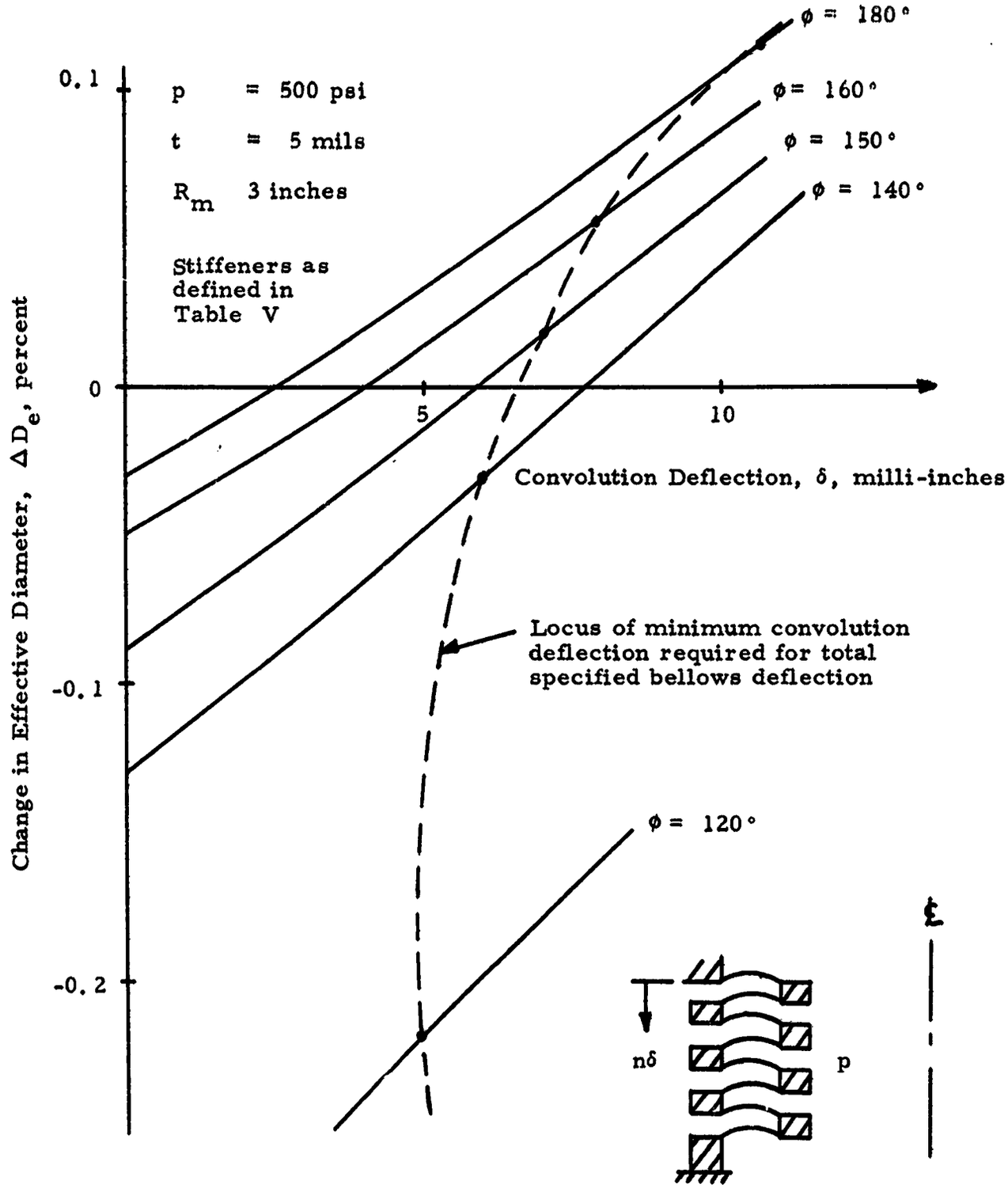

Figure 38. Change in Effective Diameter for Various Included Angles with Acceptable Combinations of Stiffener Rings and Numbers of Convolutions.

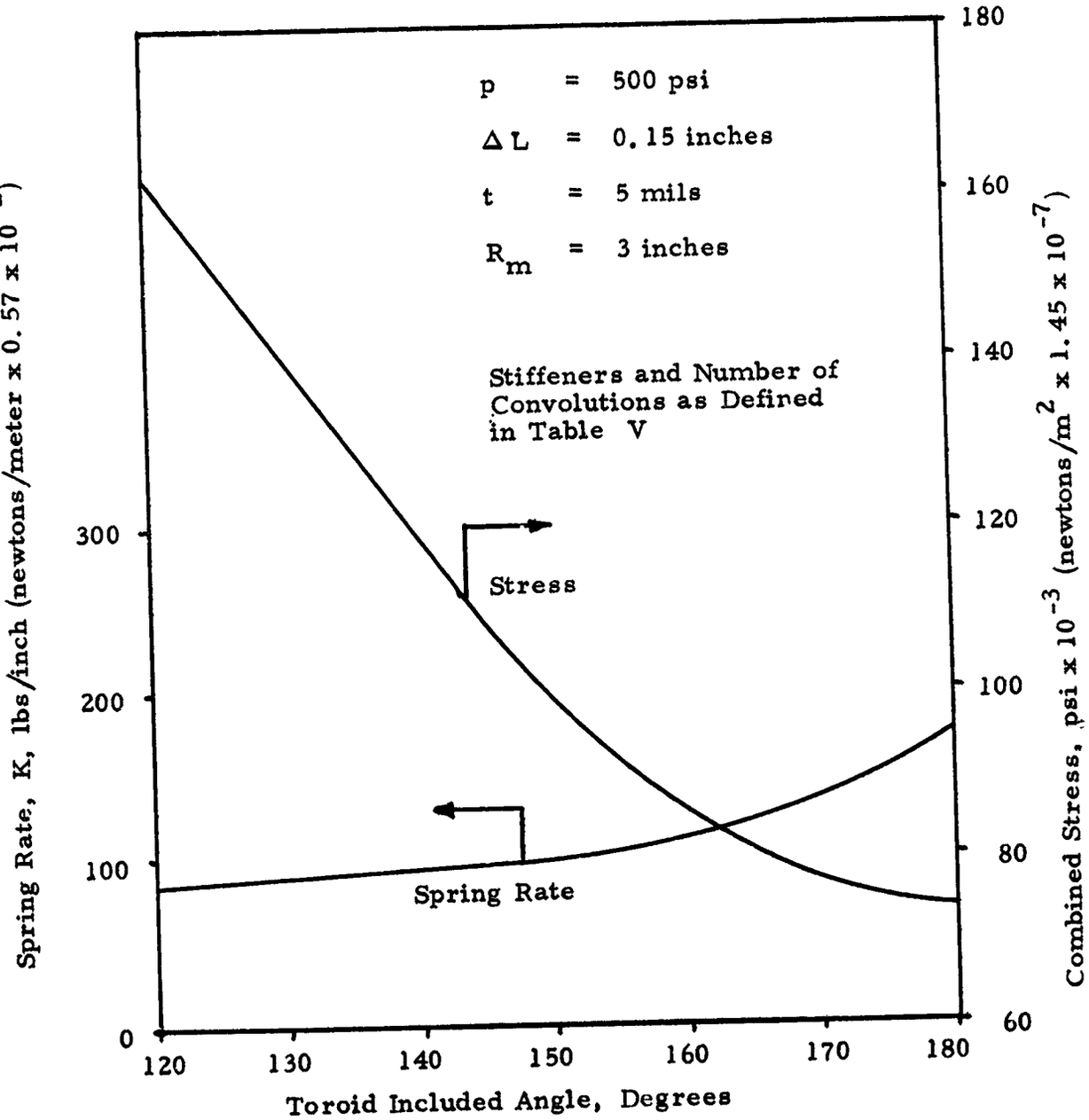

Figure 39. Maximum Combined Stress and Spring Rate Versus Included Angle for Acceptable Combinations of Stiffener Rings and Maximum Number of Convolutions.

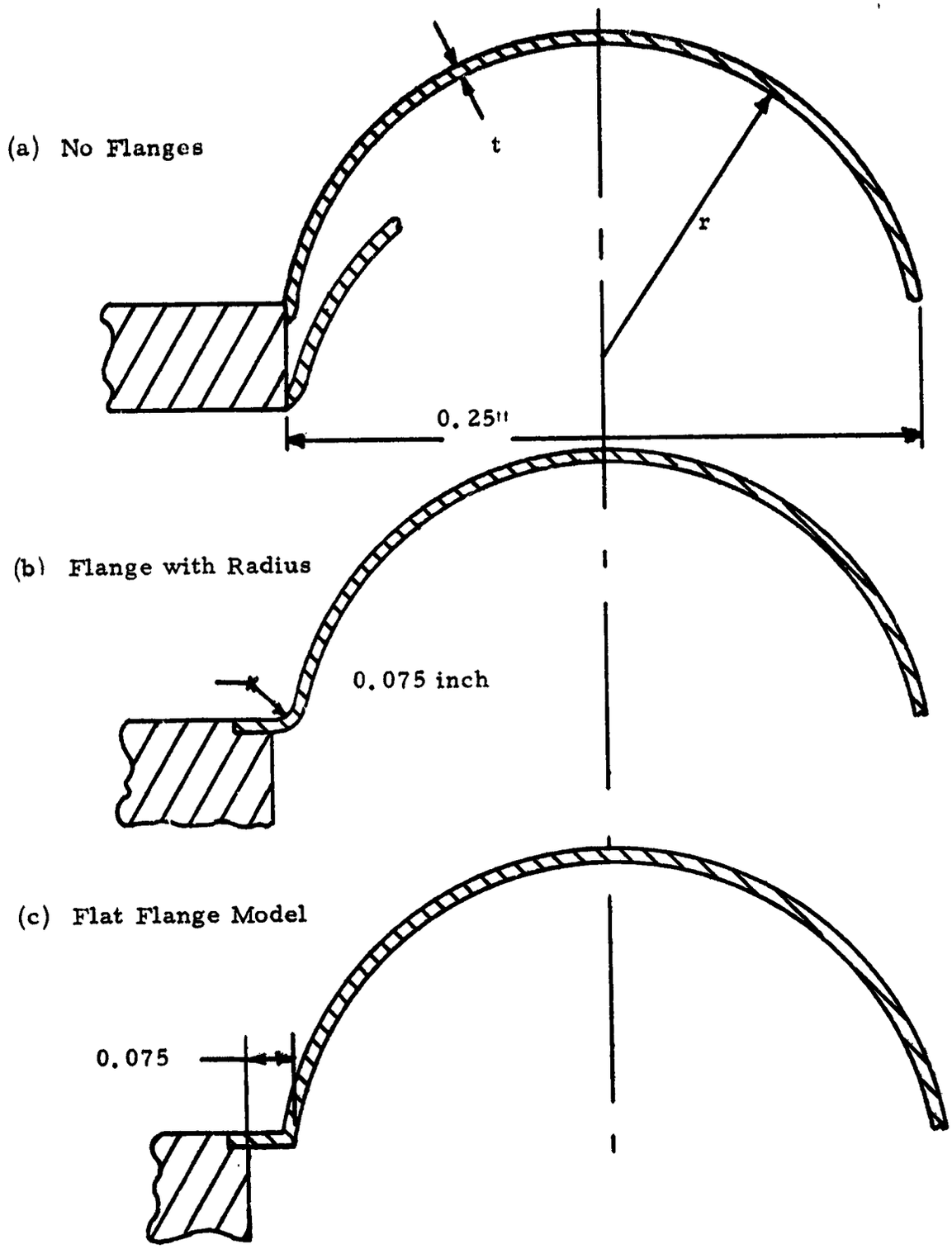

Figure 40. Definition of Edge Welding Flanges Investigated Analytically.

However, the peak stress is increased by a factor of over four (from 40,000 psi to 172,000 psi) putting it beyond the design limitation. Moreover, it is felt that this type of configuration will also impose a stress concentration further increasing local stresses beyond the analytically computed values.

Thus, it is recommended that the use of this type of flange be avoided if at all possible within the state-of-the-art in welding.

In Summary. - It is recommended that the parameters used for the experimental nested toroidal bellows be as follows:

included angle,	ϕ	= 160°
plate thickness,	t	= 5 mils
number of convolutions,	n	= 19
stiffener ring size,	L_s	= 40 mils
	ΔR_s	= 150 mils

FABRICATION STUDIES

A specific objective of the study was the experimental verification of the performance predicted by the analytical studies for the most promising bellows configurations. Thus, with the completion of the analytical work and selection of the opposed and nested toroidal configurations, effort was turned toward the fabrication of special test bellows.

The design of the bellows plate forming dies, welding fixtures, and chill rings (heat sinks), as well as the detailed design of the bellows plates, their flanges, and the mating surfaces of the interconnecting stiffener rings and end fittings was accomplished at the outset to produce optimum hardware implementing the basic designs resulting from the analytical work.

Because each of the selected configurations described in the preceding sections requires the incorporation of stiffener rings into the bellows core to achieve the desired linearity, they presented a common fabrication problem, the joining of thin gage bellows plates with relatively heavy stiffener rings as shown in Figure 41. These configurations incorporate some modifications from the recommended configurations of the preceding section designed to facilitate fabrication. In each case, however, the modification was not felt to significantly affect the basic performance of the bellows.

Several joining techniques were attempted to solve the problems associated with the plate to stiffener ring joint, but each was unsuccessful within the scope of effort possible in the program. This work is summarized in the following paragraphs in order to provide a basis for future development efforts. It is felt, at this time, that the stiffened toroidal bellows can be produced using welding techniques, but modified tooling in order to implement revised bellows plates and welding fixtures would be required to overcome the problems experienced.

Inert Gas Welding

The preferred method for joining the bellows elements was inert gas shielded-arc, non-consumable electrode fusion welding (TIG welding).

Assembly of bellows plates and stiffener rings in welding fixtures brought problems to light very early in the fabrication effort. A combination of fit-up requirements and optimum location of metal fusion resulted in unsatisfactory welds. Inner stiffener rings fabricated from annealed hot rolled Inconel 718 plate could not be produced flat enough to result in intimate contact for the full surface of the bellows

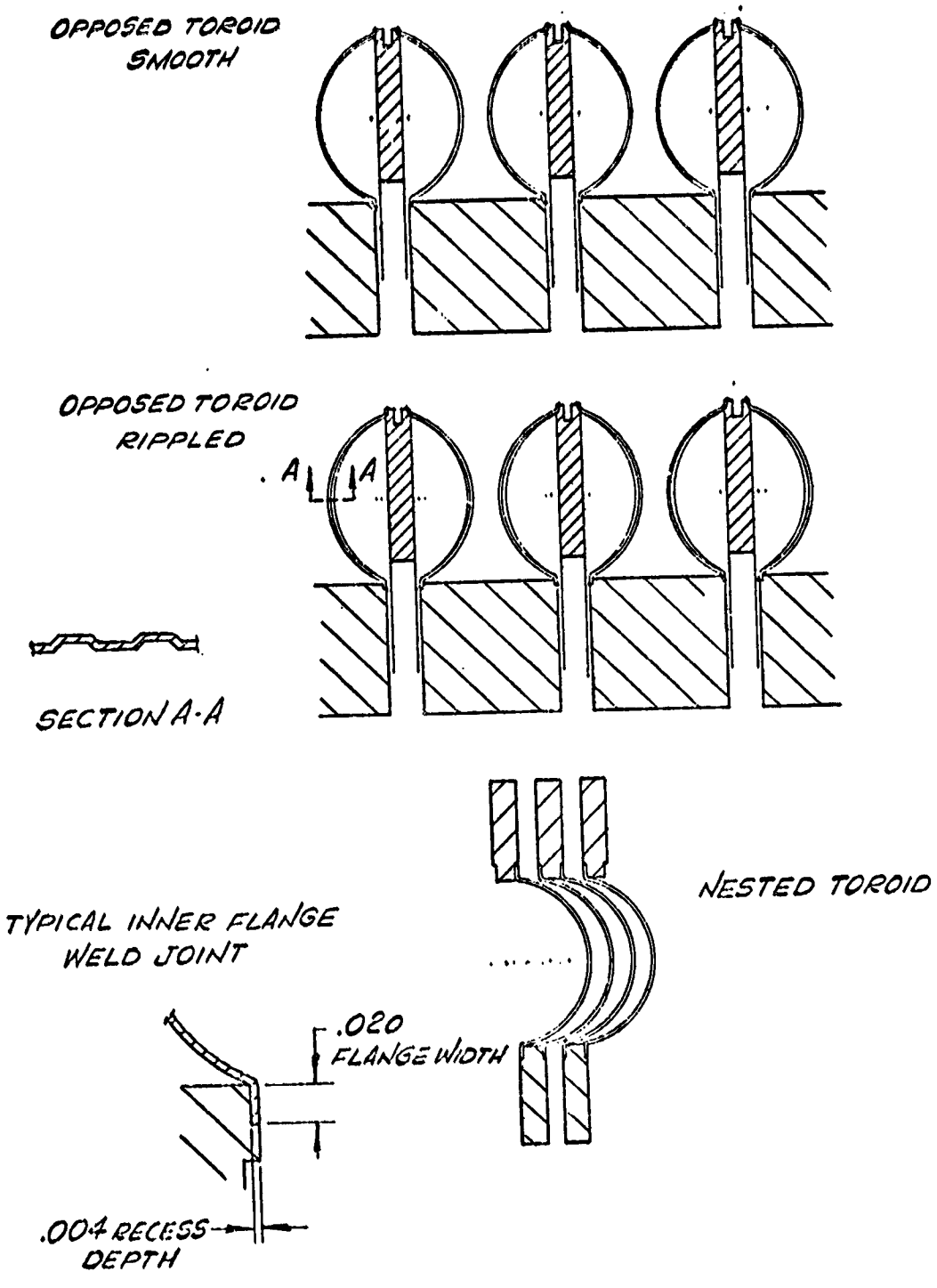

Figure 41. Bellows Configurations Selected for Fabrication Effort

plate flanges within the stiffener ring centering recesses. Blow-through was experienced in those areas where the parts were not in contact. The use of stiffener rings machined from annealed forged rings in order to effect radial grain flow and reduce the effects of the orientated grain structure of the rolled material, was indicated.

Bellows plate weld flanges were designed with what was considered the maximum practical radial dimension since the desirable characteristics of the toroidal type convolutions were predicated on close control of the geometry at the juncture of the plates and stiffener rings. The geometry of the stiffener ring as shown in the detail of Figure 41 was chosen so as to produce optimum wetting and fusion of the two elements in order to produce a weld as shown in Figure 42.

With 4 mil (1×10^{-4} m) toroid plate thickness and 10 mil (2.5×10^{-4} m) radial flange width, fixturing which would adequately centralize and bottom the plate within its recess and still allow adequate clearance between the welding electrode and the fixture elements, required great attention to detail.

Numerous fixture changes and rebuilds were made and the effects of increased ring recess depth were evaluated by welding elements incorporating these various changes. All were considered ineffective as solutions to the problem. A continuous joint of the quality depicted in the photomicrograph of Figure 42 could not be consistently produced throughout 360°.

In the light of the lack of success as recorded above, it was necessary to consider alternate means of fabrication by TIG welding techniques and the possibility of alternate welding systems.

A design change compatible with the TIG system was implemented for trial. This involved the addition of an integral lip on the stiffener ring, so located that it might be mechanically rolled over the bellows plate flange, retaining the flange in its stiffener ring recess. Figures 43(a), (b) and (c) illustrate the original and the changed design.

This innovation gave great promise on the first trial weld. One plate was satisfactorily welded throughout the 360° pass. This plate was an opposed type toroidal segment plate and was welded to its .200 inch (5×10^{-3} m) thick inner stiffener. The assembly sequence required that another similar plate be welded to the opposite side of the same stiffener ring. In the process of rolling down the retainer lip on this plate, the clamping action or lip-to-flange overlap was minimal over part of the circumference of the flange-stiffener ring interface. This was caused by out-of-roundness developed in the stiffener ring by localized heating during welding of the first plate. The actual clamping was not sufficient to retain the plate in position during this second welding operation. The same end result developed on parts having both plates lip-clamped in place prior to welding of

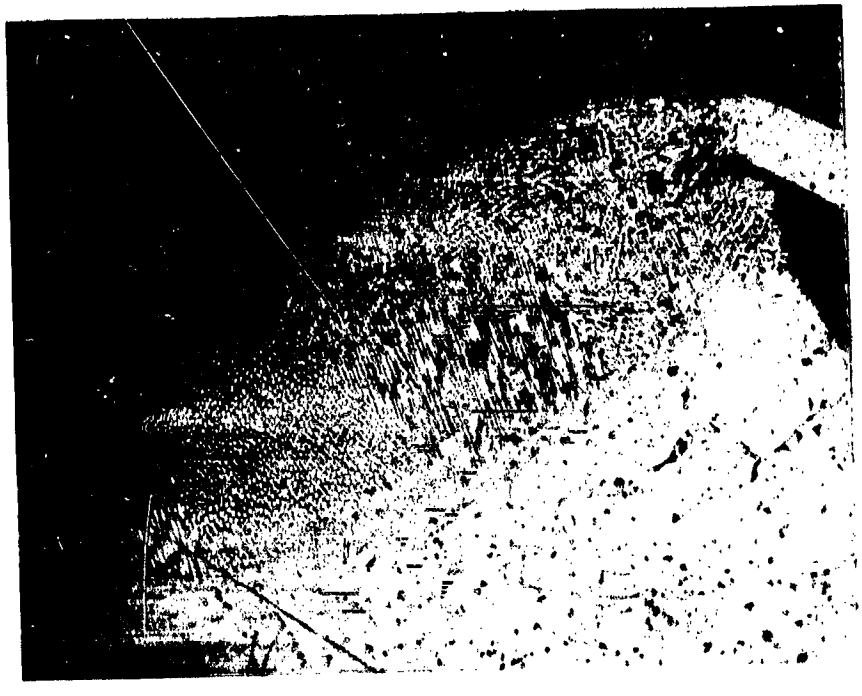

Magnification 100 x

Figure 42. Optimum TIG Weld

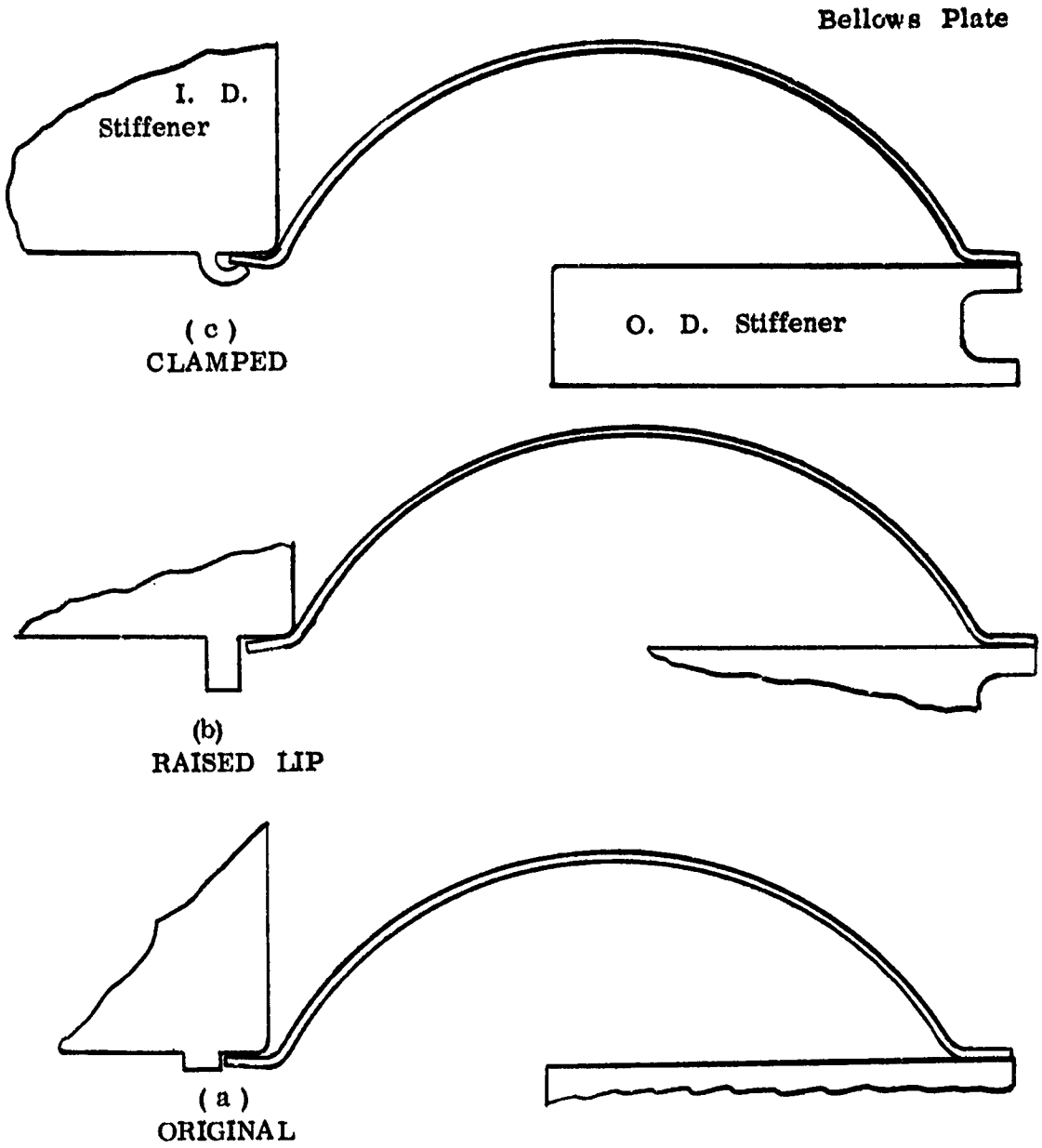

Figure 43. Stiffener Ring To Bellows Plate Joint

either plate. Changes in fixturing were not effective in the reduction of this problem.

Several trial welds were produced with variations in fixturing and stiffener ring design. Perfect 360° welds were not obtained with any degree of consistency in the production of acceptable inner stiffener ring and plate assemblies.

Electron Beam Welding

As an alternate welding system, Electron Beam Welding was selected as most promising for trial. Segmented toroidal bellows plates and inner stiffener rings for both the nested toroidal assembly and opposed plate assembly were made available to a subcontractor for production of specimen welds. Temporary fixturing was fabricated by the EB Welding contractor and trial welds were produced as depicted typically in Figure 44. As in TIG welding, parts fit-up was inadequate with fusion not occurring at the radius joining the bellows plate flange and the arcurate form of the semi-toroid. However, the experiment indicated an excellent chance of success with proper tooling and improvement in the form of the stiffener-ring recess. The sub-contractor's estimate of the funding required to fabricate proper permanent fixturing, setting up the EB equipment and producing the actual welds required for bellows assemblies was beyond the funding available in the program at this point in time.

Brazing

Another joining system, brazing, which had been considered earlier in the program and rejected because of anticipated lower joint strength as compared to the welding processes was at this point in the program given serious reconsideration as it was agreed that evaluation of bellows stability performance at less than the original test parameters would provide a contribution to the program.

General brazing experiments were performed by a source specializing in High Temperature Vacuum Brazing. The brazing alloy recommended as most suitable for production of a joint having maximum strength and compatability with Inconel 718 alloy and its final heat treating temperatures was 82-18 gold-nickel. The first process specimens consisted of an opposed type toroid brazed to an inner stiffner ring. Again, the trial of an alternate joining system produced promising results. Figure 45 is a photomicrograph of an early specimen. An excess of brazing alloy occurred at the critical point of the joint, the juncture of the outer diameter of the inner stiffener ring and the arcurate form of the semi-toroid. Several joints were produced in which the control of brazing alloy in the critical area was given special

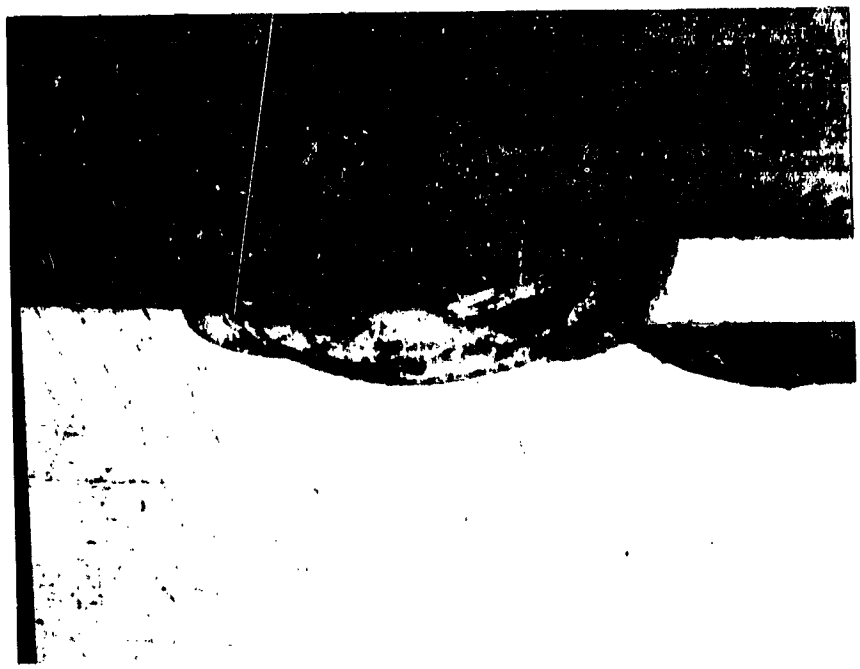

Magnification 100 x

Figure 44. Electron Beam Weld.

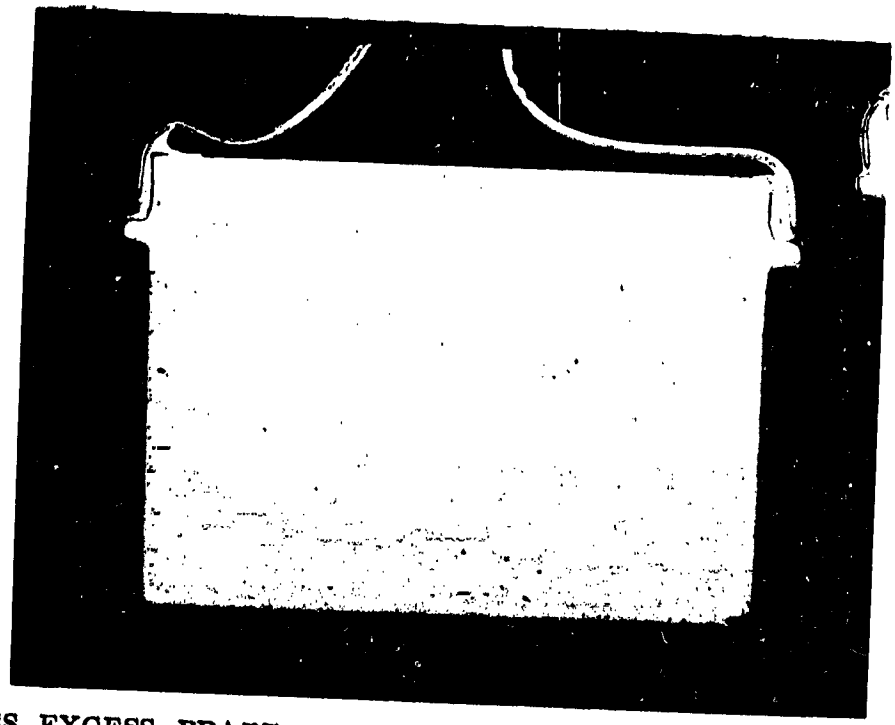

GROSS EXCESS BRAZE

SLIGHT EXCESS BRAZE

Figure 45. Braze Joint Specimen With Excess Amount Of Braze Alloy

attention. Figure 46 shows the progress made in this direction.

Figures 45 and 46 show cross-sections of the sub-assembly of an inner stiffener ring and two semi-toroid plates. The attachment of the required number of such sub-assemblies to intermediate outer stiffener rings as shown in Figure 47 was the next step in the fabrication of test bellows. The detailed parts were delivered to the brazing source for production of toroid-inner stiffener ring sub-assemblies which it was expected would be TIG welded to outer stiffener rings. TIG welds in the outer joints were expected to present no problem since they were designed geometrically similar to conventional Sealol bellows end fitting welds. Reference to the outer joint in Figure 43(c) will further explain the geometry of these welds where the weld bead joining the parts are formed by the fusion of elements having a reasonable ratio of cross-section. This ratio is in the range of two or three to one.

Sub-assemblies were brazed and tested for leak-tightness. These units required the repair of minor leaks in the brazed joint. This reheat, while it was performed in a controlled atmosphere furnace, produced an oxide layer on the surfaces of the parts. This oxidized material defied removal by bake-out in the vendor's vacuum furnace, nor could it be removed by a reverse plating process which produced unacceptable reduction in toroid plate thickness.

Although the original intent had been to TIG weld at the plate O. D.'s the brazing vendor suggested brazing all joints in each assembly simultaneously as a means of avoiding furnacing the sub-assembly units more than once. Trial of this suggestion would have required the production of additional detail parts and the purchase of considerable labor for pre-brazing preparation and expensive furnace time which could not be funded by the program at this point in time.

Surface Contamination

In addition to the problems associated with positioning of the parts and accurate fusion location control as described in the preceding sections, the quality of the fused metal was less than fully acceptable. This proved to be due to contamination traceable to tenacious surface oxides present on the 718 Inconel 4 mil plates fabricated from strip as received from the reroller supplier. Cleaning, pickling and storage in evacuated containers would not provide the program with contamination free plates. Experimentation did develop a successful electro-chemical reverse plating means for this purpose suitable for use on small numbers of plates. This process also resulted in a means of plate thickness control through the removal of surface material.

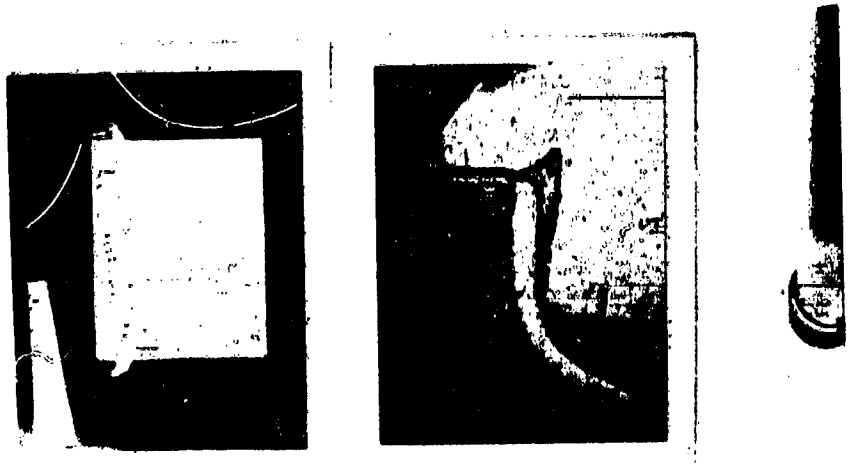

BRAZED

Figure 46 Braze Joint Specimen With Acceptible Amount Of Braze Alloy

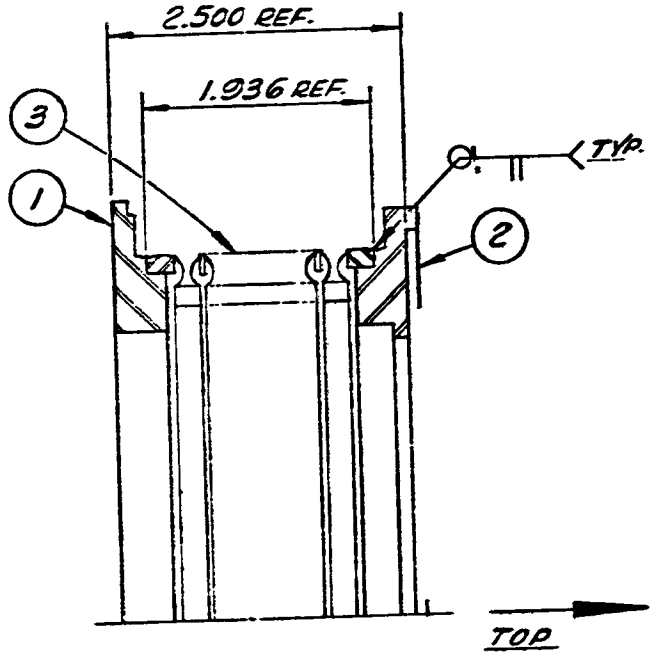

REVISIONS				
REV.	DESCRIPTION	CHANGE ORDER	BY	APP'D

DET.	PART NAME	REQ.	PART NO.
1	ADAPTOR (LOWER)	1	C-47951
2	ADAPTOR (UPPER)	1	C-47952
3	BELLOWS CORE ASSY.	1	D-47953

BELLOWS DATA: (REF.)

BELLOWS: 6.290 O.D. x 5.710 I.D.

MATERIAL: INC-718 x 4 MIL THICK

NO. CONVOLUTIONS: 6

CONSTRUCTION: SINGLE PLY

UNLESS OTHERWISE SPECIFIED	DRAWN	CHKD	PROJ ENG	ENG
REMOVE ALL BURRS. CORNER RADII & FILLETS .010-.020 DIMENSIONS ARE IN INCHES TOLERANCES ON: FRACTIONS ANGLES DECIMALS ± 0'0 ±1/2° .XX ±.0'0 .XXX ±.00'0	LS 3/19/69	3/21/69	3/27/69	
SURFACE FINISH (FINISH): ALL OVER; LAPPLAT WITHIN; LIGHT BANDS HELIUM	MATL & SPEC:			
	PROCESS SPEC.			

REFERENCED: F-MA#SE-6823-3

BELLOWS ASS'Y. (OPPOSED TOROIDAL SEGMENT)

SCALE FULL WEIGHT

SEALOL INC.
PROVIDENCE, R.I.

FIRST USED ON SO-78574

B 47950 REV.

Figure 47. Opposed Toroid Bellows Assembly

Summary

While the work to date has failed to produce bellows joints of consistent quality or test bellows for the verification of performance predictions, it is felt, at this time, that the experience gained in this program will make this goal attainable with further effort. TIG or EB welding is the recommended fabrication method because of the homogeneity of the parts and the high anticipated joint strength.

Overcoming the fusion problems will require revised plate shapes and improved welding fixtures. The plate attachment geometry would take a somewhat different form, as would the fusion area on the inner stiffener rings. Figure 48 depicts an improved weld construction which is felt to offer considerable promise.

In summary, the work to date has provided considerable experience in the welding problems for bellows of the recommended type which differ considerably from conventional bellows by virtue of the stiffener ring requirements. Also valuable expertise with the problems peculiar to Inconel 718 has been acquired as a result of this work. This work, it is felt, can provide a sound basis for the successful development of fabrication techniques for the stiffened opposed bellows configuration.

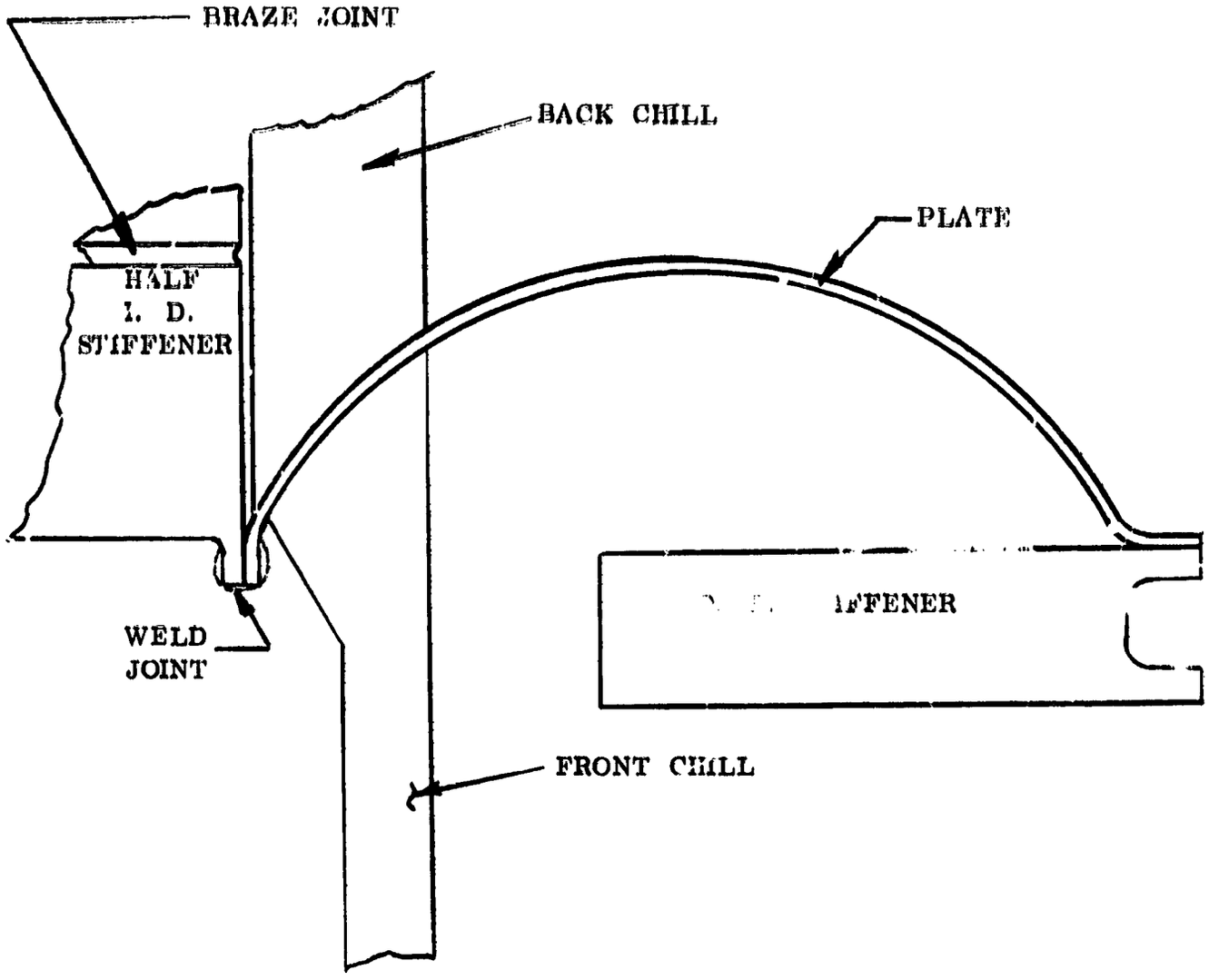

OPERATION

1. Weld Two I. D. Stiffeners
2. Braze I. D. Stiffeners (Halfs)
3. Weld or Braze Plate to O. D. Stiffener

NOT TO SCALE

Figure 48. Improved Weld Construction

DESIGN AND FABRICATION OF BELLOWS TEST APPARATUS

A test apparatus was designed and constructed for the purpose of verifying the analytical results under cryogenic conditions. Although this apparatus was not used for bellows testing in this program, it is described briefly in this section for reference purposes.

Specifications for the Test Apparatus

The basic purpose of the apparatus is, of course, the measurement of the change in effective diameter for a test bellows over the operating range of interest. Since the effective diameter or areas and pressures of interest combine to produce large pressure forces in comparison with the change due to nonlinearity, the approach adopted was to balance the pressure force on the bellows against that on a fixed, known area built into the apparatus and measure the difference. Since the expected variation in effective diameter is quite small (0.1 to 0.3 percent), the apparatus must be quite sensitive to variations in pressure force and must introduce very little friction force at its seals.

The pressure range applied to the bellows was specified to be 0 to 500 psi (345×10^6 newtons/m^2) applied internally and externally. The test bellows are to be deflected axially over a range of 0 to 0.150 inches (3.8×10^{-3} m). The fluid acting on the bellows will be both liquid and gaseous nitrogen.

In addition to the static tests above, a fatigue test consisting of cycling the test pressure with amplitudes of 0 to 500 psi (345×10^6 newtons/m^2) with a constant applied bellows deflection of 0.150 inches (3.8×10^{-3} m) was specified.

Description of the Apparatus

The apparatus, which was built and proof tested in parallel with the development of fabrication techniques is shown in the photographs of Figure 49. Figure 50 shows an overall schematic diagram of the test fixture. The description in the following paragraphs is keyed to the element numbers shown in this figure.

The overall structure of Figure 50 consists of the main support frame, base plate, and rods supporting a yoke which provides means for adjusting the axial position of a load cell relative to a basic pressure vessel in order to obtain load readings at various bellows test lengths and pressures.

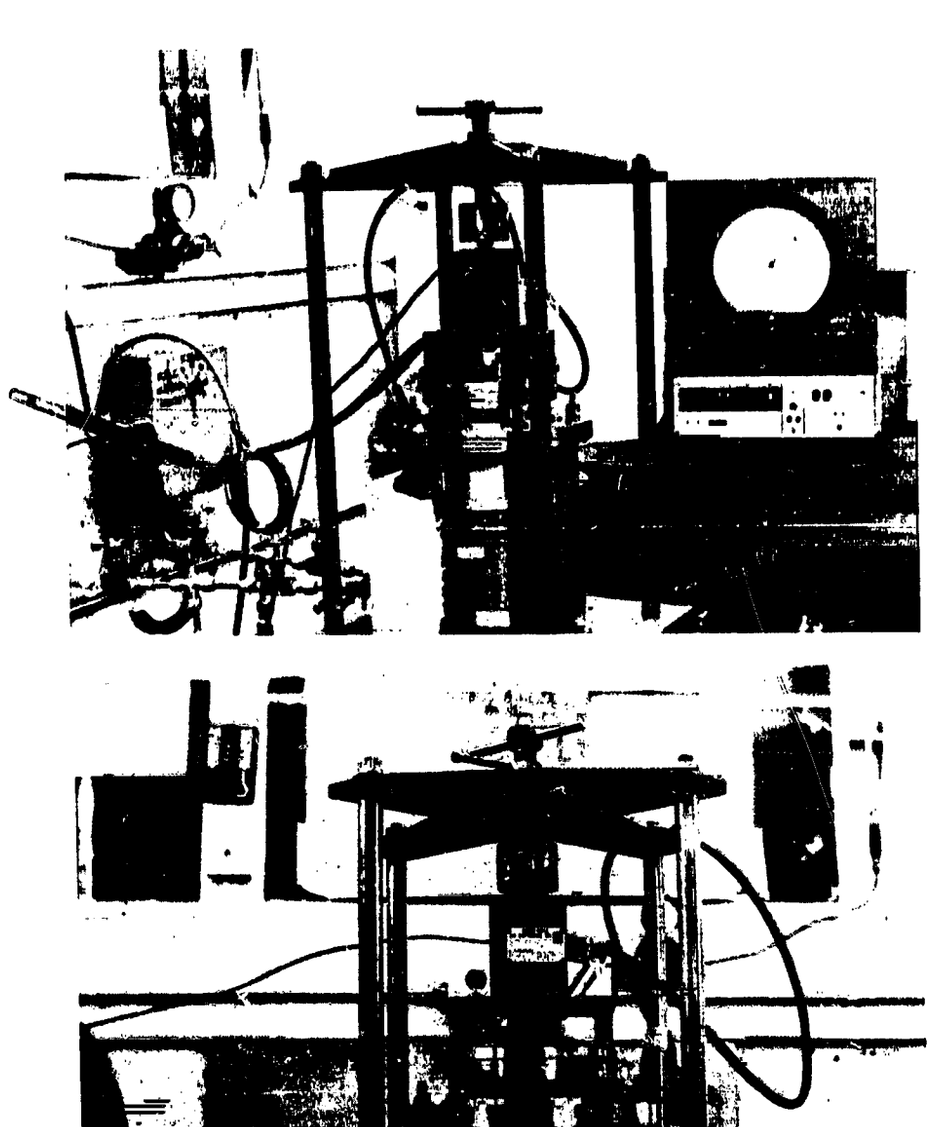

Figure 49. Bellows Test Apparatus

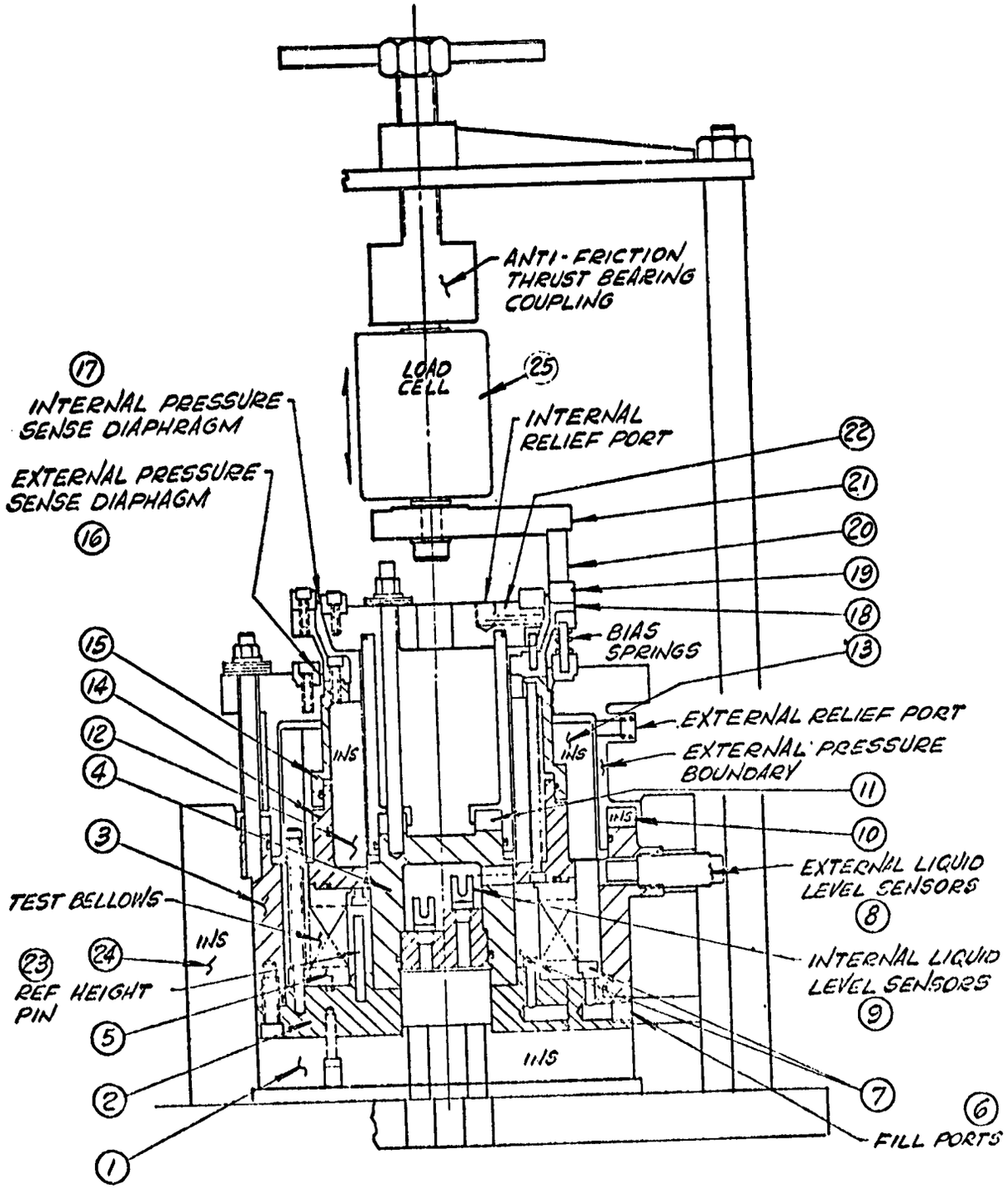

Figure 50. Bellows Test Fixture.

The pressure vessel is insulated from the frame base by Transite (1) which supports a steel pressure structure or base plate (2). Directly attached to this structure are a static separable outer pressure cylinder (3) and a multi-element static inner pressure cylinder (4) and the lower element of a Bellows Test Specimen (5). Fill ports (6) for the introduction of the cryogenic LN_2 to the inner and outer surfaces of the test bellows are provided in the base plate.

Flow spreaders (7) or baffles will direct the flow of the LN_2 to minimize the rate of localized cooling in the test bellows chamber.

Fluid level sensors (8) were designed into the outer cylinder wall to indicate the level of cryogenic liquid in the chamber outward of the Test Specimen. The sensors are upper and lower elements of an ultrasonic system indicating the range of the LN_2 liquid level and are located to indicate complete immersion of the test specimen in the LN_2 and provide assurance that the upper LN_2 level does not exceed its design limit. Control of the LN_2 level in the chamber inward of the test specimen is accomplished by a similar set of sensors (9) built into the base (2). In each case, thermal isolation of the external (16) and internal (17) diaphragms is maximized by insulating elements (10) and (11). Insulation (12) and (13) is also designed to assist in the isolation of the upper section of the apparatus. These elements are attached to cylinders (14) and (15) which transmit the forces developed by the test pressures on the specimen effective areas to the strain-gage load cell (25) which is adjustable in vertical position to effect deflection of the Bellows Test Specimen through elements 21, 20, 19, 18, 15 and 14. All elements of the pressure vessel are thus to be cooled and temperatures of the apparatus stabilized. Covering (24) was designed to provide a major means of reduction of heat input to the cold bellows test chamber.

Figure 51 shows an enlarged schematic diagram of the differential force sensing elements of the apparatus. The fixed reference areas for measurement of differential forces are defined by sealed cylindrical surfaces that allow at least 0.150 inch (3.8×10^{-3} m) relative axial movement between surfaces without friction loss. Self-compensating rolling diaphragms (16) and (17) were selected as seals having the desired characteristics. These elements, to operate properly, must be isolated thermally from the cryogenic temperature in the chamber housing. This is accomplished by means of the insulating elements described in the preceding paragraphs.

Operation

In operation the upper section of the pressurized side of the vessel relative to the Test Bellows will be filled with Gaseous Helium at test pressure to minimize loss of LN_2 and for further protection of

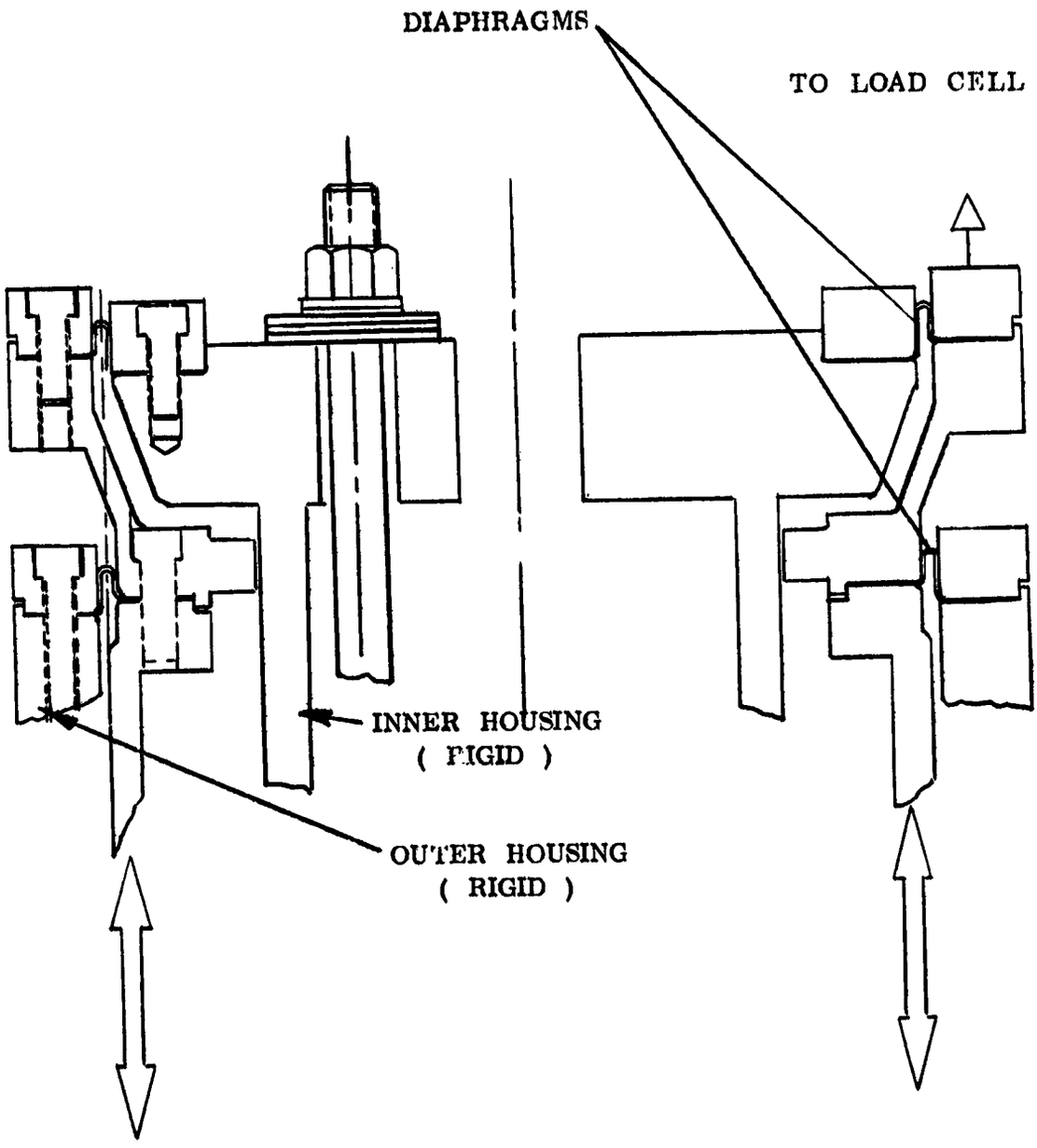

Figure 51. Differential Force Sensor

the rolling diaphragm seals. Gaseous nitrogen will be vented to the atmosphere from the low pressure side of the vessel. These conditions will, of course, be reversed as the test pressure conditions are reversed relative to the bellows.

Test Pressure measurements are intended to be read on a precision pressure gage sensing the pressure of the GHe above the LN_2 on the high pressure side of the test bellows. Loads are to be read on a digital indicator of the output signal from the strain gage load cell. Refering to Figure 50, Test Bellows deflection is determined relative to a Reference Height Pin (23) representing the compressed height of the bellows. Adjustment of the bellows height on test will be made by adjustment of the position of the load cell and actual measurements of the adjustments of the position sensing element (19) relative to the Reference Height Pin (23).

The apparatus was designed to perform Bellows Fatigue Tests by cycling the pressure applied to the LN_2 external to the bellows over a range of 0 to 500 psi (345×10^6 newtons/m^2) at a rate of 2 cycles per minute and with the Test Specimen in its compressed position. The GH3 blanket above the LN_2 fluid will be the pressure control medium handled through suitable valving and timing devices.

Testing

The Test equipment was constructed during the period of bellows fabrication and proof tested. The Apparatus was subjected to 750 psi (518×10^6 newton/m^2) water pressure at room temperature applied to the inner and outer pressure sections with a solid cylindrical element installed in place of a Test Bellows to separate the chambers. The only problem encountered concerned the rolling diaphragms (16) and (17). Clamping of the flanges of these parts proved inadequate as indicated in Figure 52 which is a photograph of a diaphragm which pulled loose from the clamping surfaces. Roughening of all clamping surfaces for each of the diaphragms shown in the partial view of Figure 51 for the upper section of the apparatus proved to be the solution to this problem. After this measure, the apparatus successfully passed the Proof Pressure Test.

Calibration Tests were not performed on this equipment as fabrication of test bellows was not successful. Verification of diaphragm areas was to be made against a telescoping cylinder having a sealed sliding diameter comparable to the designed areas of the diaphragms. Cylinder seal frictional hysteresis was to be obtained as the difference in forces in compression and extension and removed to correct the net forces, to be used in calibration of this element. Tests performed at room and LN_2 temperatures would indicate temperature sensitivity of the apparatus and need for the addition of temperature sensing.

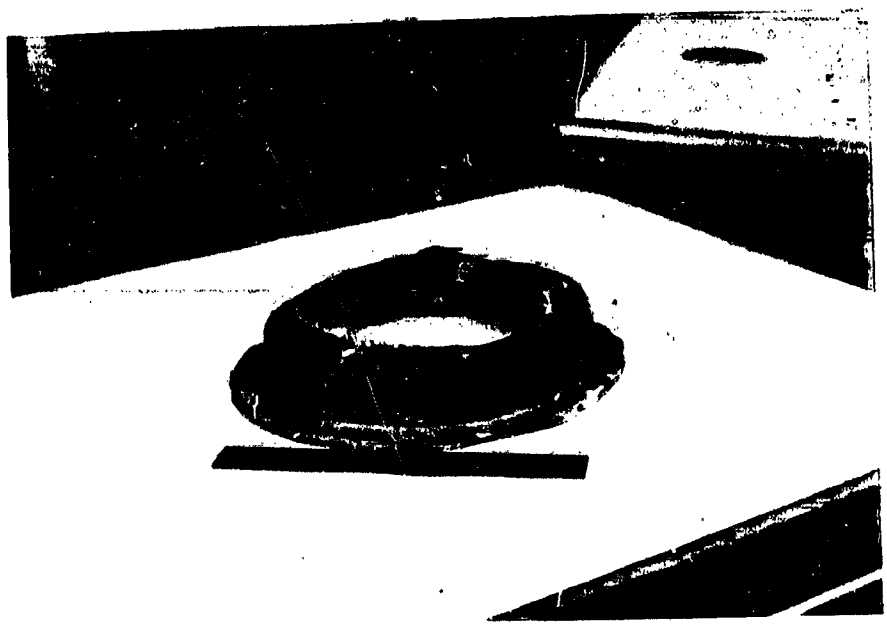

Figure 52. Subsequent to Pulling Loose From the Clamping Surfaces

CONCLUSIONS

The general overall conclusion that may be drawn from the analytical studies performed in this program is that for the range of bellows pressure, deflection, and size specified for this application, only toroidal bellows elements appear promising for achieving significant improvements in holding constant effective diameter.

Opposed toroidal plates appear capable of holding their effective diameter constant within 0.2 to 0.3 percent. Nested toroidal plates, because of their capability of providing more convolutions within the envelope appear capable of meeting the 0.1 percent goal. Even the opposed toroidal performance, should it be attained, would be significantly better than the current state of the art in seal bellows. Both configurations require a core made up of alternating flexible bellows plates and stiffener rings.

The fabrication studies pointed out the difficulty of fabricating this type of structure in the desired size range. No successful bellows was produced within the scope of work allowed by the contract, although several individual welded joints were successfully produced. The nested toroid, as was expected, proved much more difficult to fabricate. The main conclusion reached as a result of the fabrication studies is that the stiffened opposed toroid can be fabricated with further development of the configuration near the bellows plate-stiffener ring interface and improved fixturing. Considerable attention must be given to improvement of the surface quality of the Inconel 718 foil material and the use of light oxide removal procedures in order to achieve good welds.

It has been concluded as a result of the test development work that the pressure forces on the bellows in the desired range can be measured accurately enough to establish performance capability under cryogenic conditions. An apparatus for this purpose has been designed and built.

The systematic evaluation of the range of possible bellows plate configurations for this application resulted in several detailed conclusions which are summarized below for completeness:

(a) The performance predictions for the conventional corrugated plate bellows showed that it was extremely marginal in this application for meeting the nominal performance goals (spring rate and pressure resistance). Thus, it was not investigated in detail for non linear effects, and it was felt that corrugated plate bellows do not offer promise for achieving the small effective diameter change goal.

(b) The flat plate bellows suffers from the same factors that make the corrugated plate unsuitable in the specified size range.

(c) A wide variety of S-shaped plate configurations were analyzed and shown to have nominal performance characteristics comparable to, but generally inferior to, corrugated and flat plate bellows.

(d) Analysis of orthotropic plates (corrugations in a radial direction) showed that this feature has some promise, particularly on toroidal plates, for improving their linearity.

RECOMMENDATION

The bellows designs developed in this program are expected to significantly improv the state of the art in achieving small change in effective diameter fo. cryogenic seals. Accordingly, it is recommended that this work be used as a basis for continuing development toward this end.

Specifically, the next phase of the work should be aimed at developing improvements in the techniques used to weld flexible plates and stiffener rings having dissimilar sectional thicknesses. This will require modifications in both bellows plate and stiffener ring configuration near the interface. Also, improved weld fixturing will be required.

APPENDIX A

DESCRIPTION OF COMPUTER PROGRAM "SEALOL"

Computer program SEALOL predicts the stresses and deflections of a pair of metal bellows plates under combined axial force loading and pressure differential. It uses the linear shell equations and, thus, is limited to small deflections if an accurate solution is required. For the present study, SEALOL was used to conduct the screening analysis of corrugated and partial toroid plate shapes in order to establish their basic performance capabilities.

In this appendix, the capabilities, the programming basis, and a listing of SEALOL are provided.

Since NONLIN (described in Appendix B) is also capable of providing a linear range solution as well as a nonlinear one, a brief user-oriented comparison is given between the two programs in Appendix C.

Capabilities

SEALOL can treat bellows convolutions consisting of the various plate shapes shown in Figure A-1 as well as combinations of these cases. In the case of toroidal arc segments, up to four different segments having different radii can be treated.

The basic equations allow only constant plate thickness across the span. Stiffening rings can be represented only by imposing simple boundary conditions on the plate. (e. g. radially or rotationally fixed).

Both differential pressure loading and axial deflection can be treated.

Governing Equations

The program uses the classical first order shell equations reduced to two linear second order differential equations in terms of angular rotation, β , and horizontal force, rH. This formulation is similar to the Reissner-Meissner transformation.

The governing equations can be written,

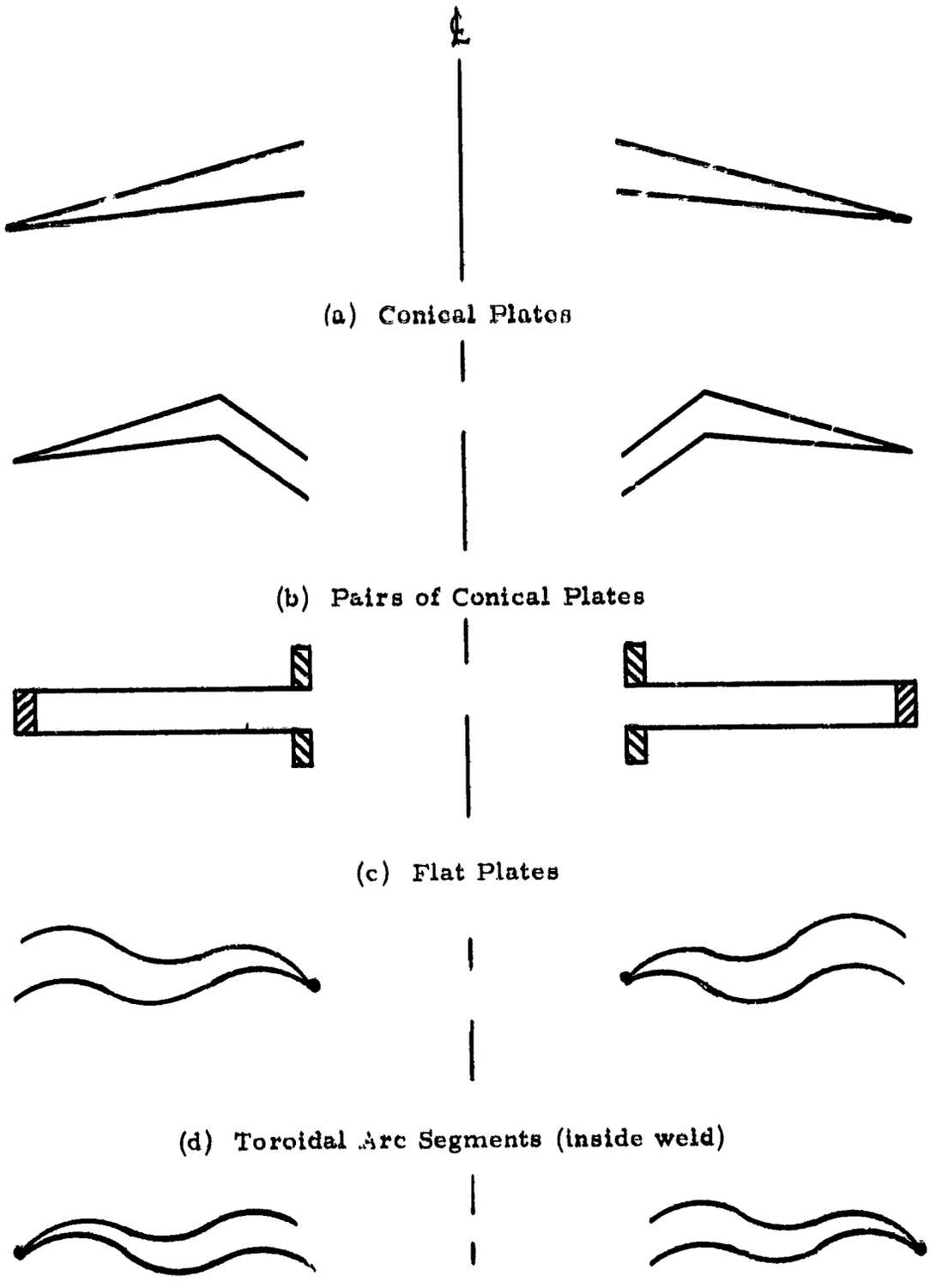

(a) Conical Plates

(b) Pairs of Conical Plates

(c) Flat Plates

(d) Toroidal Arc Segments (inside weld)

(e) Toroidal Arc Segments (outside weld)

Figure A-1. Various Shapes of Bellow Elements which can be Treated by SEALOL.

$$L_1 \beta - \frac{z\sqrt{1+z'^2}}{rD} \psi = \frac{\sqrt{1+z'^2}}{2rD} \left[p (r^2 - r_o^2) - \frac{\mathbb{P}}{\pi} \right] \quad (A-1)$$

$$L_2 \psi + \frac{z\sqrt{1+z'^2}}{rA} \beta = q_\psi \quad (A-2)$$

where the operators are defined by,

$$L_{1,2}( ) = \frac{d^2( )}{dr^2} + \left(\frac{1}{r} - \frac{z' z''}{1+z'^2} \right) \frac{d( )}{dr} - \frac{1}{r} \left[\frac{1}{r} \pm \nu \frac{z' z''}{1+z'^2} \right] ( ) \quad (A-3)$$

and q_ψ is defined as,

$$q_\psi = p \left[(z + rz'') + \left(\frac{1}{r} - \frac{z' z''}{1+z'^2} \right) (r z') \right] - \frac{1}{2\pi r} \left[\frac{z'}{r} + \nu \frac{z''}{1+z'^2} \right] \left[\pi p (r^2 - r_o^2) - \mathbb{P} \right] \quad (A-4)$$

The nomenclature for these equations is defined in Table A-1 and in Figure A-2.

The various possible prescribed boundary conditions for the plate edges are:

(a) Prescribed Rotation or Moment

$$\beta = \beta_o \text{ or } \beta_i \text{ at } r = r_o \text{ or } r_i$$

$$\frac{D}{\sqrt{1+z'^2}} (\beta' + \frac{\nu}{r} \beta) = M_o \text{ or } M_i \text{ at } r = r_o \text{ or } r_i$$

(b) Prescribed Radial Displacement or Force

$$\frac{rA}{\sqrt{1+z'^2}} \left\{ \psi' - \frac{\nu}{r} \psi - \frac{\nu z'}{2\pi r} \mathbb{P} - \left[r z' - \frac{\nu z'}{2r} (r^2 - r_o^2) \right] p \right\}$$

$$= u_o \text{ or } u_i \text{ at } r = r_o \text{ or } r_i$$

TABLE A-1

Nomenclature

A	=	$\frac{1}{Eh}$
β	=	rotation of middle plane
δ	=	axial displacement
D	=	$Eh^3/12\,(1-\nu^2)$
E	=	Young's modulus
h	=	thickness of plate
H	2	radial force
p	=	pressure load
ν	=	Poisson's ratio
ψ	=	rH
r_i	=	inner radius
r_o	=	outer radius
r, z	=	cylindrical coordinates
P	=	axial load
u	=	radial displacement
V	=	axial force
$( )'$	=	$\frac{\partial}{\partial r}( )$
$( )''$	=	$\frac{\partial^2}{\partial r^2}( )$

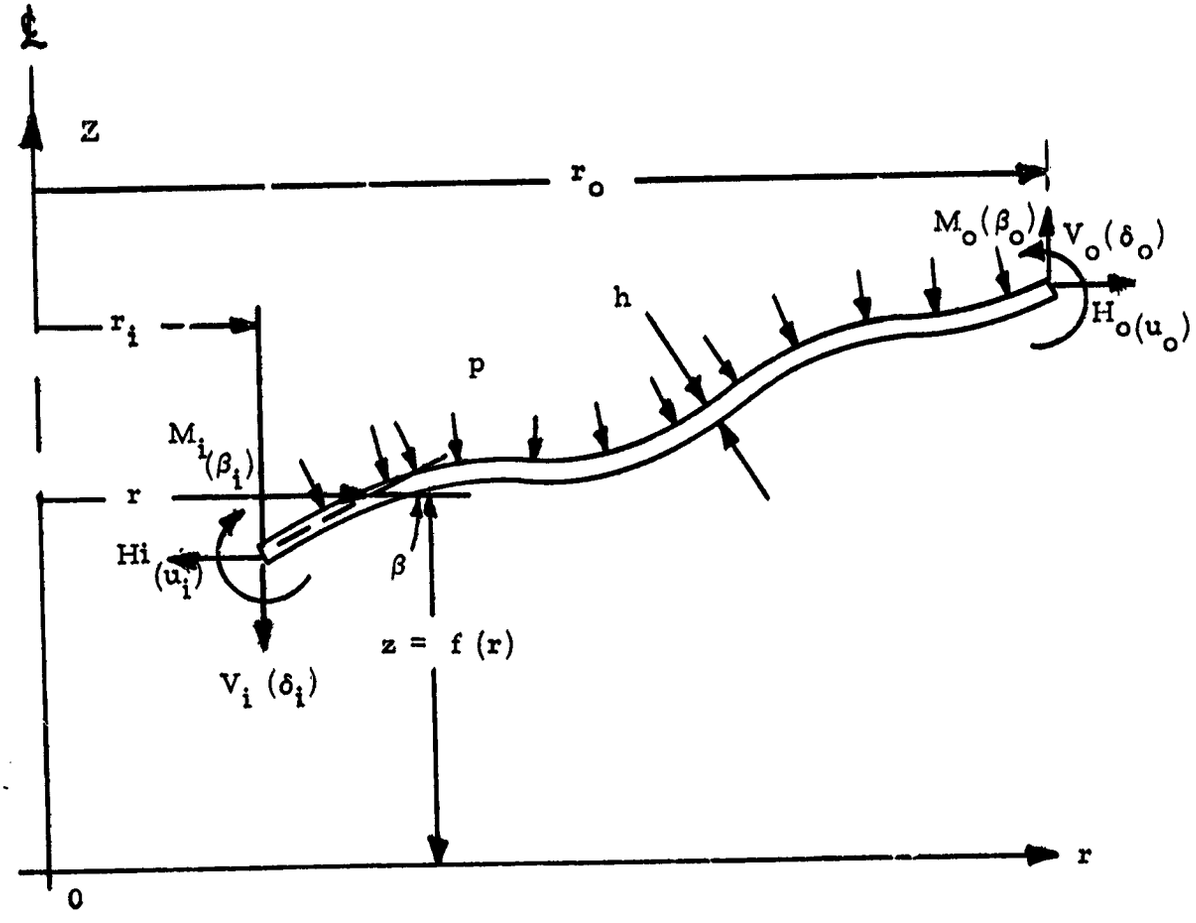

Figure A-2. Definition of Nomenclature.

$$\psi = r_o H_o \text{ or } r_i H_i \text{ at } r = r_o \text{ or } r_i$$

Method of Solution

The general computational method consists of the following steps:

(a) The computer program uses finite difference equivalents for the governing differential equations (central difference in the interior and forward or backward differences at the edges).

(b) The program determines a set of influence coefficients for each plate to represent the various deflections as functions of the imposed loadings and edge reaction forces.

(c) These coefficients are then used to formulate a set of simultaneous linear equations for each element of the bellows.

(d) This set of equations is solved for the unknown reaction forces taking into account the prescribed deflections or loads.

(e) The resulting known edge conditions can then be used to compute the displacements and stresses at any point in each bellows plate.

The computer program consists of the main program plus six subroutines. A logic flow diagram, defining the functions of the subroutines is provided in Figure A-3. The FORTRAN II listing of the program is given in the following section.

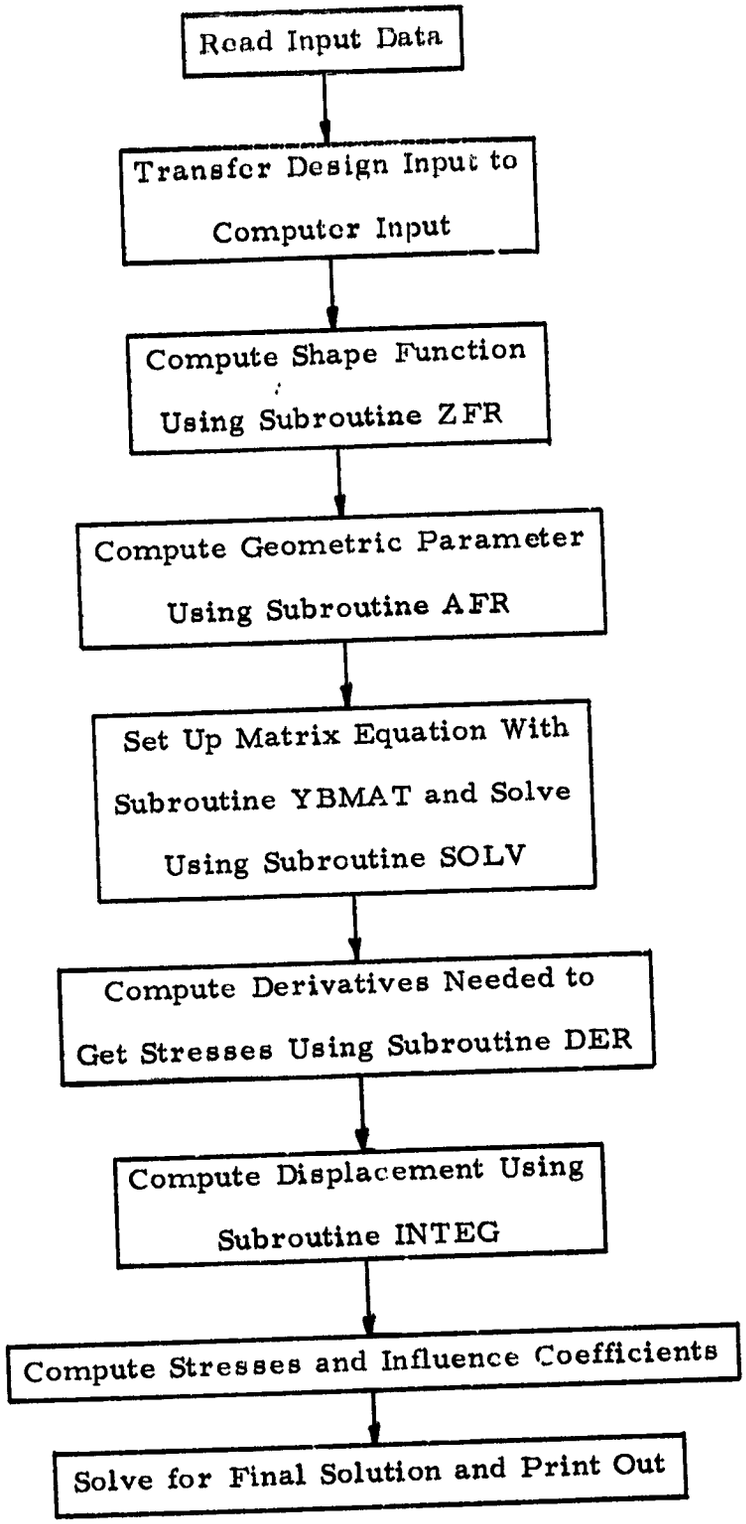

Figure A-3. Logic Flow Diagram of Program SEALOL.

```
C      MAIN PROBLEM
C      NR=1  PROBLEM NORMALLY CONTINUE
C      NR=2  CALCULATION FOR FINAL RESULT OF PLATE A ONLY
C      NGE=1  ELEMENT A OF SEALOL BELLOW PLATE
C      NGE=2  ELEMENT B OF SEALOL BELLOW PLATE
C      NGE=3  FLAT BELLOW FOR TESTING
C      NBC1, NBC2=1  GIVEN MOMENT, GIVEN HORIZONTAL FORCE
C      NBC1, NBC2=2  GIVEN ANGULAR DISP., GIVEN RADIAL DISP.
C      NBC1, NBC2=3  GIVEN ANGULAR DISP., GIVEN HORIZ. FORCE
C      NBC1, NBC2=4  GIVEN MOMENT, GIVEN RADIAL DISP.
C      BC1, BC3= MOMENT OR ANGULAR DISP.
C      BC2, BC4= HORIZ. FORCE OR RADIAL DISP.
C      NBC1, BC1, BC2= INSIDE BOUNDARY
C      NBC2, BC3, BC4= OUTSIDE BOUNDARY
C      NCONT=1, ONLY FOR GIVEN BOUNDARY CONDITION
C      NCONT=2, CALCULATE THE INFLUENCE COEFFICIENTS
C      NCONT=3, CALCULATE THE COMPLETE SOLUTIONS FOR TWO PLATE
C      STOP 111  NBC ERROR
C      STOP 444  SINGULAR MATRIX
C      SP IS SPAN
C      SENSE SWITCH 1  D=PRINT OUT NEW Y MATRIX, U=CONTINUE
C      SENSE SWITCH 3  D=CIRCULAR ARC,  U=SEALOL BELLOW
C      DELT= CORRECTION DUE TO THICKNESS
C      CPT=NORMALIZED PITCH
C      LOAD=1  INSIDE SUPPORT
C      LOAD=2  OUTSIDE SUPPORT
C      LOAD=3  COMPLETLY CLOSED BELLOW
       DIMENSION  C(10,10), Z(150), DFL(150), U(150), SRD(150), SCD(150),
      1           SRB(150),SCB(150),CA(10,10),CB(10,10),
      1            R(150), DZ(150), DDZ(150), A1(150), A2
      1            A4(150), A5(150), A6(150), A7(150), F(150), G(150),
      1          DF(150), DG(150), ZNEW(100),
      1          RMOMT(100), CMOMT(100), FH(100), COE1(10,10), COE2(10,10)
      1,COE(10,10),PR(10,2),ER(10),BD(4),
      1DSP(25,2,2),US(50,2,2),ROT(50,2,2),
      1RDS(50,2,2),CDS(50,2,2),RBS(50,2,2),CBS(50,2,2),
      1RMMT(50,2,2),CMMT(50,2,2),FHS(50,2,2)
       COMMON  R, DZ, DDZ, F, G, DF, DG, CVP, A1, A2, A3, A4, A5, A6, A7,
      1        XNU, D, A, CONST
     3 READ INPUT TAPE 5,13,((CA(I,J),I=1,7),J=1,4)
       READ INPUT TAPE 5,13,((CB(I,J),I=1,7),J=1,4)
       READ INPUT TAPE 5,10,SPT,RATA,RATB
       READ INPUT TAPE 5,10,ES,XNU,SV
     4 READ INPUT TAPE 5,10,SP,RI,TH,DELT,CPT
       READ INPUT TAPE 5,12,N,NBC1,NBC2,NCONT,LOAD
       GO TO (5,800,800),NCONT
     5 READ INPUT TAPE 5,10,BC1,BC2,BC3,BC4
   800 READ INPUT TAPE 5,801,DL,PRLD,LCONT,IRUN
    10 FORMAT(6E12.5)
   801 FORMAT(2E12.5,2I5)
    12 FORMAT(10I5)
    13 FORMAT(7F10.5)
       PLS=-1.00
       PIL=0.00
       NGE=1
       LK=1
   810 NR=1
       WRITE OUTPUT TAPE 6,812,IRUN
   812 FORMAT(///16H  ***RUN NUMBER=I5 //)
     6 T=TH
```

```
      PL=PLS
      PI=PIL
      E=ES
      GO TO (15,18,18,18),NGE
   15 DO 16 J=1,3
      DO 16 I=1,7
   16 C(I,J)=CA(I,J)*SP
      DO 516 J=4,5
      DO 516 I=1,7
  516 C(I,J)=CA(I,J)
      PTA=(SPT-CPT)*SP*RATA
      GO TO 20
   18 DO 19 J=1,3
      DO 19 I=1,7
   19 C(I,J)=CB(I,J)*SP
      DO 519 J=4,5
      DO 519 I=1,7
  519 C(I,J)=CB(I,J)
      PTB=-(SPT-CPT)*SP*RATB
      WRITE OUTPUT TAPE 6,21
   20 PT=CPT*SP
      RO=RI+SP
      A=1./(E*T)
      D1=12.*(1.-XNU**2.)
      D=E*(T**3.)/D1
C     D IS STIFFNESS OF PLATE
      WRITE OUTPUT TAPE 6, 923
      GO TO (901,902,903), LOAD
  901 WRITE OUTPUT TAPE 6,924,PL,PI
      P=PL
      GO TO 920
  902 WRITE OUTPUT TAPE 6,925,PL,PI
      P=PL-PI*(RO**2-RI**2)*3.14159
      GO TO 920
  903 WRITE OUTPUT TAPE 6,926,PL,PI
      P=PL-PI*(RO**2)*3.14159
      GO TO 920
  923 FORMAT(//20H  LOADING CONDITIONS)
  924 FORMAT(/46H  SUPPORTED INSIDE AND AXIAL LOAD              =E15.5/
     146H                          INTERNAL PRESSURE LOAD=E15.5)
  925 FORMAT(/47H  SUPPORTED OUTSIDE AND AXIAL LOAD             =E15.5/
     147H                           INTERNAL PRESSURE LOAD=E15.5)
  926 FORMAT(/39H  CLOSED BELLOW AMD AXIAL LOAD          =E15.5/
     139H                      INTERNAL PRESSURE =E15.5)
  920 PL=P
      WRITE OUTPUT TAPE 6,22
      WRITE OUTPUT TAPE 6,23,HO,RI,SP,PT,TH
      WRITE OUTPUT TAPE 6,24,PL,E,XNU,D,A
      J=N-2
      WRITE OUTPUT TAPE 6,39,J
   21 FORMAT(52H  SEALOL BELLOW ANALYSIS OF FOSTER MILLER ASSO. INC.)
   22 FORMAT(29H0  PARAMETER USED IN ANALYSIS)
   23 FORMAT(5H  RO=F8.5,6H   RI=F8.5,8H   SPAN=F8.5,9H   PITCH=F8.5,13H
     1   THICKNESS=F8.5)
   24 FORMAT(9H0   LOAD=E15.5,5H   E=E15.5,7H   XNU=E15.5,5H   D=E15.5,5
     1H   A=E15.5)
   39 FORMAT(27H   NUMBER OF DIVISION, N-2=I5)
   50 NGES=NGE
      GO TO (52,53,70,53),NGE
   52 PT=PTA+DELT
      GO TO 60
   53 PT=PTB-DELT
      NGE=2
   60 CALL SEALOL(C,RI,RO,PT,NGE)
      NGE=NGES
      CALL ZFR(C,N,H,K,Z)
```

```
      GO TO 80
   70 XN=N-2
      H=SP/XN
      J=N+1
      WRITE OUTPUT TAPE 6,73
   73 FORMAT(32H0  FLAT BELLOW PLATE FOR TESTING)
      DO 75 I=1,J
      XI=I
      R(I)=RI+(XI-2.)*H
      Z(I)=0.0
      DZ(I)=0.0
   75 DDZ(I)=0.0
   80 CALL AFR(R,Z,N,M,ANU,D,A)
   82 KONT=1
      GO TO (84,95),NR
   84 GO TO (99,85,85), NCONT
   85 BC1=0.
      BC2=0.
      BC3=0.
      BC4=0.
      P=0.
      PI=0.
      GO TO(86,87,88,89,90,91),KONT
   86 BC1=1.
      GO TO 99
   87 BC2=1.
      GO TO 99
   88 BC3=1.
      GO TO 99
   89 BC4=1.
      GO TO 99
   90 P=1.
      GO TO 99
   91 PI=1.
      GO TO 99
   95 BC1=-BC1
      BC2=-BC2
      BC3=-BC3
      BC4=-BC4
      P=PL
      PI=PIL
   99 WRITE OUTPUT TAPE 6,25
      WRITE OUTPUT TAPE 6,28
      GO TO (30,31,32,33),NBC1
   30 WRITE OUTPUT TAPE 6,35,BC1,BC2
      GO TO 40
   31 WRITE OUTPUT TAPE 6,36,BC1,BC2
      GO TO 40
   32 WRITE OUTPUT TAPE 6,37,BC1,BC2
      GO TO 40
   33 WRITE OUTPUT TAPE 6,38,BC1,BC2
      GO TO 40
   25 FORMAT(22H   BOUNDARY CONDITIONS)
   28 FORMAT(21H   AT INSIDE BOUNDARY)
   35 FORMAT(9H  MOMENT=E13.5,19H  HORIZONTAL FORCE=E13
   36 FORMAT(16H  ANGULAR DISP.=E13.5,15H  RADIAL DISP.=E13.5)
   37 FORMAT(16H  ANGULAR DISP.=E13.5,19H  HORIZONTAL FORCE=E13.5)
   38 FORMAT(9H  MOMENT=E13.5,15H  RADIAL DISP.=E13.5)
   40 WRITE OUTPUT TAPE 6,42
      GO TO (330,331,332,333),NBC2
   42 FORMAT (19H0  OUTSIDE BOUNDARY)
  330 WRITE OUTPUT TAPE 6,35,BC3,BC4
      GO TO 100
  331 WRITE OUTPUT TAPE 6,36,BC3,BC4
      GO TO 100
  332 WRITE OUTPUT TAPE 6,37,BC3,BC4
```

```
      GO TO 100
  333 WRITE OUTPUT TAPE 6,34,BC3,BC4
      GO TO 100
  100 SAVE=SV
      WRITE OUTPUT TAPE 6,639,P,PI
  639 FORMAT(/14H   AXIAL LOAD=E13.5,21H   INTERNAL PRESSURE=E13.5)
      CALL YRMAT(E,G,N,H,XNU,A,D,NBC1,NBC2,SV,P,PI,BC1,BC2,BC3,BC4,
      SV=SAVE
C     CALCULATION OF VERTICAL DEFLECTION
  120 CALL INTEG(F,H,N,DFL)
      J=N/2
      WRITE OUTPUT TAPE 6,122
      WRITE OUTPUT TAPE 6,123
      WRITE OUTPUT TAPE 6,124,(R(2*I),DFL(I),I=2,J)
      DFL(1)=0.0
      ZNEW(1)=Z(2)
      DO 130 I=2,J
  130 ZNEW(I)=Z(2*I)+DFL(I)
      WRITE OUTPUT TAPE 6,132
      WRITE OUTPUT TAPE 6,133
      WRITE OUTPUT TAPE 6,124,(R(2*I),ZNEW(I),I=1,J)
  132 FORMAT(25H0  Z(I) AFTER DEFORMATION)
  133 FORMAT(109H      R              ZNEW              R              ZNEW
     1          R              ZNEW              R              ZNEW)
  122 FORMAT(22H0  VERTICAL DEFLECTION)
  124 FORMAT (3(F16.5,E13.5))
  123 FORMAT(109H      R              DFL               R              DFL
     1          R              DFL               R              DFL)
C     DFL=VERTICAL DEFLECTION
C     U(I)=RADIAL DISPLACEMENT
C     SRD=DIRECT STRESS IN RADIAL DIRECTION
C     SCD=DIRECT STRESS IN CIRCUMFERENTIAL DIRECTION
C     SRB=BENDING STRESS IN RADIAL DIRECTION
C     SCB=BENDING STRESS IN CIRCUMFERENTIAL DIRECTION
      HINT=H
      H=T
      DO 150 I=2,N
      C1=XNU*G(I)/R(I)
      C2=A7(I)*(P-PI*(R(I)**2-RO**2)/(2.*CVP))+PI*R(I)*DZ(I)
      U(I)=A*CVP*(DG(I)-C1-C2)/A5(I)
      C1=A5(I)*R(I)/CVP
      C2=R(I)*H*C1
      SRD(I)=(G(I)+DZ(I)*CVP*(P-PI*(R(I)**2-RO**2)/(2.*CVP)))/C2
      SCD(I)=(DG(I)-PI*R(I)*DZ(I))/(H*C1)
      H2=H*H
      RMOMT(I)=-D*(DF(I)+XNU*F(I)/R(I))/C1
      CMOMT(I)=-D*(F(I)/R(I)+XNU*DF(I))/C1
      SRB(I)=6.*RMOMT(I)/H2
      SCB(I)=6.*CMOMT(I)/H2
      FH(I)=G(I)/R(I)
  150 CONTINUE
      WRITE OUTPUT TAPE 6,180
      WRITE OUTPUT TAPE 6,181
      WRITE OUTPUT TAPE 6,182
      WRITE OUTPUT TAPE 6,183,(I,R(I),U(I),SRD(I),SCD(I),SRB(I),SCB(I),
     1I=2,N)
  180 FORMAT(35H0  RADIAL DISPLACEMENT AND STRESSES)
  181 FORMAT(101H              LOCATION        RAD.DISP.  RAD.DIR.STRESS
     1TAN.DIR.STRESS RAD.BEND.STRESS TAN.BEND.STRESS)
  182 FORMAT(98H     I              R(I)              U(I)          SRD(I)
     1     SCD(I)            SRB(I)            SCB(I))
  183 FORMAT(I5,6E16.5)
      WRITE OUTPUT TAPE 6,185
      WRITE OUTPUT TAPE 6,186,(I,R(I),RMOMT(I),CMOMT(I),FH(I),F(I),I=2,
     1N)
  185 FORMAT(87H0    I              R(I)          RMOMT(I)          CMOMT(I)
```

```
     1    HOR. FORCE       ANG. OF ROT.)
186  FORMAT(I5,6F10.5)
     H=HINT
     GO TO (300,188,188),NCONT
188  GO TO (190,240,300),NGE
190  COE1(1,KONT)=F(Z)
     COE1(2,KONT)=U(Z)
     COE1(3,KONT)=F(N)
     COE1(4,KONT)=U(N)
     J=N/2
     COE1(5,KONT)=PL(J)
     IF(KONT-6) 192,195,195
192  KONT=1+KONT
     GO TO 85
195  WRITE OUTPUT TAPE 6,198
     WRITE OUTPUT TAPE 6,199
198  FORMAT(38H0     INFLUENCE COEFFICIENTS OF PLATE A)
199  FORMAT(73H0       M1              M1              M2              M2
     1  P               PI)
     WRITE OUTPUT TAPE 6, 610,((COE1(I,J),J=1,6),I=1,5)
610  FORMAT(6E13.5)
     GO TO (300,5,820),NCONT
820  NGE=2
     PLS=1.0
     PIS=0.0
     GO TO 6
240  COE2(1,KONT)=F(Z)
     COE2(2,KONT)=U(Z)
     COE2(3,KONT)=F(N)
     COE2(4,KONT)=U(N)
     J=N/2
     COE2(5,KONT)=PL(J)
     IF(KONT-6) 242,245,245
242  KONT=1+KONT
     GO TO 85
245  WRITE OUTPUT TAPE 6,248
246  WRITE OUTPUT TAPE 6,199
248  FORMAT(38H0     INFLUENCE COEFFICIENTS OF PLATE B)
     WRITE OUTPUT TAPE 6, 610,  ((COE2(I,J),J=1,6),I=1,5)
     GO TO (300,300,249),NCONT
249  DO 250 I=1,4
     DO 250 J=1,4
250   COE(I,J)=COE1(I,J)+COE2(I,J)
     DO 255 J=1,4
     PR(J,1)=COE1(J,5)+COE2(J,5)
255  PR(J,2)=COE1(J,6)+COE2(J,6)
     DS=1.0
     J=4
     M=XSIMEQF(10,J,2,COE,PR,DS,ER)
     GO TO (268,261),M
261  WRITE OUTPUT TAPE 6,263
     GO TO 267
262  WRITE OUTPUT TAPE 6,265
     GO TO 267
267  STOP 555
263  FORMAT(17H0  OVER/UNDERFLOW)
265  FORMAT(18H0  COE IS SINGULAR)
268  BC1=-COE(1,1)
     BC2=-COE(2,1)
     BC3=-COE(3,1)
     BC4=-COE(4,1)
     NCONT=1
     NGE=4
     H=HINT
     DO 830 I=1,4
830  BD(I)=-COE(I,2)
```

```
      GO TO 6
300   GO TO (302,505,506,301),NGE
301   NH=2
      NGE=1
      PLS=-PLS
      PIL=-PIL
      K=N/2
      DEL2=DFL(K)
      NRL=1
      GO TO 835
302   GO TO (502,405),NR
502   KMAX=N/2
      DEL1=DFL(KMAX)
      NRL=2
      PLS=-PLS
      PIL=-PIL
      NGE=2
      BC1=-BC1
      BC2=-BC2
      BC3=-BC3
      BC4=-BC4
      GO TO 835
505   KMAX=N/2
      DEL2=DFL(KMAX)
      NRL=3
      NR=2
      GO TO 835
405   KMAX=N/2
      DEL1=DFL(KMAX)
      NR=1
      NCONT=3
      NRL=4
835   KMAX=N/2
      DO 836 K=1,KMAX
836   DSP(K,NR,LK)=DFL(K)
      DO 838 I=2,N
      US(I,NR,LK)=U(I)
      ROT(I,NR,LK)=P(I)
      RDS(I,NR,LK)=SRD(I)
      CDS(I,NR,LK)=SCD(I)
      RBS(I,NR,LK)=SRB(I)
      CBS(I,NR,LK)=SCB(I)
      RMMT(I,NR,LK)=RMOMT(I)
      CMMT(I,NR,LK)=CMOMT(I)
838   FHS(I,NR,LK)=FH(I)
      GO TO (6,6,506,506),NRL
506   DEL=DEL2-DEL1
      SK=ABSF(1./DEL)
      GO TO (840,842),LK
840   SKF=SK
      GO TO 845
842   SKP=SK
845   WRITE OUTPUT TAPE 6,410,DEL1
      WRITE OUTPUT TAPE 6,411,DEL2
      WRITE OUTPUT TAPE 6,412,DEL
      WRITE OUTPUT TAPE 6,413,SK
410   FORMAT(20H  DEFL. OF PLATE A =E15.5)
411   FORMAT(20H  DEFL. OF PLATE B =E15.5)
412   FORMAT(20H  DEFL. PER CONV.  =E15.5)
413   FORMAT(20H  SPRING RATE      =E15.5)
849   GO TO (850,870),LK
850   LK=2
860   GO TO (862,862,865),NCONT
862   BC1=-BC1
      BC2=-BC2
      BC3=-BC3
```

```
      BC4=-BC4
      PLS=0.0
      PIL=-1.00
      NGE=1
      H=HINT
      NR=1
      GO TO 6
  865 BC1=BD(1)
      BC2=BD(2)
      BC3=BD(3)
      BC4=BD(4)
      PLS=0.0
      PIL=1.00
      NCONT=1
      NGE=4
      H=HINT
      GO TO 6
  870 PLS=-(SKF/SKP)*PRLD-DL*CPI*SP*SKF
      KMAX=N/2
      WRITE OUTPUT TAPE 6,872,PRLD,DL,PLS,SKF,SKP
  872 FORMAT(//32H    **PRESSURE LOAD                =E12.5, /
     1 32H      PRESET PREF LENGTH CHANGE =E12.5, /
     2 32H      REACTION AXIAL LOAD       =E12.5, /
     3 40H      SPRING CONSTANT FOR AXIAL LOAD    =E12.5, /
     4 40H      SPRING CONSTANT FOR PRESSURE LOAD =E12.5, / )
      DO 895 NR=1,2
      SN=1.0
      PL=SN*PLS
      PI=PRLD*SN
      GO TO (875,878),NR
  875 WRITE OUTPUT TAPE 6,876
      GO TO 880
  878 WRITE OUTPUT TAPE 6,879
  876 FORMAT (//16H     *FOR PLATE A )
  879 FORMAT (//16H     *FOR PLATE B )
  880 DO 882 K=2,KMAX
  882 DFL(K)=PL*DSP(K,NR,1)+PI*USP(K,NR,2)
      DO 890 I=2,N
      U(I)=US(I,NR,1)*PL+US(I,NR,2)*PI
      SRD(I)=RDS(I,NR,1)*PL+RDS(I,NR,2)*PI
      SCD(I)=CDS(I,NR,1)*PL+CDS(I,NR,2)*PI
      SRB(I)=RBS(I,NR,1)*PL+RBS(I,NR,2)*PI
      SCB(I)=CBS(I,NR,1)*PL+CBS(I,NR,2)*PI
      RMOMT(I)=RMMT(I,NR,1)*PL+RMMT(I,NR,2)*PI
      CMOMT(I)=CMMT(I,NR,1)*PL+CMMT(I,NR,2)*PI
      FH(I)=FHS(I,NR,1)*PL+FHS(I,NR,2)*PI
  890 F(I)=ROT(I,NR,1)*PL+ROT(I,NR,2)*PI
      SMAX=0.0
      DO 892 I=2,N
      DO 892 L=1,2
      SN=2*L-3
      S1=SRD(I)+SRB(I)*SN
      IF (SMAX-ABSF(S1)) 701,702,702
  701 SMAX=ABSF(S1)
      IMAX=I
  702 S2=SCD(I)+SCB(I)*SN
      S3=ABSF(S1-S2)
  703 IF (SMAX-ABSF(S2)) 704,705,705
  704 SMAX=ABSF(S2)
      IMAX=I
  705 IF (SMAX-S3) 891,892,892
  891 SMAX=S3
      IMAX=I
  892 CONTINUE
      WRITE OUTPUT TAPE 6,893,SMAX,R(IMAX)
  893 FORMAT (//30H     MAXIMUM STRESS INTENSITY= E12.5,/
```

```
 122H      AT LOCATION OF HH  F12.5)
     WRITE OUTPUT TAPE 6,162
     WRITE OUTPUT TAPE 6,123
     WRITE OUTPUT TAPE 6,124,(F(2*I),DEL(I),I=2,J)
     WRITE OUTPUT TAPE 6,180
     WRITE OUTPUT TAPE 6,181
     WRITE OUTPUT TAPE 6,182
     WRITE OUTPUT TAPE 6,183,(I,R(I),U(I),SRB(I),SCB(I),SRR(I),SCR(I),
    1I=2,N)
     WRITE OUTPUT TAPE 6,184,
     WRITE OUTPUT TAPE 6,185,(I,R(I),RMOMT(I),CMOMT(I),FH(I), F(I),I=2,
    1N)
 805 CONTINUE
     GO TO (3,4,5,6,1000),LCONT
 806 READ INPUT TAPE 5,801,DL,PRLD,LCONT
     GO TO 870
1000 CALL EXIT
     END
```

```
C      SUBROUTINE SEALOL(C,RI,RO,PT,NGE)
C      CALCULATION OF INPUT DATA IN MATRIX FORM
       SUBROUTINE SEALOL (C,RI,RO,PT,NGE)
       DIMENSION  C(10,10)
       TANF(X)=SINF(X)/COSF(X)
       AG=ATANF(C(1,4))
       ZH=C(1,3)*SINF(AG)-C(2,3)*COSF(AG)-C(2,2)
       DO 105 I=1,7
  105  C(I,1)=RO-C(I,1)
       IF (SENSE SWITCH 3) 100,106
  100  C(2,2)=C(2,3)**2-(C(2,1)-C(1,1))**2
       C(2,2)=SQRTF(C(2,2))
       C(2,2)=-1.*C(2,4)*C(2,2)
       GO TO 109
  106  DO 108 I=2,7
  108  C(I,2)=ZH+C(I,2)
  109  SP=RO-RI
       C(1,2)=0.0
       AGG=SP**2-PT**2
       AGG=SQRTF(AGG)
       AGG=PT/AGG
       AG=ATANF(AGG)
       GO TO (110,110,130), NGE
  110  DO 115 I=1,7
       ROLD=C(I,1)
       ZOLD=C(I,2)
       Z1=ZOLD
       R1=ROLD-RI
       C(I,1)=R1*COSF(AG)+Z1*SINF(AG)
       C(I,2)=Z1*COSF(AG)-R1*SINF(AG)
       C(I,1)=RI+C(I,1)
  115  CONTINUE
       AGL1=ATANF(C(1,4))
       AGL7=ATANF(C(7,4))
       C(1,4)=TANF(AGL1-AG)
       C(7,4)=TANF(AGL7-AG)
       GO TO (120,117,130),NGE
  117  WRITE OUTPUT TAPE 6,118
  118  FORMAT(19H0     BELLOW PLATE B)
       GO TO 123
  120  WRITE OUTPUT TAPE 6,121
  121  FORMAT(19H0     BELLOW PLATE A)
```

```
123 AG=ATAN(C(1,4))
    C(1,6)=H1*C(1,3)*COS(AG)
    DO 125 I=2,5
    J=I-1
125 C(I,6)=C(I,1)+C(I,4)*(C(J,1))-C(I,1))/(C(I,3)*C(J,3))
    AG7=ATAN(C(7,4))
    C(6,6)=RO-C(7,3)*COS(AG7)
    C(7,6)=R0+C(7,4)
    C(1,3)=0.0
    C(7,3)=0.0
    WRITE OUTPUT TAPE 6,126
    WRITE OUTPUT TAPE 6,127
    WRITE OUTPUT TAPE 6,128,((C(I,J),J=1,5),I=1,7)
126 FORMAT(31H  INPUT MATRIX OF SFALOL BELLOW)
127 FORMAT (7H     RC=,15H                ZC=,15H                AI=,15H
   1     FI=,15H                RI=)
128 FORMAT (5F15.7)
130 RETURN
    END
```

```
C       SUBROUTINE  YHMAT
C       CALCULATION OF FUNCTION BETA(=F) AND PSI(=G)
C       SUBROUTINE YH A1(F,G,N,M,ANU,A,D,NHC1,NBC2,SV,P,PI,
      1 HC1,HC2,HC3,HC4)
       DIMENSION  Y(102,102), B(102), R(150), DZ(150), DDZ(150), F(150),
      1           G(150), DF(150), DG(150), A1(150), A2(150), A3(150),
      1           A4(150), A5(150), A6(150), A7(150)
       COMMON  R, DZ, DDZ, F, G, DF, DG, CVP, A1, A2, A3, A4, A5, A6, A7,
      1        ANU, D, A
C      CALCULATION OF Y AND B MATRIX EXCEPT B.C.
       J=2*N+2
       M2=M*M
       DO 407 I=1,J
       B(I)=0.0
       DO 407 K=1,J
  407  Y(I,K)=0.0
       Y(2,1)=10.-3.*M*A1(2)
       Y(2,2)=-15.-10.*M*A1(2)-12.*M2*A2(2)
       Y(2,3)=-4.+18.*M*A1(2)
       Y(2,4)=14.-6.*M*A1(2)
       Y(2,5)=-6.+M*A1(2)
       Y(2,6)=1.
       Y(2,N+3)=-12.*M2*A4(2)/D
       B(2)=12.*M2*A6(2)*(PI*(R(2)**2-R(N)**2)/(2.*CVP)-P)/D
  415  Y(N,N-4)=1.
       Y(N,N-3)=-6.-M*A1(N)
       Y(N,N-2)=14.+6.*M*A1(N)
       Y(N,N-1)=-4.-10.*M*A1(N)
       Y(N,N)=-15.+10.*M*A1(N)-12.*M2*A2(N)
       Y(N,N+1)=10.+3.*M*A1(N)
       Y(N,2*N+1)=-12.*M2*A4(N)/D
       B(N)=-12.*M2*A6(N)*P/D
  422  Y(N+3,N+2)=Y(2,1)
       Y(N+3,N+3)=-15.-10.*M*A1(2)-12.*M2*A3(2)
       Y(N+3,N+4)=Y(2,3)
       Y(N+3,N+5)=Y(2,4)
       Y(N+3,N+6)=Y(2,5)
       Y(N+3,N+7)=1.
       Y(N+3,2)=12.*M2*A4(2)/A
       B(N+3)=12.*M2*(A6(2)*(P-P1*(R(2)**2-R(N)**2)/(2.*CVP))
      1  +PI*(DZ(2)+M*(2)*DDZ(2)+A1(2)*R(2)*DZ(2)))
  429  Y(2*N+1,2*N-3)=1.
```

```
      Y(2*N+1,2*N-2)=B1(I,J)
      Y(2*N+1,2*N-1)=B2(I,J)
      Y(2*N+1,2*N)=B3(I,J)
      Y(2*N+1,2*N+1)=-10.+10.*H*A1(I)-12.*H2*A3(N)
      Y(2*N+1,2*N+2)=B4(I,J)
      Y(2*N+1,N)=12.*H2*A4(I)/A
      B(2*N+1)=12.*H2*(A5(N)*P+P1*(DZ(I)+B(I)*DDZ(N)+A1(N)*R(N)*DZ(I)))
      J=N-1
      DO 450 I=3,J
      K=I+N+1
      Y(I,I-2)=H*A1(I)-1.
      Y(I,I-1)=16.-30.*H*A1(I)
      Y(I,I)=-30.-12.*H2*A2(I)
      Y(I,I+1)=16.+30.*H*A1(I)
      Y(I,I+2)=-1.-H*A1(I)
      Y(I,K)=12.*H2*A4(I)/D
      Y(K,K-2)=Y(I,I-2)
      Y(K,K-1)=Y(I,I-1)
      Y(K,K)=-30.-12.*H2*A3(I)
      Y(K,K+1)=Y(I,I+1)
      Y(K,K+2)=Y(I,I+2)
      Y(K,I)=12.*H2*A4(I)/A
      B(I)=12.*H2*A5(I)*(P1*(R(I)**2-R(N)**2)/(2.*CVP)-P)/D
  450 B(K)=12.*H2*(A5(I)*(P-P1*(R(I)**2-R(N)**2)/(2.*CVP))
     1   +P1*(DZ(I)+B(I)*DDZ(I)+A1(I)*R(I)*DZ(I)))
      WRITE OUTPUT TAPE 6,210
      WRITE OUTPUT TAPE 6,211
  210 FORMAT (3RH0  Y MATRIX CALCULATED EXCEPT FOR B,C,)
  211 FORMAT (3RH0  B MATRIX CALCULATED EXCEPT FOR B,C,)
      GO TO (462,468,468,462),NBC1
  462 Y(1,1)=-3.
      Y(1,2)=-10.+12.*ANU*H/R(2)
      Y(1,3)=18.
      Y(1,4)=-6.
      Y(1,5)=1.
      B(1)=-12.*H*A5(2)*P(2)*BC1/(D*CVP)
      GO TO (465,468,468,475),NBC1
  465 Y(N+2,N+3)=1.
      B(N+2)=R(2)*BC2
      GO TO 483
  468 Y(1,2)=1.
      B(1)=BC1
      GO TO (482,475,465,482),NBC1
  475 Y(N+2,N+2)=-3.
      Y(N+2,N+3)=-10.-12.*H*ANU/R(2)
      Y(N+2,N+4)=18.
      Y(N+2,N+5)=-6.
      Y(N+2,N+6)=1.
      B(N+2)=12.*H*(A5(2)*BC2/(CVP*A)
     1   +P1*R(2)*DZ(2)
     1   +A7(2)*(P-P1*(R(2)**2-R(N)**2)/(2.*CVP)))
      GO TO 483
C     STOP 111 NBC ERROR
  482 STOP 111
  483 GO TO (484,490,490,484),NBC2
  484 Y(N+1,N-3)=-1.
      Y(N+1,N-2)=6.
      Y(N+1,N-1)=-15.
      Y(N+1,N)=10.+12.*H*ANU/R(N)
      Y(N+1,N+1)=3.
      B(N+1)=-12.*H*A5(N)*R(N)*BC3/(D*CVP)
      GO TO (487,488,482,497),NBC2
  487 Y(2*N+2,2*N+1)=1.
      B(2*N+2)=R(N)*BC4
      GO TO 504
  490 Y(N+1,N)=1.
```

```
      R(N+1)=RC3
      GO TO (402,49,50,402),NRC2
  407 Y(2*N+2,2*N-2)=1.
      Y(2*N+2,2*N-1)=0.
      Y(2*N+2,2*N)=10.
      Y(2*N+2,2*N+1)=10.-12.*H*XNU/R(N)
      Y(2*N+2,2*N+2)=12.*H*(P*A7(N)+A5(N)*RC6/(CVP*A))
     1 +BI*B(N)*DZ(N-1)*12.*H
      GO TO 504
  504 WRITE OUTPUT TAPE 6,212
  212 FORMAT (32H0  BOUNDARY CONDITIONS COMPLETED)
      REWIND 3
      J=2*N+2
      WRITE TAPE 3,Y
      REWIND 3
      WRITE OUTPUT TAPE 6,213
  213 FORMAT (14H0      I  MATRIX)
  214 FORMAT (8E14.5)
      WRITE OUTPUT TAPE 6,214,((I,I=1,J),I=1,J)
  511 CALL SOLV (Y,J,1,0.E-6,0,5V)
      CALL DER (H,N,F,DF)
      CALL DER (H,N,G,DG)
      WRITE OUTPUT TAPE 6,215
      WRITE OUTPUT TAPE 6,216
      WRITE OUTPUT TAPE 6,217,(I,R(I),F(I),G(I),DF(I),DG(I),I=2,N)
  215 FORMAT (43H0  SOLUTION OF THE EQUATION,  F(I) AND G(I))
  216 FORMAT (7RH    I              R                F                G
     1  DF                DG)
  217 FORMAT (14,5E13.5)
      RETURN
      END
```

```
C     SUBROUTINE ZERO(C,N,H,R,Z)
*     LIST
C     CALCULATION OF R(I), Z(I), DZ(I), DDZ(I),
      SUBROUTINE ZERO(C,N,H,R,Z)
C     SENSE SWITCH  3  U=CIRCULAR ARC
C                      U=SEALOL BELLOW
      DIMENSION  C(10,10), R(150), Z(150), DZ(150), DDZ(150)
      COMMON  R,DZ,DDZ
C     CALCULATION OF R(I)
      RI=C(1,1)
      RO=C(7,1)
      ZI=C(1,2)
      ZO=C(7,2)
      XN=N-2
      SP=RO-RI
      H=SP/XN
      H2=H*H
      J=N+1
      DO 210 I=1,J
      XI=I
  210 R(I)=RI+(XI-2.)*H
C     CALCULATION OF Z(I),DZ(I),DDZ(I)
      K=1
      IF(SENSE SWITCH 3) 215,217
  215 WRITE OUTPUT TAPE 6,300
  300 FORMAT (28H0  CIRCULAR ARC BELLOW PLATE)
      DO 216 I=1,4
  216 C(1,I)=C(2,I)
      C(2,5)=C(2,5)+3.*H
```

```
217 DO 240 I=1,J
    IF (K-7) 214,226,226
214 CV1=ABSF(C(K,3)**2.-(R(I)-C(K,1))**2.)
    CV2=SQRTF(CV1)
    Z(I)=C(K,2)+C(K,4)*CV2
    GO TO 218
226 Z(I)=C(K,2)+C(K,4)*(R(I)-C(K,1))
218 IF(C(K,5)-R(I+1)) 235,235,240
235 IF (C(K+1,5)-R(I+1)) 239,239,237
237 K=K+1
    GO TO 240
239 K=K+2
240 CONTINUE
    J=N-1
    DO 245 I=3,J
    DZ(I)=(Z(I-2)-8.*Z(I-1)+8.*Z(I+1)-Z(I+2))/(12.*H)
245 DDZ(I)=(-Z(I-2)+16.*Z(I-1)-30.*Z(I)+16.*Z(I+1)-Z(I+2))/(12.*H2)
    DZ(2)=(-3.*Z(1)-10.*Z(2)+18.*Z(3)-6.*Z(4)+Z(5))/(12.*H)
    DDZ(2)=(10.*Z(1)-15.*Z(2)-4.*Z(3)+14.*Z(4)-6.*Z(5)+Z(6))/(12.*H2)
    DZ(N)=(-Z(N-3)+6.*Z(N-2)-18.*Z(N-1)+10.*Z(N)+3.*Z(N+1))/(12.*H)
    DDZ(N)=(Z(N-4)-6.*Z(N-3)+14.*Z(N-2)-4.*Z(N-1)-15.*Z(N)
   1+10.*Z(N+1))/(12.*H2)
    WRITE OUTPUT TAPE 6,250,H
    WRITE OUTPUT TAPE 6,251
    WRITE OUTPUT TAPE 6,252,(I,R(I),Z(I),DZ(I),DDZ(I),I=2,N)
250 FORMAT (35H0  INTERVAL SIZE OF BELLOW PLATE H=E13.5)
251 FORMAT (4H    I,10H       R(I),15H            Z(I),16H            DZ(I
   1),17H             DDZ(I))
252 FORMAT(I5,4E15.5)
    RETURN
    END
```

```
C       CALCULATION OF COEFICIENT AI
        SUBROUTINE AFM (R,Z,N,H,XNU,D,A)
*       LIST
        DIMENSION  R(150), Z(150), DZ(150), DDZ(150), A1(150), A2(150,
       1           A3(150), A4(150), A5(150), A6(150), A7(150), F(150),
       1           G(150), DF(150), DG(150)
        COMMON  R, DZ, DDZ, F, G, DF, DG, CVP, A1, A2, A3, A4, A5, A6, A7,
       1        ANU, D, A
        J=N-1
        DO 305 I=1,J
        CVP=0.159155
        ZP1=1.+DZ(I)**2.
        ZP2=D/(I)*DDZ(I)/ZP1
        RC=1./R(I)
        ZP3=SQRTF(1.+DZ(I)**2.)
        A1(I)=RC-ZP2
        A2(I)=RC*(RC+XNU*ZP2)
        A3(I)=RC*(RC-XNU*ZP2)
        A4(I)=RC*DZ(I)*ZP3
        A5(I)=CVP*RC*ZP3
        ZP4=D/(I)*RC+XNU*DDZ(I)/ZP1
        A6(I)=CVP*RC*ZP4
        A7(I)=CVP*DZ(I)*RC*XNU
  305 CONTINUE
        WRITE OUTPUT TAPE 6,315
        WRITE OUTPUT TAPE 6,316
        WRITE OUTPUT TAPE 6,317,(I,A1(I), A2(I), A3(I), A4(I), A5(I), A6(I
       1), A7(I), I=1,J)
  315 FORMAT (16H0  FUNCTION A(I))
  316 FORMAT (5H    I,10H       A1(I),13H          A2(I),13H          A3(I),13
```

```
     1H         A4(I),13H         A5(I),13H         A6(I),13H         A7(I))
 317 FORMAT (I6, 7E13.5)
     RETURN
     END



C    SUBROUTINE DER
     SUBROUTINE DER (N,H,Z,DZ)
     DIMENSION  Z(150), DZ(150)
     DZ(2)=(-3.*Z(1)-10.*Z(2)+18.*Z(3)-6.*Z(4)+Z(5))/(12.*H)
     DZ(N)=(-Z(N-3)+6.*Z(N-2)-18.*Z(N-1)+10.*Z(N)+3.*Z(N+1))/(12.*H)
     J=N-1
     DO 708 I=3,J
 708 DZ(I)=(Z(I-2)-8.*Z(I-1)+8.*Z(I+1)-Z(I+2))/(12.*H)
     RETURN
     END
C    SUBROUTINE INTEG
     SUBROUTINE INTEG (F,H,N,S)
     DIMENSION  F(150), S(150)
     CONV=0.0
     J=N/2-1
     DO 20 K=1,J
     I=2*K
     S(K)=CONV*H/3.
     CONV=CONV+4.*F(I+1)+F(I+2)+F(I)
  20 CONTINUE
     J=N/2
     S(J)=CONV*H/3.
     RETURN
     END



C    SUBROUTINE SOLV
C    STOP 444  SINGULAR MATRIX
     SUBROUTINE SOLV (Y,B,N,F,G,D)
 214 FORMAT (8F14.5)
 218 FORMAT (19H      B MATRIX CHECK)
     DIMENSION  Y(102,102), B(102), F(150), G(150), F(150)
     CONST=0.1000
 200 FORMAT(5E13.5)
     WRITE OUTPUT TAPE 6,202,CONST
 202 FORMAT(33H0  SCALE FACTOR USED IN YBMATRIX=E13.5)
C    CALCULATION OF NEW Y, B MATRIX
     J=2*N+2
     DO 300 I=1,J
     B(I)=CONST*B(I)
     DO 300 K=1,J
 300 Y(I,K)=CONST*Y(I,K)
     WRITE OUTPUT TAPE 6,310
 310 FORMAT(15H0  NEW B MATRIX)
     WRITE OUTPUT TAPE 6,312,(B(I),I=1,J)
 312 FORMAT(8E14.5)
     IF(SENSE SWITCH 1) 313,606
 313 WRITE OUTPUT TAPE 6,314
 314 FORMAT(15H0  NEW Y MATRIX)
     WRITE OUTPUT TAPE 6,316,((Y(I,K),K=1,J),I=1,J)
 316 FORMAT(9E13.5)
 606 M=XSIMEQF(102,J,1,Y,B,D,E)
     WRITE OUTPUT TAPE 6,600,D
```

```
      GO TO (600,601,602),M
  601 WRITE OUTPUT TAPE 6,603
      GO TO 607
  602 WRITE OUTPUT TAPE 6,604
      GO TO 607
  600 FORMAT(5H0   DET=E15.6)
  603 FORMAT(17H0   OVER/UNDERFLOW)
  604 FORMAT(16H0   IS SINGULAR)
  607 STOP  444
  608 J=N+1
      DO 611 I=1,J
      K=I+N+1
      F(I)=Y(I+1)
  611 G(I)=Y(K+1)
      J=2*N+2
      DO 616 I=1,J
      B(I)=0.0
      E(I)=0.0
  616 E(I)=F(I)+Y(I+1)
      DO 619 I=1,J
      DO 619 K=1,J
  619 Y(I,J)=0.0
      READ TAPE 3,Y
      REWIND 3
      DO 624 I=1,J
      DO 624 K=1,J
  624 B(I)=B(I)+Y(I,N)*E(K)
      WRITE OUTPUT TAPE 6,218
      WRITE OUTPUT TAPE 6,214,(B(I),I=1,J)
      RETURN
      END
```

APPENDIX B

DESCRIPTION OF COMPUTER PROGRAM "NONLIN"

Program NONLIN was developed by Battelle Memorial Institute, under Air Force contract. It is generally capable of predicting the nonlinear behavior of bellows plates under a wide range of conditions. It was used in this study for all nonlinear range analysis and for the linear range analysis of the S-shaped bellows plates.

Because NONLIN is described in detail for the interested reader in Reference (6) which is available from the DDC collection, only a brief description will be presented here.

Capabilities

NONLIN can treat any bellows plate or shell which can be divided into segments having the following basic chapes:

(a) cylinder

(b) spheroid

(c) ellipsoid

(d) parabaloid

(e) conical section

(f) toroid

The thicknesses of these elements can vary along the meridional direction. Thus, it can be seen that virtually any axisymmetric plate shape can be treated.

The possible applied loadings are as follows:

(a) pressure acting normal to the plate surface (lb/in^2)

(b) weight of the shell itself (lb/in^3)

(c) dead weight acting on the shell (lb/in^2)

(d) boundary forces, moments, or displacements acting at the initial and final edges of the structure.

Load (a) can be specified to vary along the radial direction but must be axisymmetric unless it can be expressed by a Fourier harmonic series with eight or less terms. Loads (b) and (c) must be constant over the element and the shell centerline must be vertical.

The elastic properties of the shell (i.e. Young's modulus and Poisson's ratio) can vary along the meridional direction.

Computational Method

NONLIN uses a method developed by Kalnins (7, 8). The general nonlinear shell equations are reduced to a set of six first order nonlinear differential equations. These are solved by a multi-segment model which combines direct numerical and finite difference methods. This method is coupled with a systematic iteration procedure to solve the nonlinear equations.

Program Limitations

The program was written in FORTRAN IV for the CDC-6400 computer. It consists of one main program and 15 subroutines and is self-contained except for standard library functions.

The major inherent limitation is that the total number of segments which can be treated is 60. For simple plate shapes, this is not a serious limitation, but the number of convolutions for a complex plate shape becomes limited. This precludes the study of the effect of edge conditions several convolutions away from the boundary or the simulation of a convolution in the center of a long bellows core.

Occasionally, in runs for this study where near 60 segments were used, the iteration procedure required for the nonlinear solution did not converge.

Other than this segment size limitation, the program was found to be extremely flexible, and economic for predicting bellows plate behavior.

APPENDIX C

COMPARISON BETWEEN "SEALOL" AND "NONLIN" FOR LINEAR RANGE ANALYSIS

Program NONLIN can also be used to obtain a linear solution for the stresses and deflections in bellow. Thus, for the benefit of a potential future investigator who requires linear range solutions, the following user-oriented information is documented.

For linear solutions, the required computer time for the two programs is comparable, NONLIN probably being somewhat faster for most shapes. Preparation of input data is complex for both programs and requires comparable time. Here NONLIN is probably also more convenient due to the documentation available in Reference (6).

If the desired solution is for a single convolution in the central portion of a long bellows core, SEALOL is likely a more accurate tool because SEALOL treates a single convolution whose boundary conditions are provided by an adjacent entirely similar convolution. It, thus, is not capable of predicting the influence of the end fixtures on the behavior of the convolution. NONLIN, on the other hand, is capable of treating only 3 or 4 convolutions adjacent to the end fixture. Thus, it is capable of predicting end effects but cannot represent a convolution far away from the end fixture.

Both programs are capable of treating a variety of basic plate shapes. Because of the method used for describing plate shapes, however, NONLIN, is more suitable for treating complex convolutions consisting of coupled segments of basic shapes or stiffening rings. It also is capable of treating variations in plate thickness across the span where SEALOL is not.

Another fundamental shape limitation for SEALOL which does not apply for NONLIN is that it should not be used to treat any shape where the local plate inclination approaches 90° (e.g. near the edges of a full toroidal span) since the form of the equations used has a singular point in this case. Thus, it is suitable only for shallow plate elements.

Finally, the programs were each developed for a different computer although each is written in FORTRAN. Modifications in control and format statements are often required in adapting a program written for one machine to another machine. This was found to be the case for NONLIN which was originally written for a Control Data computer. Modifications would have been required in the program to use it on an IBM machine. Thus, for convenience, it was used on a CDC-6600. The FORTRAN II used for SEALOL is compatible with the IBM 7090 and 7094 systems.

Another factor affecting the use of program NONLIN is the large memory required, approaching 100,000 words. This again is compatible with the CDC 6600 system which has a 100K memory, but is too large for those systems which only have 32K available without augmentation. Thus, a dimension statement modification would be necessary and the number of plates treated is limited.

On balance, it is recommended that the Battelle program, NONLIN, be used for any case where it is suitable, because of the available documentation and its inherent flexibility and generality in treatment of plate shapes.

APPENDIX D

TABULATION OF COMPUTER RUNS AND PLOTS OF THE STRESS DISTRIBUTIONS FOR THE SYMMETRICALLY-STACKED TOROIDAL BELLOWS

Computor Runs

A tabulation of all computer runs made on Program NONLIN to investigate the behavior of the symmetrically-stacked toroidal bellows plates is given in Table D-1. This data is plotted and discussed in the main body of this report.

The nomenclature used in Table D-1 is defined in Figure D-1.

Stress Distributions

Figures D-2, D-3, and D-4 shows the distribution of the four principal stress components as predicted for opposed plates having included angles of 180°, 120° and 60°, respectively. The loading assumed for these plates was a combined 500 psi pressure differential and an axial plate deflection of 5 mils. For each plate, a 5 mil thickness was used.

In Table D-1, the maximum combined stress intensity (twice the maximum shear stress) is tabulated for the various critical cases. This value is obtained by taking the maximum local difference between principal stress components.

Table D-1

Tabulation of Computer Results

Symmetrically Stacked Toroids

Run Number	Geometric Parameters			Loads and Boundary Conditions				Output Results			Comments
	$\Delta\alpha$ degrees	r inches	t mils	δ_{xi} mils	δ_{ri} mils	δ_{rf} mils	p psi	ΔN_p lbs/in	ΔD_e percent	σ_{max} Kpsi	
1	180	1/8	5	0	0	0	500	.015	0.001	16.6	Effects of δ_x
2	180	1/8	5	5	0	0	500	1.65	0.11	33.3	
3	180	1/8	5	10	0	0	500	3.15	0.21	51.9	
4	180	1/8	5	15	0	0	500	4.8	0.32	70.1	
5	180	1/8	3	10	0	0	500	3.3	0.22	48.2	Effects of Thickness
6	180	1/8	4	10	0	0	500	3.3	0.22	-	
7	180	1/8	6	10	0	0	500	3.15	0.21	-	
8	180	1/8	7	10	0	0	500	3.15	0.21	57.2	
9	180	1/8	5	10	0	0	0	--	-	40.1	For Spring Rate
10	180	1/16	5	5	0	0	0	0	-	64.0	Effects of r
11	180	1/16	5	0	0	0	500	0	0	7.0	
12	180	1/16	5	5	0	0	500	1.5	0.10	.0	
13	180	1/8	5	0	1	1	500	-0.045	-0.003	28.1	Effects of δ_r
14	180	1/8	5	10	1	1	500	3.0	0.20	45.4	

Table D-1 (Cont.)

Run Number	Geometric Parameters			Loads and Boundary Conditions				Output Results			Comments
	$\Delta\phi$ degrees	r inches	t mils	δ_{xi} mils	δ_{ri} mils	δ_{rf} mils	p psi	ΔN_p lbs/in	ΔD_e percent	σ_{max} Kpsi	
15	140	1/8	5	10	0	0	500	3.3	0.22	55.2	$\Delta\phi$ Effects
16	120	1/8	5	0	0	0	500	0.045	0.003	17.4	Run 17 same as run 16
17	120	1/8	5	0	0	0	500	0.045	0.003	17.4	but tilted by 2.5 degrees
18	120	1/8	5	2.5	0	0	500	0.9	0.06	-	Effects of δ_x
19	120	1/8	5	5	0	0	500	1.8	0.12	-	
20	120	1/8	5	7.5	0	0	500	2.7	0.18	-	
21	120	1/8	5	10	0	0	500	3.6	0.24	85.2	
22	120	1/8	5	15	0	0	500	5.25	0.35	-	
23	120	1/8	5	10	0	0	0	--	-	70.6	For Spring Constant, k.
24	120	1/8	3	10	0	0	500	3.45	0.23	-	Effects of Thickness
25	120	1/8	4	10	0	0	500	3.45	0.23	-	
26	120	1/8	6	10	0	0	500	3.45	0.23	-	
27	120	1/8	7	10	0	0	500	3.6	0.24	-	
28	120	1/8	5	10	0	0	50	3.75	0.25	-	Effects of p
29	120	1/8	5	10	0	0	250	3.6	0.24	-	
30	120	1/8	5	10	1	1	500	3.45	0.23	-	Effects of δ_r
31	120	1/8	5	0	1	1	500	0.03	0.002	-	
32	60	1/4	5	10	0	0	0	--	-	83.1	Spring Constant

Table D-1 (Cont.)

Run Number	Geometric Parameters			Loads and Boundary Conditions				Output Results			Comments
	$\Delta\phi$ degrees	r inches	t mils	δ_{xi} mils	δ_{ri} mils	δ_{rf} mils	p psi	ΔN_p lbs/in	$\Delta\Gamma_e$ percent	σ max Kpsi	
33	60	1/4	5	0	0	0	500	0.06	0.004	40.2	δ_x Effects
34	60	1/4	5	10	0	0	500	6.45	0.43	116.4	
35	60	1/4	3	10	0	0	500	5.55	0.37	-	Effects of t
36	60	1/4	3	0	0	0	500	0.015	0.001	-	
37	60	1/4	3	10	0	0	0	--	-	-	
38	180	1/8	5	0	0.3*	0.2*	500	0	0	12.9	* Boundary Condition is free edge, and the values given are output results
39	270	1/8	5	10	0	0	0	--	-	-	3/4 Toroid to study the effects due to edge locations
40	270	1/8	5	0	1	1	500	0.045	0.003	-	
41	270	1/8	5	10	1	1	500	2.55	0.17	-	
42	180	1/8 $\pm$ 0.005*	5	0	0	0	500	-0.6	-0.04	-	Study of variable r * non-symmetric for $90 < \phi < 180$ r = 0.130 for $180 < \phi < 270$ r = 0.120 ** peaked for $132 < \phi < 150$, $210 < \phi < 228$, r = 0.250 for $150 < \phi < 210$, r = 0.125
43	180	1/8 $\pm$ 0.005*	5	10	0	0	500	3.15	0.21	-	
44	180	1/8 $\pm$ 0.005*	5	20	0	0	500	6.3	0.420	-	
45	96	1/4 ~ 1/8**	5	10	0	0	500	3.6	0.240	128.0	

Table D-1 (Cont.)

Run Number	Geometric Parameters			Loads and Boundary Conditions				Output Results			Comments
	$\Delta\phi$ degrees	r inches	t mils	δ_{xi} mils	δ_{ri} mils	δ_{rf} mils	p psi	ΔN_ρ lbs/in	ΔD_e percent	σ_{max} Kpsi	
46	180	1/8	5 15*	10	0	0	0	--	-	-	Study of variable t compliant edge * for $90 < \Phi < 110$, $t = 5$, $E = 29 \times 10^6$ for $250 < \Phi < 270$, $t = 15$, E 10^7 ** for $90 < \Phi < 100$, and $260 < \phi < 270$, $t = 2.5$ $E = 29 \times 10^6$ for $100 < \Phi < 260$, $t = 15$, $E = 10^7$
47	180	1/8	5 15*	10	0	0	500	3.15	0.21	-	
48	180	1/8	5 15**	10	0	0	0	--	-	-	
49	180	1/8	5 15**	10	0	0	500	--	0.21	-	
50	144	1/8	5	10	0	0	0	--	-	-	Spring Constant, k, for $\Delta\phi = 144$

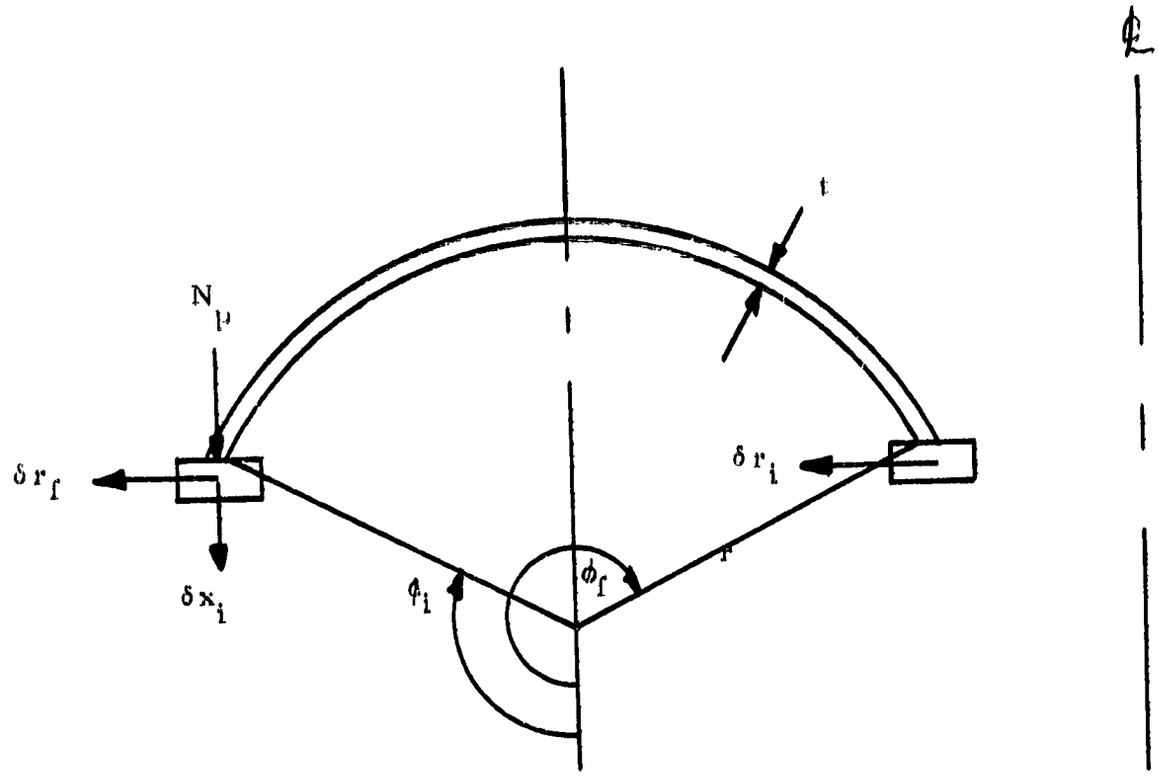

$\Delta\phi$ = $\phi_f - \phi_i$ = included angle of the toroid, degrees

r = radius of the toroidal arc, inches (2.54×10^{-2} m)

t = plate thickness, inches (2.54×10^{-2} m)

δ_{x_i} = axial plate deflection, mils (2.54×10^{-5} m)

δ_{r_i} = radial plate deflection at inner edge, mils (2.54×10^{-5} m)

δ_{r_f} = radial plate deflection at outer edge, mils (2.54×10^{-5} m)

p = pressure load, psi (6.89×10^{3} newtons/m^2)

N_p = axial reaction force per unit circumference at the sealing diameter, lbs/in (5.67×10^{-3} newton/m)

ΔN_p = the difference between the actual axial force, N_p, under the applied loads and that calculated from a linear ^{p} solution with the applied loads, lbs/in (5.67×10^{-3} newton/m)

ΔD_e = change in effective diameter, percent

σ_{mm} = meridional maximum stress, Kpsi (6.89×10^{6} newton/m^2)

σ_{mb} = meridional bending stress, Kpsi (6.89×10^{6} newton/m^2)

σ_{max} = combined maximum stress, Kpsi (6.89×10^{6} newton/m^2)

Figure D-1. Definition of Nomenclature.

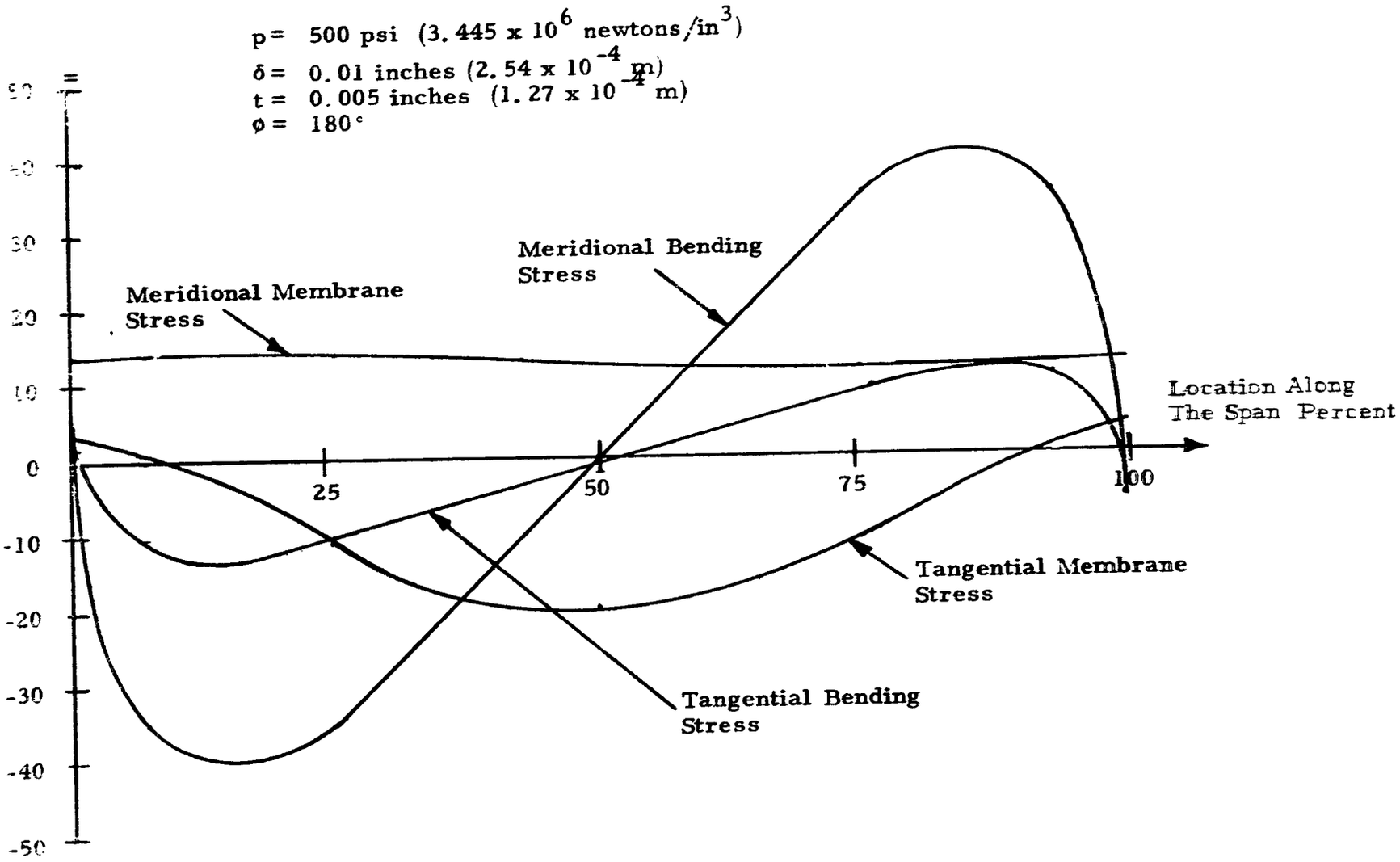

Figure D-2 Stress Distributions in a 180° Toroidal Plate.

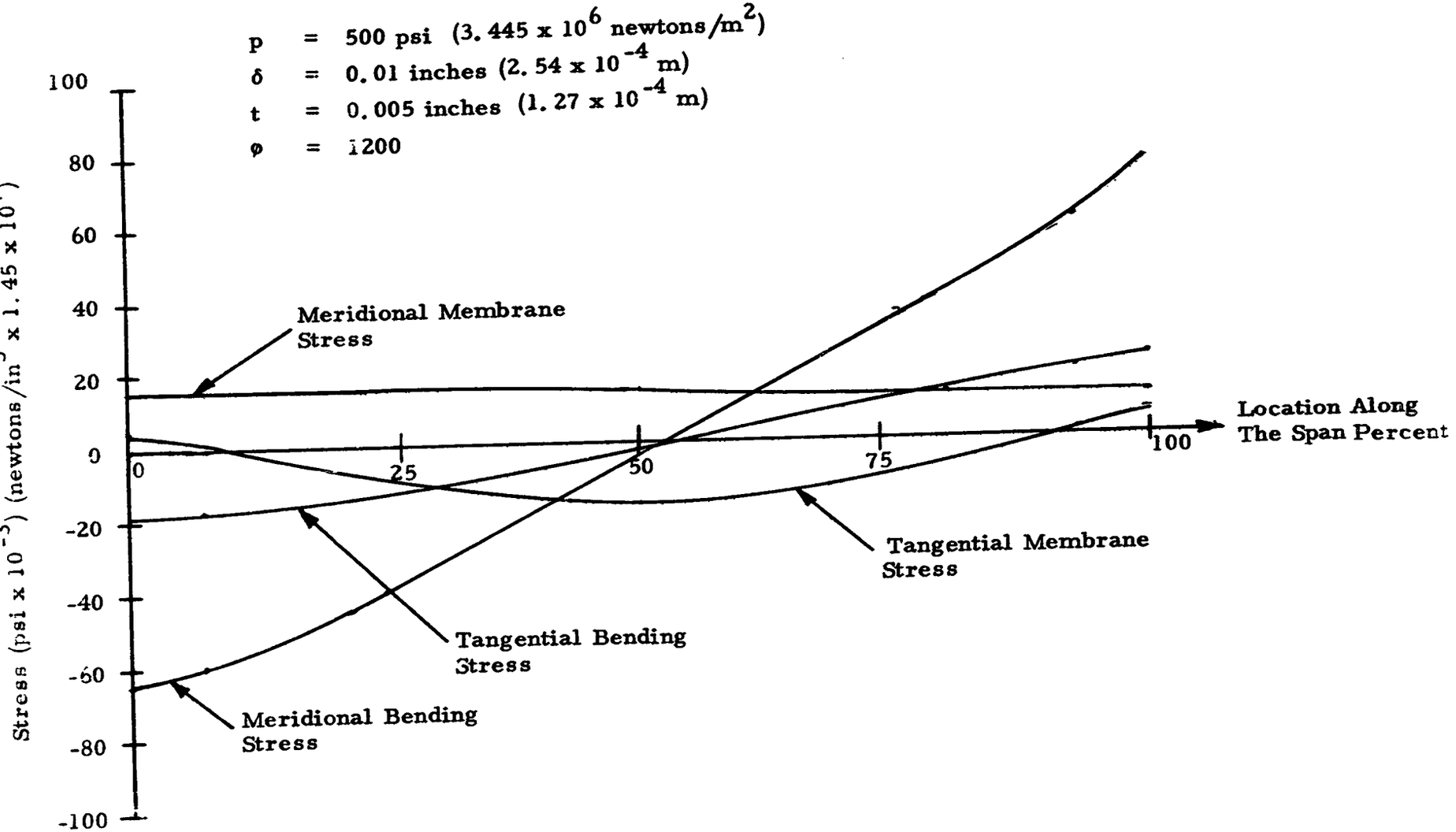

Figure D-3 Stress Distributions in a 120° Toridal Plate

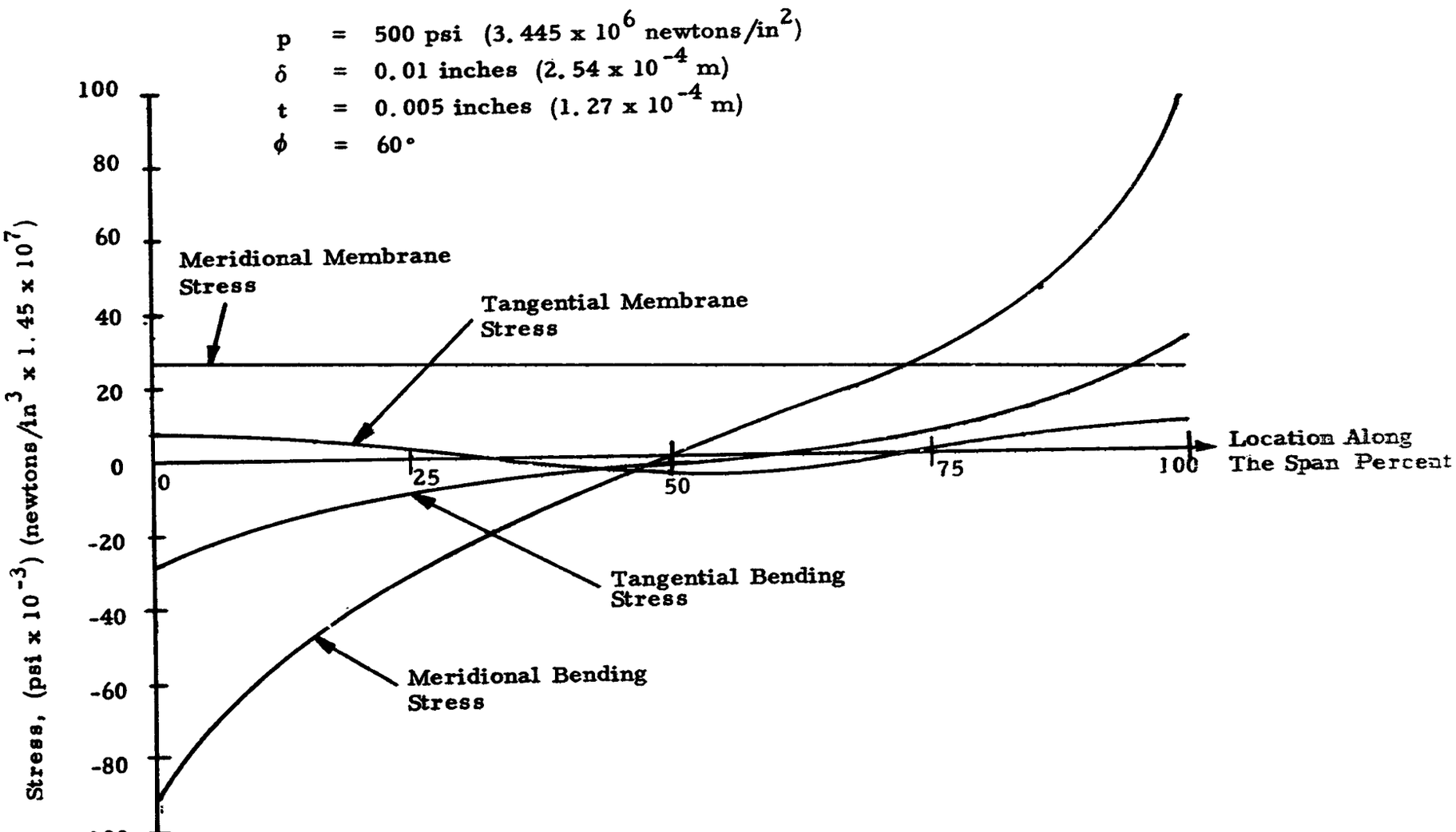

Figure D-4 Stress Distributions in 60° Toroidal Plate.

APPENDIX E

TABULATION OF COMPUTER RUNS AND PLOTS OF SAMPLE STRESS DISTRIBUTIONS FOR THE NESTED TOROIDAL BELLOWS

Computer Runs

This appendix presents the data obtained from computer runs made using program NONLIN to perform a parametric analysis of the nested toroidal bellows. The definition of nomenclature is given in Table E-1. Most of the variables are also shown graphically in Figure 21 of the main body. A tabulation of the computer results if given in Table E-2.

Stress Distributions

In order to illustrate the nature of the stress distributions which occur in the nested toroidal bellows, the case of Run No. 29 which is close to the final recommended configuration was chosen as an example. The general configuration of the four convolution stack used for the computer run is shown in Figure E-1. The shells have an included angle of 160° and the dimensions of the shells and the stiffener plates are shown in the figure.

The four principal stress components are plotted in Figures E-2 through E-5 for four successive plates from the fixed boundary or end. The stresses are plotted across the span versus angle, ϕ, which is defined as increasing from the inner to the outer edge as shown in Figure E-1.

Comparing the first shell to the third shell, it can be seen that some variation occurs near the outer edge which would be expected since the first shell is at the fixed boundary at the outer edge. The distributions for the second and fourth shells, however, are essentially identical. Thus, it appears that the influence of the boundary dies out quickly and that the results will not vary between the two similar plates of succeeding convolutions beyond the second.

Table E-1

Definition of Nomenclature

P	=	pressure, psi
δ_x	=	axial deflection, milli-inches
δ_r	=	radial deflection, milli-inches
S	=	span, inches
R_m	=	mean radius, inches
r	=	radius of toroid, inches
t	=	shell thickness, milli-inches
L_s	=	length of stiffener ring, inches
ΔR_s	=	thickness of stiffener ring, inches
$\Delta\phi$	=	included angle of toroid, degrees
β	=	angular deflection, milli-radians
n	=	number of convolutions
F_x	=	axial reaction force per unit circumference, lbs/inch
F_r	=	radial reaction force per unit circumference, lbs/inch
M	=	reaction moment per unit circumference, in-lbs/inch
ΔN_p	=	the difference between the actual axial reaction force per unit circumference at the sealing diameter under the applied loads and that calculated from a linear solution under these loads, lbs/in (5.67×10^{-3} newtons/m)
σ_{max}	=	combined maximum stress, K psi (6.89×10^{6} newtons/m^2)

Table E-2

Tabulation of Computer Results

Run Number	Geometry					Load		Boundary Conditions	ΔN_p (lbs/in)	ΔD_e Percent	σ_{max} (K psi)	Comments
	$\Delta\varphi$ degrees	r inches	t mils	L_s mils	n	p psi	δ_x/n mils conv.					
1	180	1/8	5	50	1	0	10	Fixed	$\simeq 0$	$\simeq 0$	20.2	Boundary Condition effects for a single convolution
2	180	1/8	5	50	1	500	0	$\beta = 0$ $\delta_r = 1$ mil	-0.675	-0.045	40.8	
3	180	1/8	5	50	1	500	10	$\beta = 0$ $\delta_r = 1$ mil	1.5	0.10	49.3	
4	180	1/8	5	50	1	500	10	Fixed	1.95	0.13	67.9	
5	180	1/8	5	10	1	500	5	Fixed	0.93	0.062	42.7	
6	180	1/8	5	10	1	500	5	$M = 0$ $\delta_r = 0$	0.945	0.063	43.4	
7	180	1/16	3	10	1	500	5	Fixed	0.90	0.060	54.8	r effect
8	180	1/8	5	50	1	500	10	Fixed	2.21	0.147	66.6	E for stiffner ring equal 2,900 psi
9	180	1/8	5	10	1	500	10	Fixed	2.21	0.147	66.6	E for stiffner ring equal 290×10^3 psi
10	140	1/8	5	10	1	0	5	Fixed	$\simeq 0$	$\simeq 0$	11.7	Effect of φ

Table E-2 (Continued)

Run Number	Geometry					Load		Boundary Conditions	ΔN_p (lbs/in)	ΔD_e Percent	σ_{max} (K psi)	Comments
	$\Delta\phi$ degree	r inches	t mils	L_s mils	n	p psi	δ_x/n mils/conv.					
11	140	1/8	5	10	1	500	5	Fixed	0.45	0.03	48.3	Effect of ϕ
12	140	1/8	5	10	1	500	0	Fixed	-0.975	-0.065	49.9	
13	140	1/8	5	5	1	500	5	Fixed	-1.32	-0.088	58.9	ΔR_s = 10 mils
14	140	1/8	5	5	1	500	5	M = 0 δ_r = 0	-1.455	-0.097	59.6	ΔR_s = 10 mils
15	120	1/8	5	25	1	500	0	Fixed	-1.995	-0.133	143	Reference cases for ϕ = 120°
16	120	1/8	5	25	1	500	5	Fixed	-0.39	-0.026	134	
17	140	1/8	55	30	1	500	0	Fixed	-1.005	-0.067	106	Reference cases for ϕ = 140°
18	140	1/8	5	30	1	500	5	Fixed	0.51	0.034	100	
19	140	1/8	5	30	1	500	0	M = 0 δ_r = 0	-1.101	-0.0734	107	Effects of Boundary Conditions
20	140	1/8	5	30	1	500	5	M = 0 δ_r = 0	0.51	0.034	109	
21	140	1/8	10	30	1	500	0	Fixed	-0.801	-0.0534	37.4	Effects of thickness t
22	140	1/8	10	30	1	500	5	Fixed	-0.51	-0.034	40	
23	160	1/8	5	40	1	500	0	Fixed	-0.435	-0.029	33.7	Reference cases for ϕ = 160°

Table E-2 (Continued)

Run Number	Geometry					Load		Boundary Conditions	ΔN_p (lbs/in)	ΔD_e Percent	σ_{max} (K psi)	Comments
	$\Delta\phi$ degree	r inches	t mils	L_s mils	n	p psi	δ_x/n $\frac{\text{mils}}{\text{conv.}}$					
24	160	1/8	5	40	1	500	10	Fixed	1.59	0.106	85 0	Reference case for $\phi = 160^o$
25	160	1/8	5	40	2	500	0	Fixed	- .066	-0.044	71	Effects of number of convolutions
26	160	1/8	5	40	2	500	10	Fixed	1.335	0.089	75	
27	160	1/8	5	40	4	500	0	Fixed	-0.75	-0.05	73	
28	160	1/8	5	40	4	500	5	Fixed	-0.21	-0.014	71	
29	160	1/8	5	40	4	500	10	Fixed	1.275	0.085	76	
30	120	1/8	5	25	4	500	0	Fixed	-4.71	-0.314	162	Effects of number of convolutions for other ϕ's
31	120	1/8	5	25	4	500	5	Fixed	-3.24	-0.216	153	
32	140	1/8	5	30	4	500	0	Fixed	-1.965	-0.131	117	
33	140	1/8	5	30	4	500	5	Fixed	-0.72	0.048	119	
34	140	1/8	5	30	4	500	10	Fixed	0.645	0.043	112	
35	140	1/8	5	30	4	100	5	Fixed	-0.176	-0.0117	34	Effect of p
36	150	1/8	5	40	4	500	0	Fixed	-13.28	-0.885	103	Effects of ϕ for multi convolutions
37	150	1/8	5	40	4	500	10	Fixed	0.939	0.0626	112	
38	180	1/8	5	55	4	500	0	Fixed	-0.48	-0.032	37.5	
39	180	1/8	5	55	4	500	10	Fixed	1.575	0.105	73	

Table E-2 (Continued)

Run Number	Geometry					Load		Boundary Conditions	ΔN_p (lbs/in)	ΔD_e Percent	σ_{max} (K psi)	Comments
	$\Delta \phi$ degree	r inches	t mils	L_s mils	n	p psi	δ_x/n $\frac{\text{mils}}{\text{conv}}$					
40	160	1/8	8	45	4	500	0	Fixed	-1.028	-0.0685	46.2	Effects of thickness
41	160	1/8	8	45	4	500	5	Fixed	-0.519	-0.0346	58	
42	160	1/8	8	45	4	500	10	Fixed	-0.159	-0.0106	72.4	
43	160	1/8	5	40	3	500	0	Fixed	-1.23	-0.082	189	Circular Flanges at the edge (radius of the curvature of flange equals 7.5 mils) No convergence of solutions
44	160	1/8	5	40	3	500	5	Fixed	0.126	0.0084	151	
45	160	1/8	5	40	3	500	10	Fixed	1.335	0.089	148	
46	160	1/8	5	40	2	500	0	Fixed	-1.098	-0.0732	152	
47	160	1/8	5	40	2	500	5	Fixed	-5.13	-0.342	146	
48	160	1/8	5	40	2	500	10	Fixed	-4.08	-0.272	160	
49	160	1/8	5	40	2	500	0	Fixed	-0.669	-0.0446	164	7.5 mils flat flange at the edge Convergence of solutions
50	160	1/8	5	40	2	500	10	Fixed	1.4775	0.0985	172	

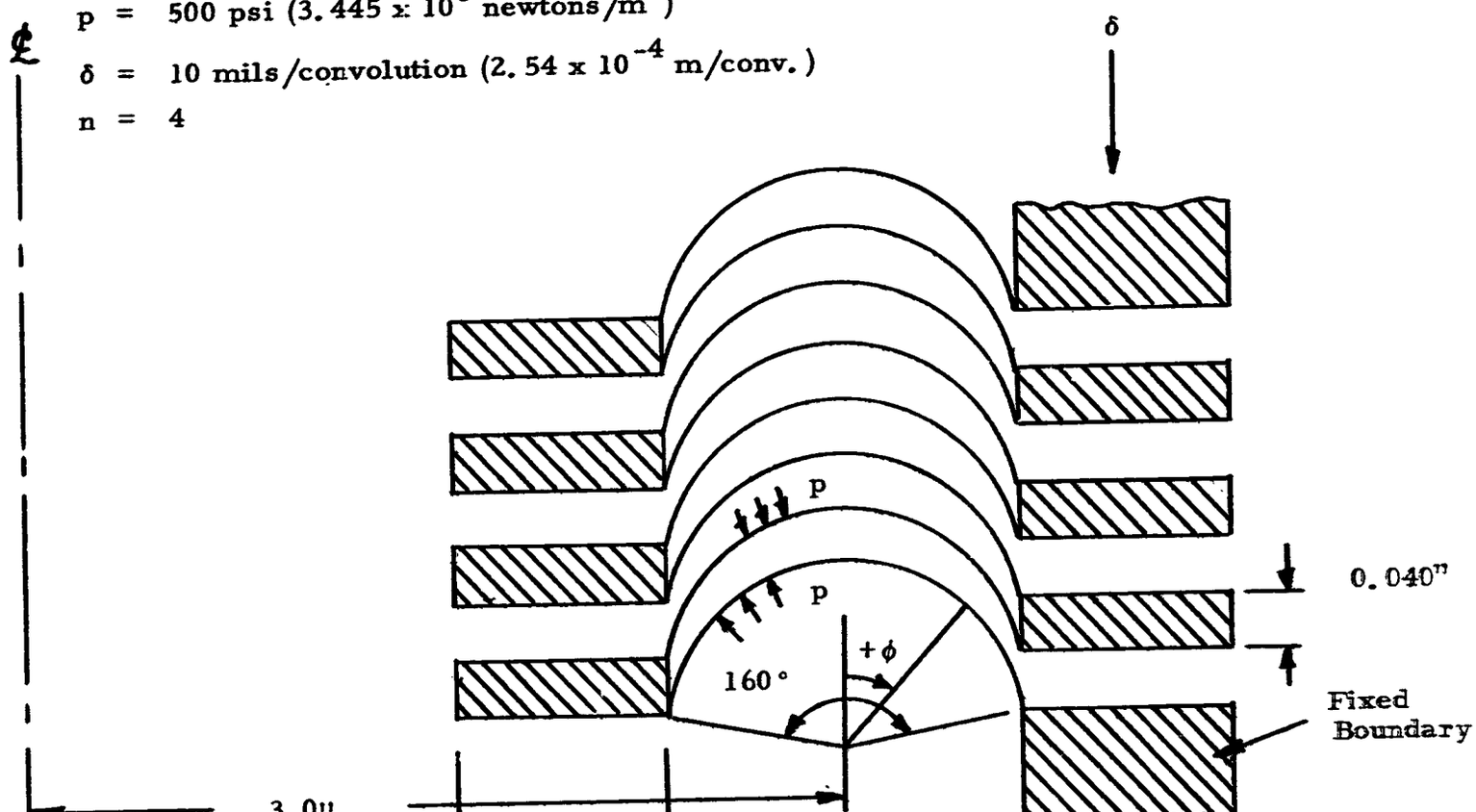

Figure E-1. Geometry for Run No. 29.

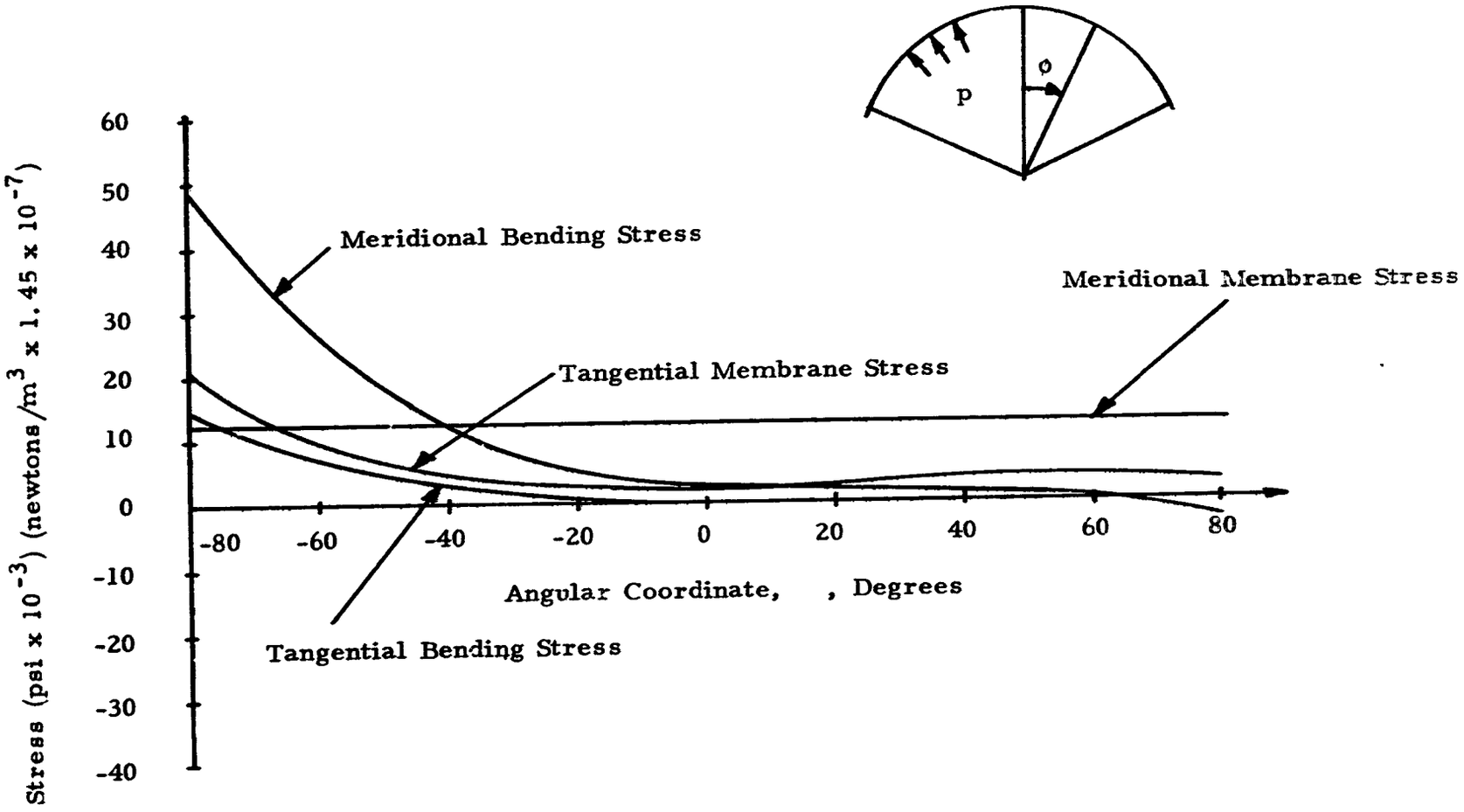

Figure E-2. Stress Distributions for the First Shell from the Fixed End, Run No. 29.

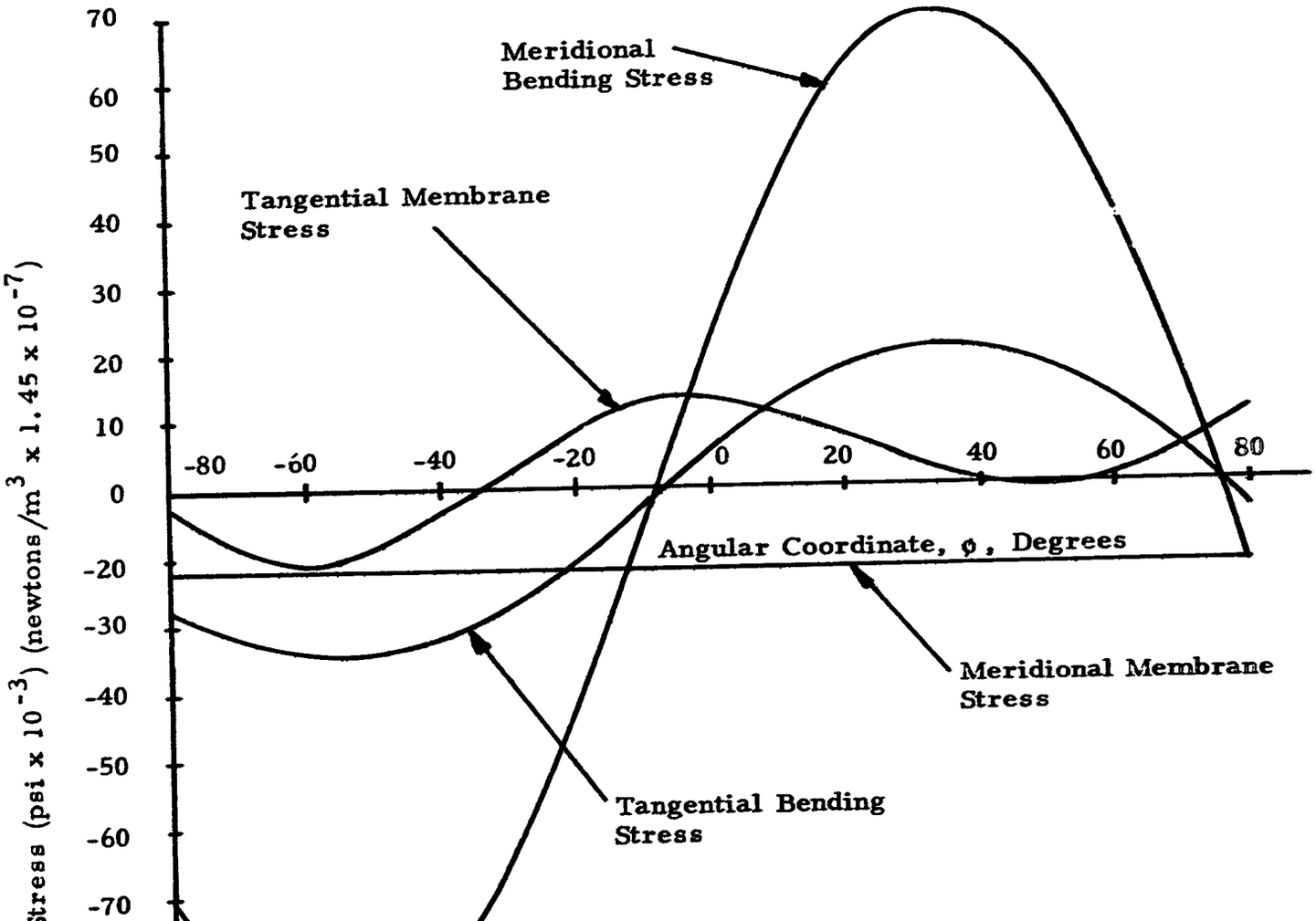

Figure E-3. Stress Distributions for the Second Shell from the Fixed End, Run No. 29.

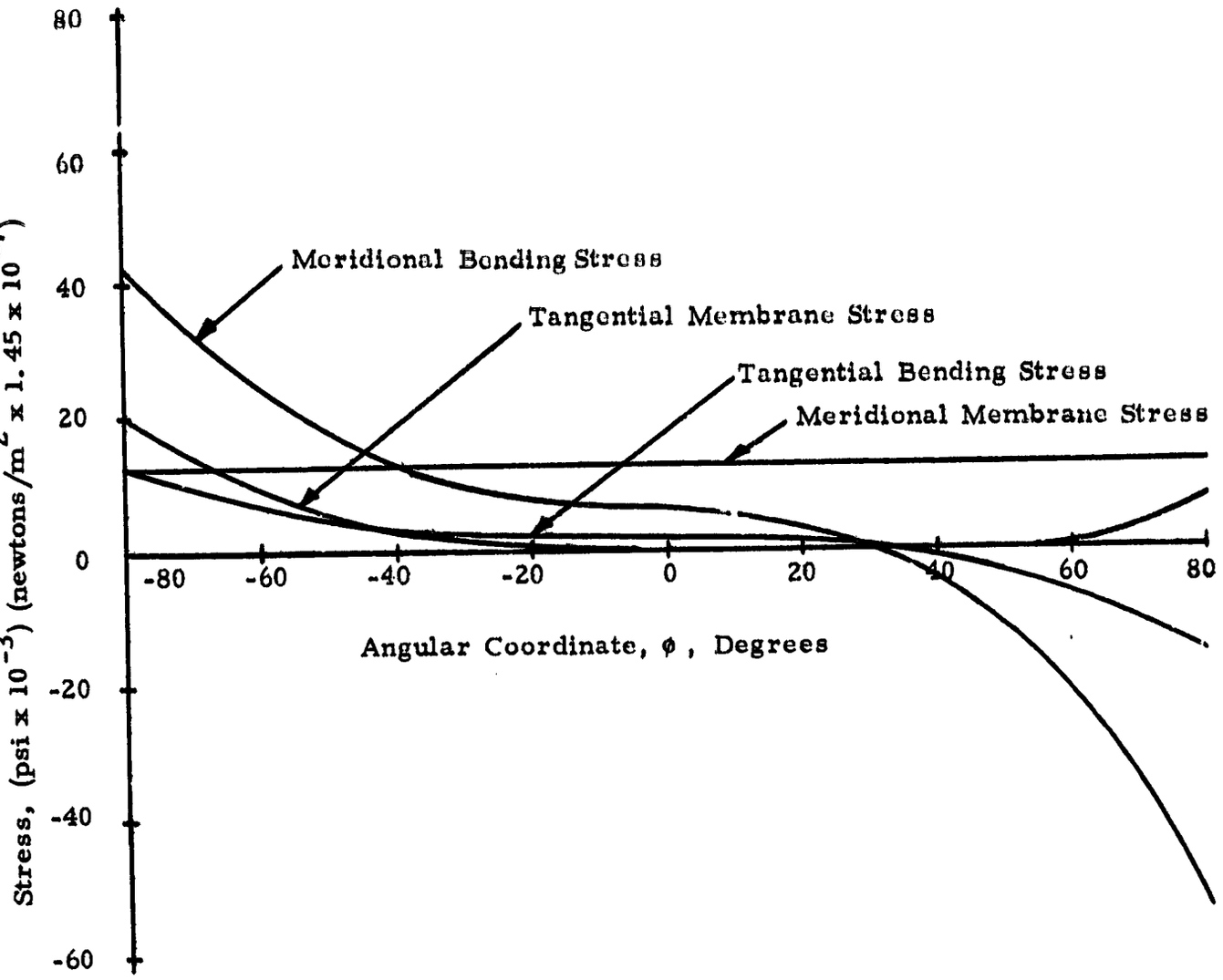

Figure E-4. Stress Distributions for the Third Shell from the Fixed End, Run No. 29.

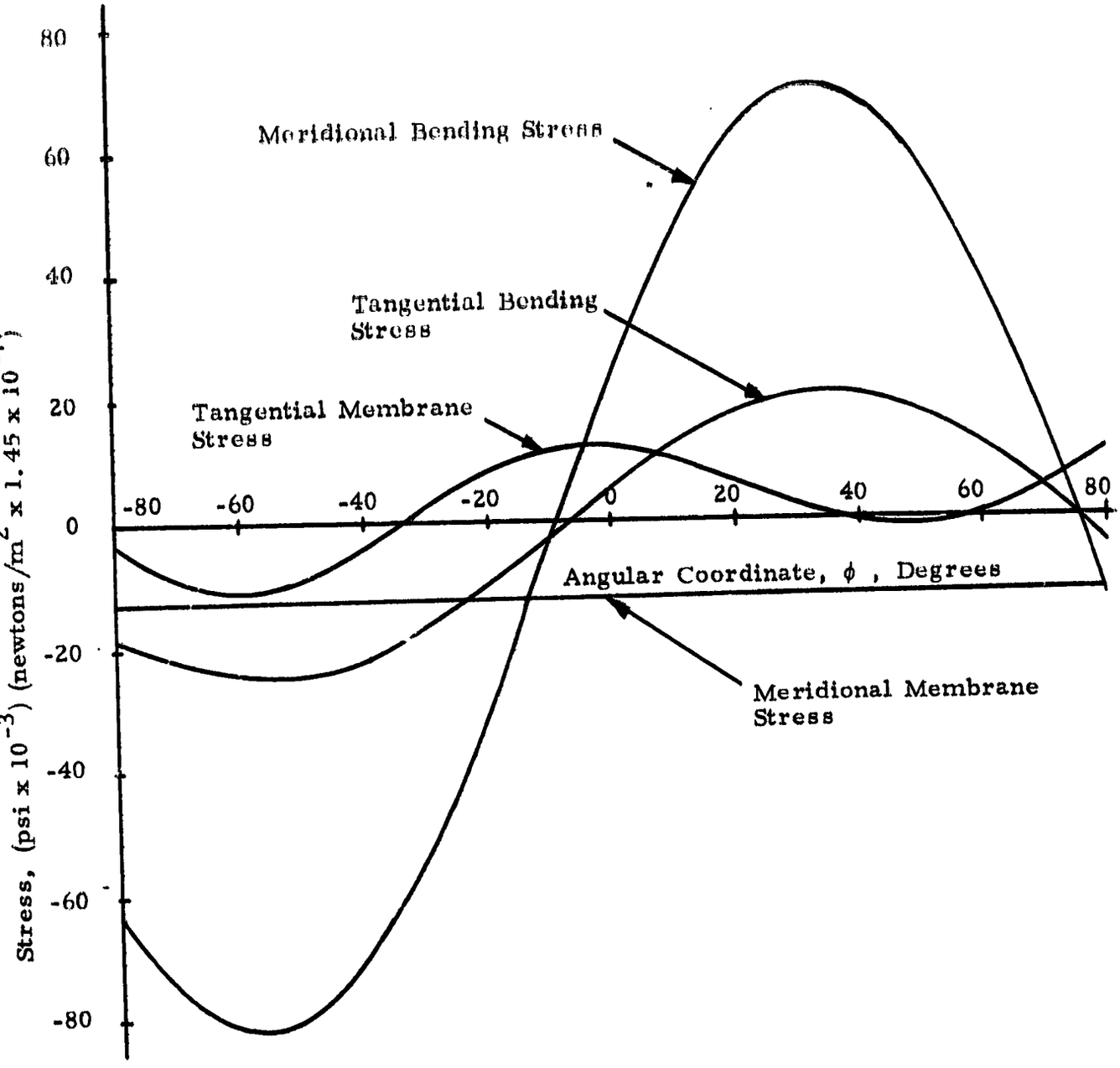

Figure E-5. Stress Distributions for the Fourth Shell from the Fixed End, Run No. 29.

APPENDIX F

STIFFNESS RELATIONSHIPS FOR THE RADIALLY CORRUGATED BELLOWS

Introduction

The nonlinear analysis of the simple opposed toroidal bellows showed that the change in effective diameter over the desired range of axial deflection is beyond the design goal.

The normal toroidal plate is very stiff circumferentially. Thus, as it is deflected, each plate fiber resists moving in or out with respect to the plate centerline. This produces radial bending or curvature change in order to accommodate the deflection. The curvature change or angular deflection across the span is plotted in Figure 30 of the main body of this report. The plate distortion produced in this manner could have the effect of altering the reaction forces and moments produced by subsequent pressure loading and, thus, change the effective diameter.

It has been hypothesized that the corrugation of the bellows plate around its circumference (corrugation peak lines and valleys lying in the radial direction) would mitigate the plate distortion produced by axial deflection and, thus, improve linearity or constancy of effective diameter.

Unfortunately, analytical techniques within the scope of this study cannot treat a non-isotropic bellows plate of this type. Thus, it is recommended that a radially corrugated opposed toroid bellows be fabricated and tested for linearity compared with a similar uncorrugated one. In order to arrive at a design for this experimental bellows which produces significant variations in the relevant plate stiffnesses, a simplified analysis was performed to determine the important stiffness ratios as functions of corrugation geometry. This analysis is summarized in this appendix.

Geometry

The geometry assumed for the analysis is shown in Figure F-1, where the principal nomenclature is also defined. For simplicity, a flat-topped corrugation was used, However, it is felt that the results provide a good approximation for the characteristics of any corrugations having a half wavelength, λ , and a mean height, h.

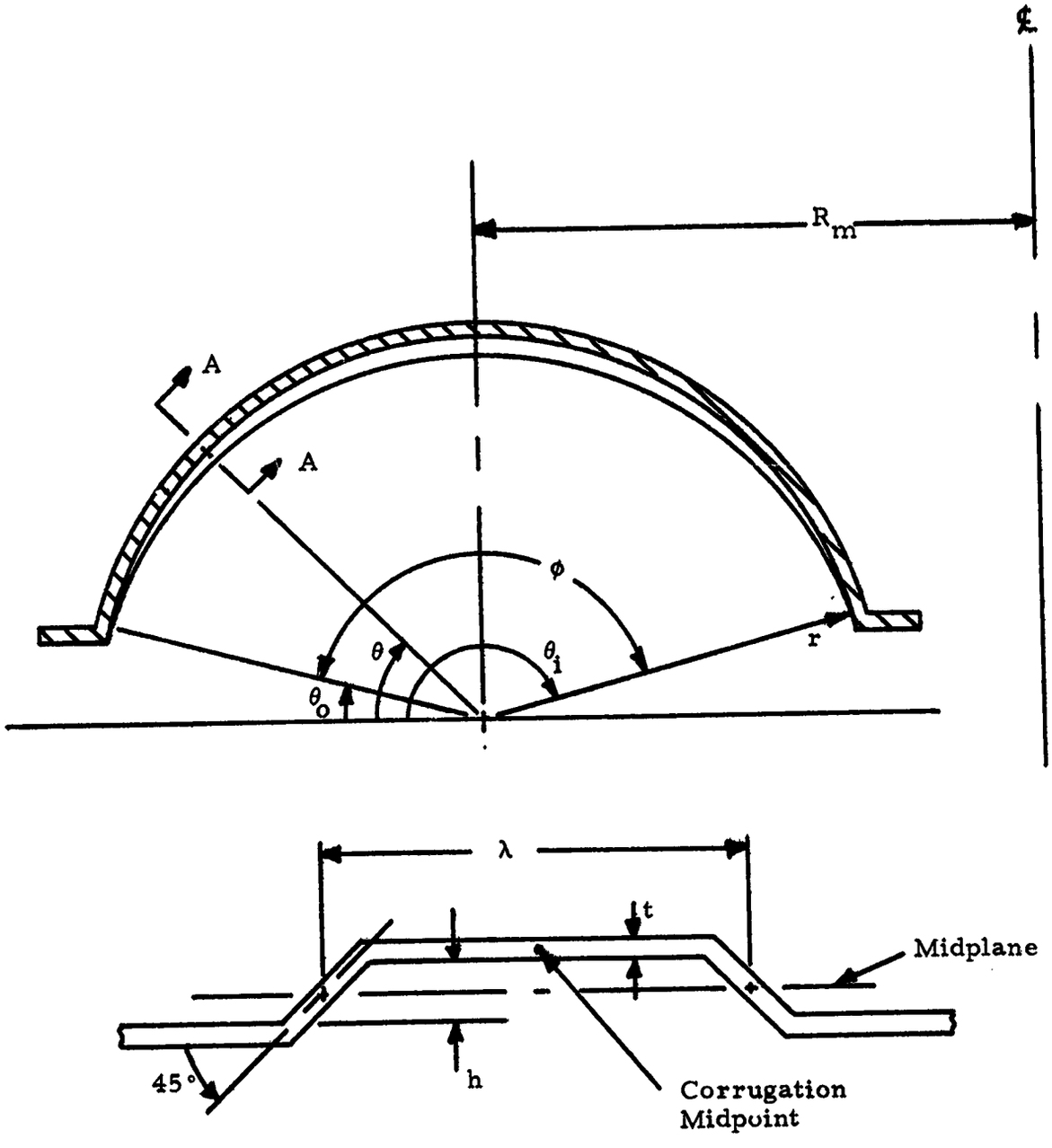

Section A-A

ϕ	-	included angle of the toroid
t	-	plate thickness
θ	-	angular coordinate
r	-	radius of the base toroid
h	-	height of the corrugation
λ	-	half wavelength of the corrugation

Figure F-1. Schematic Diagram and Definition of Nomenclature for the Radially Corrugated Toroid

Radial Direct Stiffness

The radial direct stiffness per unit length for an uncorrugated plate is simply

$$K_{RD} = A_o E = Et \tag{F-1}$$

since the area per unit length is

$$A_o = t \tag{F-2}$$

For the corrugated case of Figure F-1, the total area per half wavelength, λ, is,

$$A_\lambda = t\,(\lambda - h + \sqrt{2}\,h) \tag{F-3}$$

Thus, the radial direct stiffness becomes,

$$(K_{RD})_{corr.} = \frac{A_\lambda}{\lambda} E = Et \left[1 + (\sqrt{2} - 1)\,\frac{h}{\lambda}\right] \tag{F-4}$$

and the correction factor or ratio of corrugated stiffness to uncorrugated stiffness is given by,

$$f_{RD} = \frac{(K_{RD})_{corr.}}{K_{RD}} = 1 + (\sqrt{2} - 1)\,\frac{h}{\lambda} \tag{F-5}$$

Radial Bending Stiffness

Neglecting Poisson effects as an approximation, the radial bending stiffness for the uncorrugated plate is,

$$K_{RB} = I_o E = \frac{t^3}{12} \tag{F-6}$$

Taking the bending moment of inertia of one half wavelength of the corrugated plate about its midplane gives,

$$I_\lambda = \frac{(\lambda - h)\, t^3}{12} + (\lambda - h)\, t \left(\frac{h}{2}\right)^2 + \frac{2\sqrt{2}\, t}{12} \left(\frac{h}{2}\right)^3 + 2\sqrt{2}\, t\, \frac{h}{2} \left(\frac{h}{4}\right)^2$$

$$= \frac{t^3}{12} \left\{ (\lambda - h) + \left[3\,(\lambda - h) + \sqrt{2}\, h \right] \left[\frac{h}{t} \right]^2 \right\} \qquad \text{(F-7)}$$

Thus, the correction factor for the corrugated case becomes,

$$f_{RB} = \frac{I_\lambda / \lambda}{I_o} = 1 - \frac{h}{\lambda} + 3 \left[1 - \left(1 - \sqrt{\frac{2}{3}}\right) \frac{h}{\lambda} \right] \left[\frac{h}{t} \right]^2 \qquad \text{(F-8)}$$

Circumferential Direct Stiffness

For the uncorrugated case the circumferential direct stiffness is the same as the radial direct stiffness or,

$$K_{CD} = Et \qquad \text{(F-9)}$$

For the corrugated case, one must consider the quarter wavelength free body diagram of Figure F-2 where symmetry dictates that the corrugation midpoint is equivalent to a fixed boundary and that the midplane is an inflection point with no moment. At the corner of the corrugation segment, equilibrium dictates that,

$$M_1 = F\, \frac{h}{2} \qquad \text{(F-10)}$$

and the deflections can be written as,

$$\left.\begin{aligned} \delta_1 &= \frac{F\,(\lambda - h)}{2\,Et} \\ \theta &= \frac{M_1\,(\lambda - h)}{2\,EI} = \frac{Fh\,(\lambda - h)}{4\,EI} \end{aligned}\right\} \qquad \text{(F-11)}$$

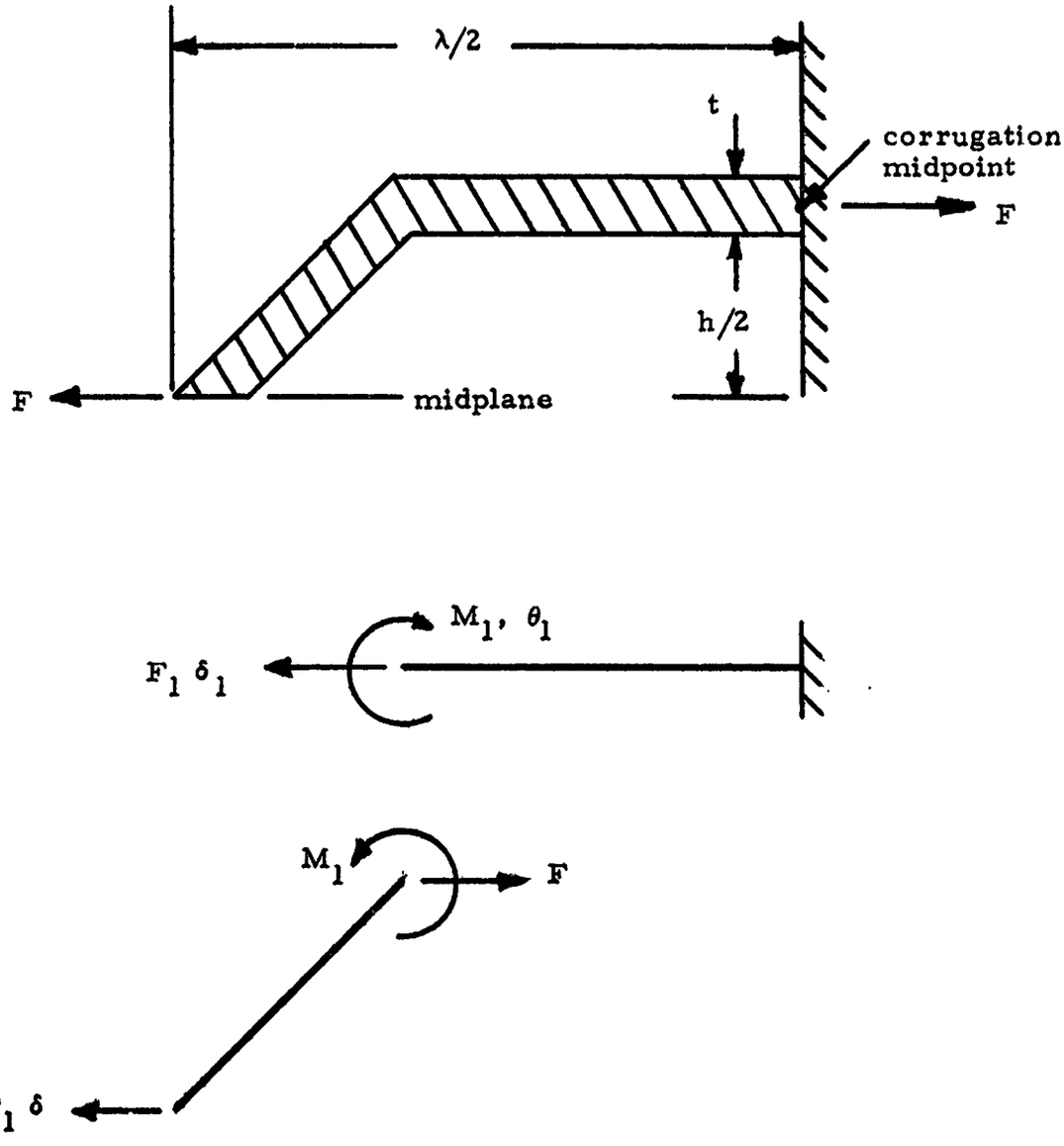

Figure F-2. Free Body Diagram of a Quarter Wavelength of a Corrugation Under Circumferential Load

where

$$I = \frac{t^3}{12} \tag{F-12}$$

Defining δ_2 as the deflection at the end under F when the corner is fixed gives,

$$\delta_2 = \frac{F}{\sqrt{2}} \left(\frac{1}{Et}\right) \left(\frac{h}{2}\right) + \frac{F}{\sqrt{2}} \left(\frac{h}{\sqrt{2}}\right)^3 \frac{1}{3} \frac{1}{EI} \frac{1}{\sqrt{2}} \tag{F-13}$$

The total deflection, δ, can be obtained by adding the effects of the above according to,

$$\delta = \delta_1 + \theta_1 \frac{h}{2} + \delta_2$$

$$= \frac{I}{2E} \left\{ \left[\frac{\lambda - h}{t} + \frac{h}{\sqrt{2}\, t} \right] + \left[\frac{h^2 (\lambda - h)}{4} + \frac{h^3}{6\sqrt{2}} \right] \frac{1}{I} \right\} \tag{F-14}$$

Thus, the equivalent direct stiffness is,

$$(K_{CD})_{corr.} = \frac{F}{\delta} \left(\frac{\lambda}{2}\right).$$

$$= ET \left\{ 1 - \left(1 - \frac{1}{\sqrt{2}}\right) \left(\frac{h}{\lambda}\right) + 3 \left[1 - \left(1 - \frac{\sqrt{2}}{3}\right) \frac{h}{\lambda} \right] \left[\frac{h^2}{t^2} \right] \right\}^{-1} \tag{F-15}$$

and the correction factor is

$$f_{CD} = \left\{ 1 - \left(1 - \frac{1}{\sqrt{2}}\right) \left(\frac{h}{\lambda}\right) + 3 \left[1 - \left(1 - \frac{\sqrt{2}}{3}\right) \frac{h}{\lambda} \right] \left[\frac{h}{t} \right]^2 \right\}^{-1} \tag{F-16}$$

Circumferential Bending Stiffness

The corrugations will not have an effect on the circumferential bending stiffness. Thus, the correction factor is simply,

$$f_{CB} = 1 \tag{F-17}$$

Numerical Values

If it is assumed that the corrugation amplitude varies across the span from zero to a maximum amplitude, H, at the midpoint according to the relations,

$$h = 2H\left(\frac{\theta - \theta_o}{\phi}\right) \qquad \theta_o < \theta < \frac{\pi}{2}$$

$$h = 2H\left(\frac{\theta_i - \theta}{\phi}\right) \qquad \frac{\pi}{2} < \theta < \theta_i \tag{F-18}$$

then the following values can be found at the midpoint, $\theta = \frac{\pi}{2}$, for the four correction factors,

$$f_{RD} = 1.083$$

$$f_{RB} = 17.5$$

$$f_{CD} = 0.056$$

$$f_{CB} = 1$$

where

$$H = 10 \text{ mils } (2.54 \times 10^{-4} \text{ meters})$$

$$\lambda = 50 \text{ mils } (1.27 \times 10^{-3} \text{ meters})$$

$$t = 4 \text{ mils } (1.016 \times 10^{-4} \text{ meters})$$

This typical case shows that the radial bending stiffness increases by a factor 17 while the cirvumferential stiffness decreases by a factor of 18. It is felt that a variation of this magnitude from the uncorrugated case should be sufficient for experimental evaluation.

Use of the various relationships of this appendix also allows prediction of the effect of any other corrugation configuration of this type.

REFERENCES

1. Morton, H. L., et. al., Effects of Low Temperatures on the Mechanical Properties of Structural Metals, Revised and Enlarged Edition, NASA Special Publication SP-5012 (01), Washington, D. C. 1968.

2. Schwartzberg, F. R., et. al., Cryogenic Materials Data Handbook, Air Force Materials Laboratory, Air Force Systems Command, Technical Documentary Report No. ML-TDR-64-280 (AD-609 562), Wright-Patterson Air Force Base, Ohio, August, 1964, (Supplement, February, 1965).

3. Roark, R. J., Formulas for Stress and Strain, Fourth Edition, McGraw-Hill Book Co., New York, 1965.

4. Wahl, A. M., Mechanical Springs, Second Edition, McGraw-Hill Book Co., New York, 1963.

5. Bessarabov, Y. P., and Rudis, M. A., On the Symmetrical Deformation of an Orthotropic Toroidal Shell, Published in the Proceedings of the Fourth All-Union Conference, U. S. S. R., October 1962, translated and published for NASA.

6. Trainer, T. M., et. al., Development of Analytical Techniques for Bellows and Diaphragm Design; Technical Report No. AFRPL-TR-68-22; Air Force Rocket Propulsion Laboratory, Edwards Air Force Base, California, March, 1968.

7. Kalnins, A., "Analysis of Shells of Revolution Subjected to Symmetrical and Nonsymmetrical Loads," ASME Transactions, Volume 86, September 1964.

8. Kalnins, A. and Lestingi, J. F., "On Nonlinear Analysis of Elastic Shells of Revolution," ASME Transactions, Volume 89, March, 1967.